Doctoral theses at NTNU, 2012:329

Li Zhou

Numerical and Experimental Investigation of Stationkeeping in Level Ice

ISBN 978-82-471-3980-6 (printed version)
ISBN 978-82-471-3981-3 (electronic version)
ISSN 1503-8181

NTNU – Trondheim
Norwegian University of
Science and Technology

Doctoral Thesis

Li Zhou

Doctoral theses at NTNU, 2012:329

NTNU

NTNU
Norwegian University of Science and Technology
Thesis for the degree of Philosophiae Doctor
Faculty of Engineering Science and Technology
Department of Marine Technology

NTNU – Trondheim
Norwegian University of
Science and Technology

Li Zhou

Numerical and Experimental Investigation of Stationkeeping in Level Ice

Thesis for the degree of philosophiae doctor

Trondheim, November 2012

Norwegian University of Science and Technology
Faculty of Engineering Science and Technology
Department of Marine Technology

NTNU – Trondheim
Norwegian University of
Science and Technology

NTNU
Norwegian University of Science and Technology

Thesis for the degree of philosophiae doctor

Faculty of Engineering Science and Technology
Department of Marine Technology

ISBN 978-82-471-3980-6 (printed version)
ISBN 978-82-471-3981-3 (electronic version)
ISSN 1503-8181

Doctoral Theses at NTNU, 2012:329

Printed by Skipnes Kommunikasjon as

Abstract

Stationkeeping method is crucial for successful marine operations in ice-covered waters. Depending on the type of structure, two methods are used in the numerical study, namely mooring system and DP combined mooring system.

For stationkeeping operations in ice, ice loads represent the dominant load and it is important to estimate global ice loads on stationkeeping structures and the resulting structures response. Therefore, focus in the present thesis is put on both numerical model for simulating ice–structure interaction during stationkeeping operations in level ice and experimental investigation of ice loading process.

The numerical model includes ice force model, mooring system model and heading control model. Ice force model reproduces continuous icebreaking process and considers the actions of ice cusps fragmented from the intact ice sheet on the structures. The mooring system mainly provides restoring forces to balance the ice loads. Heading control model is mainly used to align the ship-shaped structure with the incoming drift ice. In the simulation of an icebreaking tanker with a mooring system, the three degree-of-freedom (DOF) rigid body equations of surge, sway, and yaw are solved by numerical integration. The thickness and strength properties of the ice encountered by the structures are assumed to be constant. Accordingly the global ice loads on structures and corresponding behavior are obtained in a deterministic way.

The icebreaking tanker MT Uikku in level ice was tested in the multifunctional ice basin of the Marine Technology Group at the Aalto University. The ship model was mounted on a rigid carriage and towed through an unbroken ice sheet with different carriage speeds, heading angles of the model ship, and ice thickness. The phenomena of ice loading process were observed. The resulting ice forces, accelerations, ice cusp sizes, and ice pile dimensions under the intact ice sheets were measured.

In order to validate the numerical model, the simulated results with both conical and ship-shaped structures are compared with full scale and model scale measurements. Depending on the scenario occurred to the submerged ice blocks fragmented from intact ice sheet, two ice submersion models are used in the numerical simulation. It is expected that numerical simulations can supplement full-scale tests in providing more

details about the continuous icebreaking processes and the global ice load effects on stationkeeping operations of structures.

The simulation results are discussed in a case study with the tanker MT Uikku based on the heading control, in which the effects of ice thickness, ice drift speed, and global mooring stiffness on mooring forces and responses of the moored vessel are analyzed. Then the performances of the moored tanker with heading control are simulated in time domain to estimate stationkeeping capability of the tanker in level ice.

Up to now the knowledge about stationkeeping in ice is still at an early stage. The author believes that the present numerical model is suited for studies of the ice loads and dynamic response of structures with stationkeeping operation in level ice and can be extended to level ice with variable ice drift direction. It is hoped that further studies on this numerical model can supplement the full and model scale measurements in establishing a design basis for the structure stationkeeping.

Acknowledgements

Three years as a PhD candidate has come to an end and there are many people I would like to thank for making it an unforgettable experience.

First of all, I would like to express my sincere gratitude to my main supervisor, Prof. Torgeir Moan. Thank him for providing the PhD opportunity in the unique research environment at CeSOS to me. During the past three years, I learned a lot from his broad professional knowledge, innovative thinking, positive attitudes, novel ideas, and extensive experience. Without his patient and consistent guidance, the present work would not have been possible. Deep inside, it is my honor to be one of his students. A special thanks goes to my co-supervisor Prof. Kaj Riska for his valuable discussion and guidance throughout the present work. I would also like to thank Professors Ian Jordaan, Pentti Kujala and Roger Skjetne as well as Dr. Arne Gürtner for serving on my thesis committee.

I would like to express my appreciation to all professors, research fellows and staffs at CeSOS and the Department of Marine Technology for creating a friendly and collaborative environment. The administrative assistance and help I received from Ms. Sigrid Bakken Wold, Ms. Marianne Kjølås, Ms. Linda Grønstad and Ms. Annika Klinger are acknowledged.

During my postgraduate study, many other people helped and supported me and I want to thank all of them. I would like to acknowledge my senior fellow, Dr. Biao Su for his efforts on developing the initial computer program, great help with doing the model tests and pleasant discussions. Sincere thanks are given to associate Prof. Zhen Gao for his useful advice on mooring system and help with usage of software Riflex. I am grateful to all my friends who make my life meaningful in Norway. Among them, I would like to mention Dr. Huirong Jia, Dr. Yanlin Shao, Dr. Jingzhe Jin, Decao Yin, Bo Zhao, Marit Kvittem, Ida Aglen, Seyed Behzad Hatefi and many others for kind help during my PhD study.

Last, but definitely not least, I would like to thank my family for their continued encouragement and unconditional support throughout the years, especially my mother Cuilan Li as well as my in-laws Yaqin Liu and Hengmian Chuang. I would like to

express my special thanks to my father in heaven for his endless and permanent love to me. Most of all, I am deeply grateful to my dear wife Zhenju Chuang. Her love and continuous confidence in me and my work have carried me through the hard times in my life. Through this work, I also wish to express love to my little son Lukas Haozhe Zhou.

Li Zhou

September 13, 2012

Trondheim, Norway

Table of Contents

List of Appended Papers

The core of this thesis is constituted by Papers 1-5 which are included in Appendix C.

Paper 1:

Numerical simulation of moored structure station keeping in level ice
Li Zhou, Biao Su, Kaj Riska and Torgeir Moan
Published in Cold Regions Science and Technology 71(2012), 54-66

Paper 2:

Heading control for turret-moored vessel in level ice based on Kalman filter with thrust allocation
Li Zhou, Torgeir Moan, Kaj Riska and Biao Su
Accepted by Journal of Marine Science and Technology (2011)

Paper 3:

Station Keeping Capacity of a Moored Structure with Heading Control in Level Ice
Li Zhou, Kaj Riska and Torgeir Moan
Published in the 21st IAHR International Symposium on Ice, Dalian, China, 2012

Paper 4:

Experiments on level ice loading on an icebreaking tanker with different ice drift angles
Li Zhou, Kaj Riska, Rüdiger von Bock und Polach, Torgeir Moan and Biao Su
Published in Cold Regions Science and Technology 85 (2013), 79-93

Paper 5:

Numerical modeling of ice load on an icebreaking tanker: comparing simulations with model tests
Li Zhou, Kaj Riska, Torgeir Moan and Biao Su
Accepted by Cold Regions Science and Technology (2012)

The following publication is not included in the thesis since it was an earlier, shorter version of paper and overlaps with this paper to some extent.

Other Paper 1:

Numerical Simulation of Moored Ship in Level Ice
Li Zhou, Biao Su, Kaj Riska and Torgeir Moan
Published in Proceeding of the 30th international Conference on Offshore Mechanics and Arctic Engineering, Rotterdam, The Netherlands, 2011

Declaration of Authorship

As for the authorship of these five papers and my contributions, I have been the first author of all these papers and I was responsible for establishing the numerical models, performing the simulations, carrying out the ice model tests, analyzing the model test data, providing the results and writing the papers under the supervision of Prof. Torgeir Moan and Kaj Riska. They are both co-authors of these papers and made great help with respect to comments and corrections. As the second author of Paper 1, the fourth author of Papers 2, 5 and the fifth author of Paper 4, Dr. Biao Su was also involved in developing the initial computer program for an icebreaker in level ice and providing great help in the ice model test. As the manager of Marine Technology Multifunctional Ice Basin in Aalto university, Rüdiger von Bock und Polach is the contact person for the ice model tests and provided help on technical matters relating to the experimental setup reported in Paper 4.

Chapter 1

Introduction

1.1 Background and motivation

There is an increasing interest in oil and gas activities for the petroleum industry in Arctic waters. The illustration, Fig.1.1, presents a number of locations in Arctic and Subarctic regions where ice loads and ice operations pose major challenges for year-around operations. It will bring in new engineering challenges with respect to design of offshore structures exposed to the sea ice, as exploitation of offshore hydrocarbon resources moves to Arctic regions.

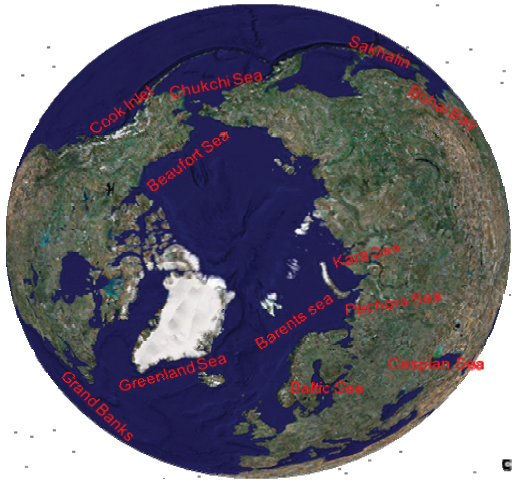

Fig.1.1 Sketch of the Northern Hemisphere showing main ice-covered waters with hydrocarbon fields

1.1.1 Offshore Structures

Depending on ice conditions, operation season and location of operation, different types of offshore structures are developed and applied to the oil and gas activities. Some possible types of offshore structures for operation in ice-covered areas are illustrated in Fig.1.2. From the stationkeeping point of view, there are three kinds of structures commonly used, comprising fixed structure, moored floating structures, and dynamic positioning based structures. The main industrial activities using the various structures will be described more in details in the following.

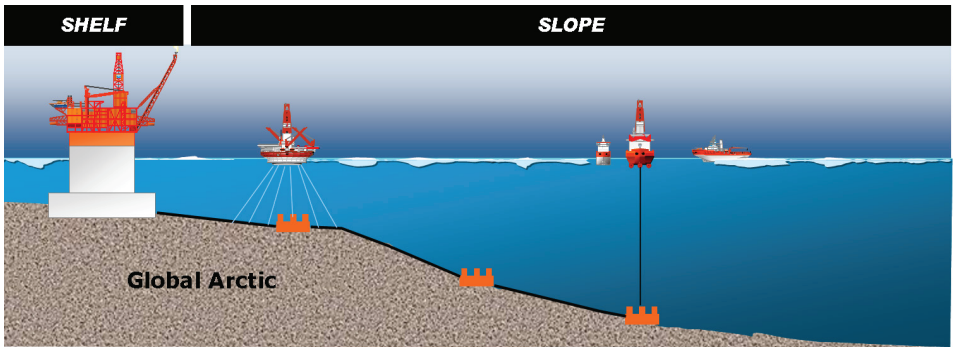

Fig.1.2 Different offshore structures employed in ice-infested areas

1) Fixed structures

Fixed structures are most attractive in shallow waters, such as on the shelf or edge of the shelf. The limitation of water depth for operations is about 100 m. The structures of this type mainly pertain to gravity base structures (GBS), artificial island, lighthouses, and jacket type platforms.

The Molikpaq platform, with sand filled inside the caisson, was used to drill in the Canadian Beaufort Sea in 1984 (Fig.1.3). The water depth was about 32 m. The moving ice actions on the platform were at significant levels (>100 MN) due to its nearly vertical sides (Jefferies & Wright, 1988). Severe vibrations were observed onboard. However, the platform endured successfully these vibrations.

Fig.1.3 The Molikpaq platform, Beaufort Sea

The development of the Beaufort Sea was initiated in quite shallow water (< 12 m) using artificial islands (Timco & Johnston, 2002). In the early 1970s, Esso Resources Canada Ltd. and Exxon Production Research measured the in-situ ice pressures around their dredged exploration drilling islands at Adgo, Netserk, Arnak, Kannerk and Issungnak (Fig.1.4). Urethane button-type sensors were used to measure the pressure, with supplementary information on ice/island movements.

Some lighthouses were constructed and deployed in the Gulf of Bothnia in the 1950's and 1960's. These lighthouses were installed at a water depth of less than 20 m. There are some accidents with these structures. Failures occurred due to the large vibration and loss of stability which resulted in the destruction of the equipments on the structures.

Fig.1.4 The Esso artificial island at Issungnak (Timco & Johnston, 2002)

Fig.1.5 Platforms in the Bohai Bay (Yue and Li, 2003)

Critical vibrations were also observed for the jacket type platforms operating in the Bohai Bay (Fig.1.5). Moving pack ice interaction with legs of the platforms caused severe vibrations, although the ice conditions were relatively mild with ice thickness in the range of 0.2-0.4 m (Yue and Li, 2003). The vibrations also caused fatigue failure problems to the structures, which needs to be taken into consideration in the design.

Based on the significant industrial experiences, it is clear that the fixed structure is a good solution in shallow waters. The benefit of this approach is that a fixed structure will experience little, if any, production downtime due to adverse environmental conditions. Special attention should be paid to the vibration of structures during ice loading processes and the resulting problems such as destruction of the equipment,

fatigue failure, or even collapse. A fixed structure may experience severe ice loads and thus a large overturning moment which leads to loss of stability. There may also exist some difficulties when moving the structure to other sites. Therefore, floating structures provide another solution in the ice covered waters.

2) Moored floating structures

Moored floating structures are relatively popular in drilling, production, and offloading of hydrocarbons. Both the ship-shaped structures and conical structures have been used. Relevant experience with moored structures in ice is obtained from drilling operations in the Beaufort Sea. Starting in the mid 1970s to the late 1980s, Dome Petroleum deployed floating drill-ships named Canmar during the summer months (Fig.1.6). These were moored on site during the summer (open water) months, where relatively light ice conditions were encountered (Wright, 1999). With support of icebreakers, these drillships developed the capability of stationkeeping in a variety of ice conditions. This extended their open water operating season, although they did not work extensively in heavy ice. Unfortunately, although Canmar gained a great deal of experience with their Beaufort Sea drillships, there is very little documentation about their operations, particularly with regard to the load levels experienced by these moored vessels in ice.

Fig.1.6 The Canmar drillship, Beaufort Sea (Timco & Johnston, 2002)

For the development of the Grand Banks oil fields, the Terra Nova scheme was implemented (Wright, 1998). It involves a floating ship-shape production vessel with integrated storage and offloading systems (FPSO), which is designed to continue operations in most environmental conditions. The FPSO could disconnect with the mooring lines and risers system and move off the site when avoiding severe ice actions. This approach is attractive for operations. The vessel has been operating year-around with light ice conditions encountered. The advantage is that capital cost is low and response to the ice conditions is quick, but the disadvantage is the potential for much downtime due to ice, and the associated production delays.

It is expected that the gas-condensate field Shtokmanovskoye, located in the central part of the Barents Sea (Fig.1.7a), will be developed in the near future. The water depth is

340 m. At this field, both occurrences of sea ice and icebergs have to be expected during operations. As shown in Fig.1.7b, the general offshore facilities development scheme that has been selected is based on the Subsea Production System (SPS) tied-back through a system of umbilical, flow line, and riser (UFR) to the ice-resistant ship-shaped Floating Production Unit (FPU) hosting gas processing, gas compression, living quarter, power generation, and all other utilities required to operate.

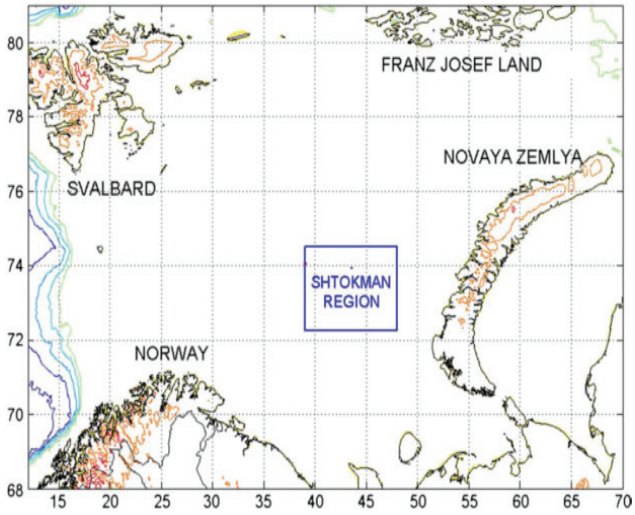

Fig.1.7a The Barents Sea and the Shtokman region (Web)

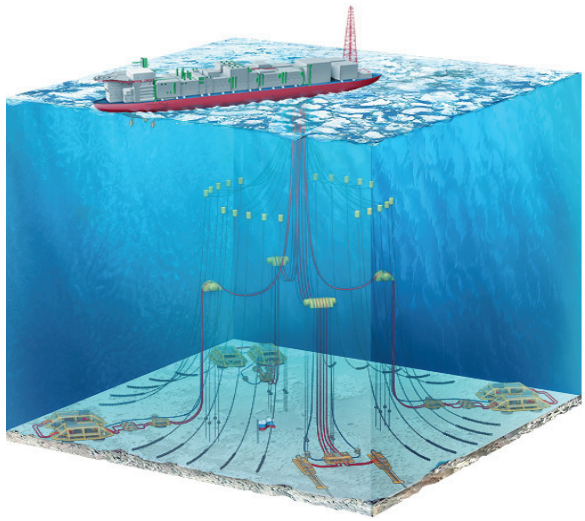

Fig.1.7b Offshore Facilities at Shtokman field (Web)

As a conical drilling unit, the Kulluk platform (Fig.1.8) was designed with a variety of special features to improve the performance under ice conditions in the shallow water (Wright, 1999). It was deployed in water depths ranging from 20m to 60m. The system

has a downward sloping circular hull near the waterline that breaks the oncoming ice mainly in flexure and an outward flare near the bottom that clears the broken ice cusps away from the moon pool and mooring lines. The strong mooring system could resist ice forces up to 450 tonnes. It worked successfully with the downtime in operations less than 10%, but at a cost of extensive ice management by three icebreakers.

Fig.1.8 The Kulluk platform, Beaufort Sea

A number of model tests have been carried out for various moored offshore structures operating in ice covered waters. Løset et al. (1998) performed a series of model-scale tests with the Submerged Turret Loading concept (STL) for loading oil offshore in the Hamburgische Schiffbau-Versuch-sanstalt GmbH (HSVA) ice tank in Hamburg. The modelled ship had a conventional icebreaking bow at a scale of 1:36. The purpose of the tests was to study the feasibility of the STL concept in level ice, broken ice, and pressure ridges. It was found that pressure ridges produced for the model tests may cause forces over the capacity of the STL system. Later, a number of model tests with another concept were conducted in the HSVA ice tank (Løset et al., 2003). The concept comprises a single anchored moored ship located in the wake behind a moored buoy floating freely on the surface. The buoy with smooth surface was expected to break the ice in upward bending, also ridges. However, the results show that it is probably not practical feasible to apply a buoy with enough buoyancy to break the design ridges since ridges may exceed the breaking capacity of the buoy unless disconnection of the ship can be done.

Bonnemaire et al. (2008) proposed a new concept for offshore offloading operations in ice. The concept named Arctic Tandem Offloading Terminal (ATOT), is composed of a turret moored offloading icebreaker and an offloading tanker in tandem. It was tested in the HSVA ice tank with focus on the measurement of mooring loads during interactions with ice ridges in head on drift.

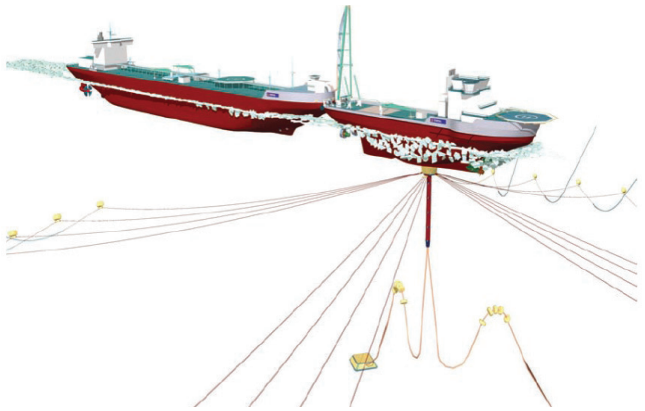

Fig.1.9 Sketch of the ATOT concept (Bonnemaire et al., 2008)

Considering the possible change in ice drift direction which may lead to a significant increase in ice load on the hull, some buoy shaped structures based on prototype of the Kulluk were tested. The structure of this sort is attractive in that the need to keep heading towards the ice drift is no longer required. The conical structure FPU-Ice (by SEVAN Marine) was tested in the spring 2008 at HSVA (Løset and Aarsnes, 2009). The purpose was to study the ice load level on the structure and its response in extreme first-year ice including the interaction with unmanaged ice ridges exceeding 20 m draft (Fig.1.10).

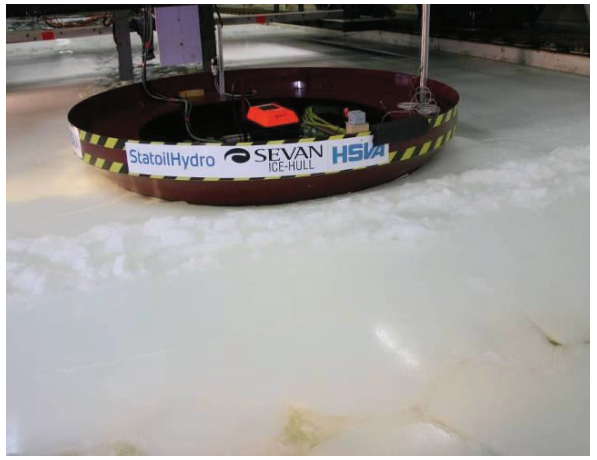

Fig.1.10 Photos from Test 3100 entering Ridge 2 (Løset & Aarsnes, 2009)

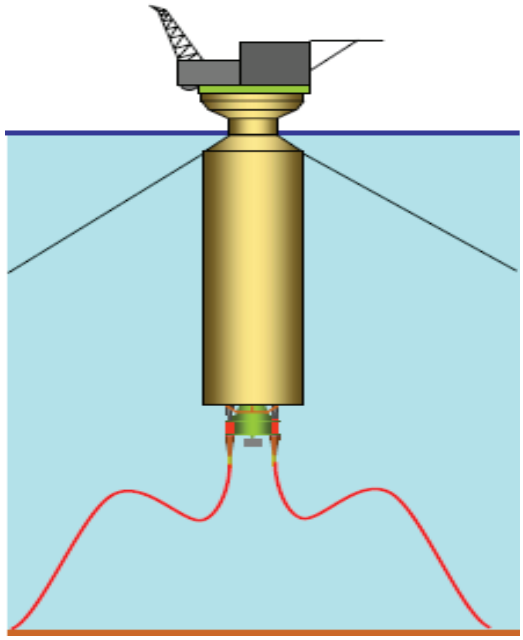

Fig.1.11 Arctic SPAR Platform (Bruun et al, 2011)

A Joint Industry Project was reported by Bruun et al. (2011) on development of conical floaters in ice. A typical SPAR platform developed during the project is shown in Fig.1.11. Two large ice model test campaigns were performed in the period 2007-2010. The objectives were to investigate different floater geometries and ice model test setups (model fixed to a carriage and pushed through the ice vs. ice pushed towards a floating model moored to the basin bottom) and their influence on the ice failure mode and structure responses in the various tested ice conditions.

1.1.2 DP vessels

Another method is to use dynamic positioning systems for stationkeeping. The solution requires marine propulsion units consisting of electrically driven azimuth thrusters. It is attractive for drilling operations in deep waters as illustrated in Fig.1.12. Up to now, the industrial applications of DP to the operations in ice are limited.

Keinonen et al. (2000) reported that stationkeeping with dynamic positioning systems was employed for drilling and diving operations in heavy ice conditions in the offshore Sakhalin. The water depth is 30 m. As the first ever such operation, the DP operation was supported by two icebreakers; Smit Sakhalin and Magadan. The operation lasted six weeks in varying ice conditions including ten tenths of ice cover and ice pressure for a level ice thickness ranging from 0.7 m to 1.5 m. The operation was carried out successfully with the total ice downtime 22%. The limitations on overall performance were believed to be caused by the limited ability of the icebreakers to manage the ice.

The related drilling operations using dynamic positioning in ice in the Arctic Ocean to recover deeply buried sediments was also reported by Moran et al. (2006). In 2004, a

convoy of three icebreakers headed north to begin the Arctic Coring Expedition, IODP Expedition 302. The site water depth ranges from 1100 meters to 1300 meters. Ice floes with thickness of 1-3 m covered 90% of the ocean surface, and ice ridges with several meters high were encountered where floes converged. The ice drifted at speeds of up to 0.15 m/s and changed direction over short time periods, sometimes within 1 hour. Three icebreakers comprising a Russian nuclear vessel, the Sovetskiy Soyuz, a Swedish diesel-electric vessel, the Oden, protected the Vidar Viking by circling on the upstream of the drifting ice, breaking the floes into smaller pieces that would not displace the drilling vessel more than 75 m from its fixed position. The operation of the fleet and ice management is shown in Fig.1.12. The fleet and ice management teams successfully ensured the smooth drilling operations to recover cores from three sites despite severe ice conditions. The manual positioning instead of automatic DP operation was applied to achieve a successful stationkeeping with nearly no downtime when good ice management with icebreakers was used.

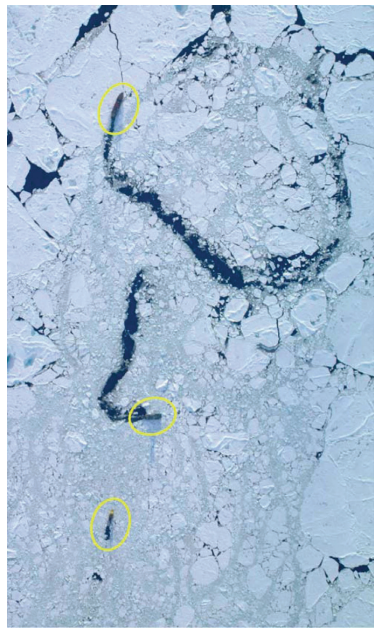

Fig.1.12 The Expedition 302 fleet during drilling operations. The Sovetskiy Soyuz (circled at the top of the image) is breaking a large floe. The Oden (middle circle) is breaking the broken floe into smaller and smaller pieces. The Vidar Viking is holding position (bottom circle) (photo taken by Per Frejvall from Moran et al., 2006).

The Aurora Borealis (as shown in Fig.1.13), a dynamically-positioned vessel for the European Polar Research Icebreaker Consortium was designed as a combination of a heavy icebreaker, a deep-sea drilling ship, and a multi-purpose research vessel (Deter & Doelling, 2009). This multipurpose research vessel is a heavy icebreaker with the highest ice class for worldwide operation. It is powered to continuously break in more than 2.5 m of multi-year ice and enables to manage ridges up to 15 m. The ship shall perform research tasks including scientific drilling year-round in the Arctic and

Antarctic without any support vessels. The capacity of performing stationkeeping operations in drifting solid ice of more than 2.0 m thickness during drilling and other research tasks is a mandatory requirement. A powerful propulsion system with a capacity up to 108 MW is installed for the various tasks including transit at 16 knots, icebreaking, and stationkeeping in ice. The ice model tests for stationkeeping in drifting solid ice of up to 2.0-meter thickness, i.e., icebreaking in a practically stationary mode, were carried out in two ice tanks in Helsinki and Hamburg. Based on the results of the Aurora Borealis icebreaker design effort, it was concluded that stationkeeping operation in solid drift ice is feasible.

Fig.1.13 The sketch of Aurora Borealis (Deter& Doelling, 2009)

Compared to the mooring solution, dynamic positioning (DP) operations in ice covered waters in general achieves success in stationkeeping, but those operations were feasible based on extensive icebreaking management with assistance of 2 to 3 icebreakers. This of course implies high cost of operations, which is undesirable.

1.2 Stationkeeping challenges in level ice

Sea ice may exist in a number of types depending on the physical processes that ice has undergone after formation. A typical first-year ice field often comprises some portion of open water, broken ice, and level ice with ice ridges scattered among the relative level ice. As a major type of ice-surface feature, the level ice is the sea ice which is unaffected by deformation and basic component in all ice interactions. For instance, consolidated layers of ice ridges, broken, or managed ice when the floes are relatively large can be modeled with level ice methodology (Zhou et al., 2012a). Thus, the investigation of stationkeeping in ice begins with level ice.

Stationkeeping for structures in both waves and ice-covered areas can be achieved by three methods: a mooring system; a dynamic positioning system; or a combination of the two. The former two methods have been used in the ice covered waters for the oil and gas related activities. The main challenges in operations could be summarized as follows.

1) Sea ice often drifts along paths with varying direction under the effects of tidal, current, waves, wind, and so on in ice covered waters. Ice loads can possibly act on an offshore structure from any direction and interact with the structure. For a ship-shaped structure, interaction geometry will vary with the relative ice drift direction, which induces different ice failure modes along the hull and changes the ice loads on the hull. In the most extreme case the drift reversal occurs.

2) Extremely high load events experienced by moored conical structures have been observed and reported in field operations when ice accumulated in front of the structures. An efficient ice clearing strategy to avoid ice accumulation surrounding the structure is difficult to develop. In general, the width of conical structure exposed to the drifting ice is often lager than the width of the ship-shaped vessels and thus cause a higher ice load and lower capacity of stationkeeping, although the ice vaning capacity of the conical structures is better. Floating conical structures may experience a significant pitch motion in ice, which could endanger the stability of the structure.

3) When ice cusp is broken from an intact ice sheet, it may be pushed underwater and cause damage to appendices, such as risers system, mooring lines, and propellers. This could be solved by increasing the draughts of appendices, or installing additional protection devices.

4) For a ship-shaped structure with self-power, transversal motion is almost impossible in that the ice load is roughly one order of magnitude higher than the bollard pull delivered by general icebreakers due to the high length of the structure exposed to the ice and nearly vertical sides of hulls. The head motion is also available in light ice conditions.

5) Many ice breakers are used in extensive ice management to reduce ice loads on the structure with stationkeeping operations. It shows from industrial experience that the effect is acceptable, but the cost of ice management may be too high to be accepted.

1.3 Thruster-assisted mooring

Thruster assisted mooring provides a promising way of stationkeeping. Considering the water limitation for DP operations and extensive ice management for mooring system, an appropriate allowance may be made for the effectiveness of thruster systems in reducing mooring loads. In addition, there is also a potential of lowering fuel consumption in shallow and intermediate open water through mooring systems (Strand et al. 1998). Kjerstad (2011) pointed out that it will be important that the ship's heading is towards the direction of ice drift. Kuehnlein (2009) discussed the main challenges for dynamic stationkeeping in ice, of which he also mentioned that the vessels need to be always oriented against the drifting ice with the bow or the aft end, as the side motions involve excessive ice load. Therefore, a heading controller must keep the vessel aligned with the drifting ice while a mooring system needs to provide a reactive force to compensate for the mean drift loads of the environment due to ice. Wilkman (2009) summarized some problems that will be challenging for DP operations in ice, such as the forces acting on the vessel, the forces caused by ice dynamics, turning yaw moment, changes in ice movement direction, new type of thrust allocation, and so on.

1.4 Objectives and scope of the thesis

The primary aim of this thesis is to introduce a numerical model for simulating ice–hull interaction in level ice during stationkeeping operations, with focus on global ice loads on moored or dynamically positioned structures, and performance of structures. Both mooring and the combination of DP and mooring are considered.

MT Uikku, an icebreaking tanker navigating in the Baltic Sea, is selected for the specific case studies, in which the global ice load effects on ship's performance, the responses of the hull, and the horizontal stability in stationkeeping mode are, respectively, analyzed. The present numerical model is established to deal with multiple subjects, including the ice–hull interaction, ice accumulation, the overall performance of icebreaking ships with mooring or dynamic positioning system, which can be used to supplement the field and laboratory measurements in establishing a design basis for stationkeeping oriented offshore structures, especially in first-year level ice conditions. The Kulluk platform, a conical structure operated in the Beaufort Sea is also chosen for validation of the numerical model.

In this thesis, dynamic ice forces and turning yaw moment exposed to the MT Uikku under 0° and 10° ice drift angle are also simulated based on the mathematical model of level ice during level ice-hull interaction in Zhou et al. (2011b) and Zhou et al. (2012b). The aim is to propose a method for simulating the behavior of a moored vessel with heading control based on kalman filter for a vessel in level-ice under different ice drift angles. The overall schematic of control strategy is shown in Fig.1.14.

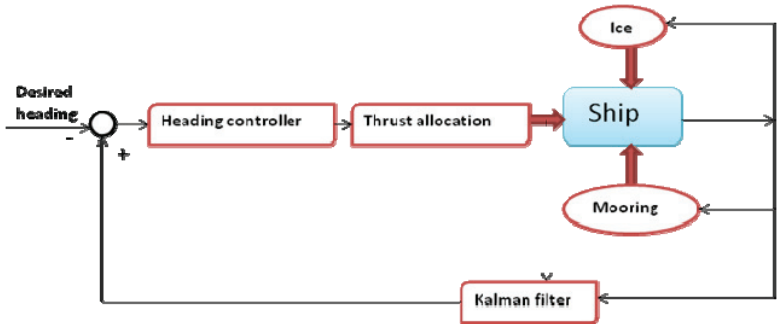

Fig.1.14 Block diagram of control strategy

The present work in this thesis is constituted by the following sub-tasks:

1) To reproduce the continuous icebreaking process of a moored structure in level ice by considering the interdependence between the ice loads and the planar motion of the structure in a numerical way;

2) To calculate the ice load exposed to the moored structures with stationkeeping operations in level ice and the resulting structure's response;

3) To propose a stationkeeping method based on mooring with a heading control system for structures operated in level ice and numerically implement it;

4) To develop a thrust allocation method specific to the heading control in level ice;

5) To analyze the main ice loading phenomena from model tests and identify the effects of some key factors on the ice load;

6) To simulate the ice force component from ice rotation and sliding and ice accumulation in front of the station-kept structure after ice floes break from intact ice sheet;

7) To validate the developed numerical model by comparison with the model test and field measurement.

This thesis is presented in the form of a collection of five papers in the Appendix C.

1.5 Thesis overview

The present thesis consists of the following chapters: **Chapter 1** describes the background, motivation, main challenges of stationkeeping, and scope of the thesis. **Chapter 2** presents the numerical model. Papers 1, 2, and 5 are associated with this chapter. **Chapter 3** addresses model tests with the icebreaking tanker MT Uikku performed in the ice Basin of Aalto University. The setup and results of model tests are presented. **Chapter 4** deals with comparison between the numerical simulation and model test data and field measurements. The ice forces exposed to the Kulluk platform are calculated with the numerical model and compared to the model test and field data. The level ice loads exposed to the MT Uikku are calculated with the numerical model and compared to the model test data. The stability and stationkeeping capability of the moored structure with heading control are estimated. Finally, the summary of conclusive remarks and several recommendations are given in **Chapter 5.**

The interconnection between the papers and the scope of the work in this thesis is shown in Fig.1.15.

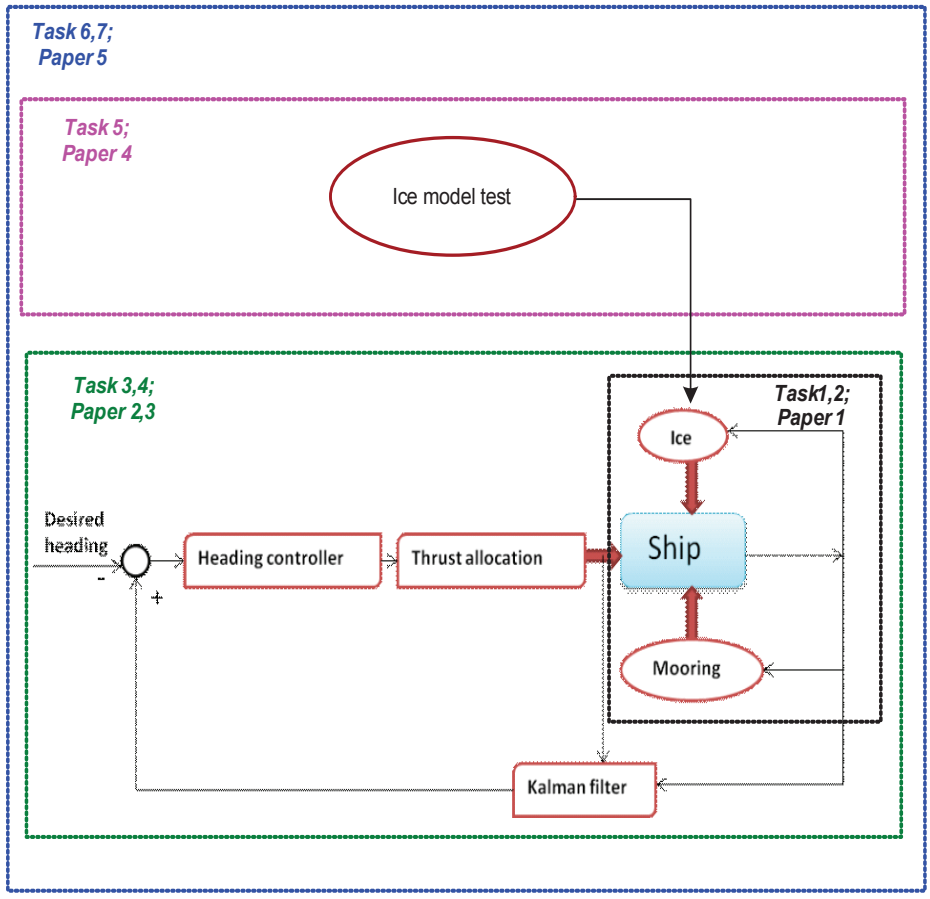

Fig.1.15 Relationships and scope of the thesis among the appended papers

Chapter 2

Numerical Model of Ice Forces and Heading Control

2.1 General

Level ice loads have been studied by many researchers. Early research on level ice resistance was usually carried out based on this break–displace process, including ice breaking, ice rotating, ice sliding, and so on. Although it may be questionable (Enkvist et al., 1979), most of the ice resistance formulas were established on this assumption (e.g. Enkvist, 1972, Lewis, 1982, and Lindqvist, 1989). Recent research on the numerical modeling of ice–hull interaction and ship maneuvering in level ice can be found for example in Valanto (2001), Liu et al. (2006), Martio (2007), Nguyen et al. (2009), Sawamura et al. (2010) and Lubbad & Løset (2011). For the simulation of full-scale icebreaking runs, a more integrated model was developed and improved by Su et al. (2010). This model is partly based on the empirical data, and the simulation program has been established to reproduce the observed icebreaking patterns and the continuous ice loading processes in a uniform level ice and the ice with randomly varying thickness and strength properties.

The ice forces encountered by a ship transiting in a level sheet of ice depend primarily on the processes, by which its hull breaks and displaces the ice. First, when the ice sheet contacts the hull, crushing happens. The crushing force will keep growing with an increasing contact area until its vertical component is large enough to cause a bending failure of ice. After the ice floes have been broken from the ice sheet, the advance of ship will force them to turn on edge until parallel with the hull. Then, the floes will become submerged and slide along the hull until they can not maintain contact with the hull.

The action of drifting level ice on a moored object is also complex, and several ice failure patterns occur, primarily crushing and bending. The resulting broken ice pieces from the intact ice may rotate, collide, accumulate, slide along the surface of the structure, and be pushed away from the structure. Nonlinear interactions among the water, structure, and ice floes such as ventilation and slamming can arise during this process, especially when the relative speed between the ice and the structure is high. Therefore some assumptions have to be made to simplify the problem. The main methodology and assumptions used in the present simulation for ice–hull interaction are summarized as follows:

1) Wave, wind, and current forces in ice covered waters are neglected as they are minor forces compared to the ice forces;

2) Only level ice with uniform ice properties is considered since it is a basic ice feature in ice covered areas;

3) The waterline of the ship and the edge of the ice are both discretized;

4) The motions of the ship on the horizontal plane are taken into account and the icebreaking forces are assumed to act at the waterline;

5) Ice interaction with a moored vessel is assumed to be a continuous icebreaking process;

6) It is assumed that the ice drift speed is low and thus ventilation and slamming are neglected;

7) The contact zones around the hull and the resulting ice forces and icebreaking patterns are numerically determined based on the empirical estimates of the geometry of the vessel and ice sheet;

8) Only the local crushing between the structure and the ice and the bending failure that occurs at a distance from the crushing region are included, although in some hull zones, typically at the very bow and at the shoulders which have large slope angles (almost vertical), crushing may be the only failure mode (Lindqvist, 1989), which can lead to a considerable ice resistance;

9) Sliding and rotating forces induced after the ice cusps are broken from the ice edge are taken into account based on a method by Croasdale (1980);

10) If ice accumulation occurs, the resulting force components are calculated based on the Croasdale model (Croasdale et al., 1994);

11) The hydrodynamic effects on the ship's motion (drag and added mass) are derived from a numerical calculation before the simulation in ice;

12) The rigid-body equations of motion are solved by numerical integration with iterations performed at each time step to find a balance between the indentation into the ice and the contact forces;

13) The mooring system is mainly used to keep the position of the structures and the heading controller is used to maintain the heading of the structures during stationkeeping operation in the simulation.

2.2 Overview of the numerical method

In the present simulation, there are two reference frames used, see Fig. 2.1.

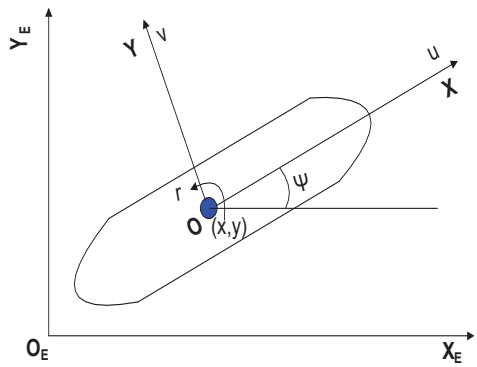

Fig.2.1 Earth-fixed ($X_EY_EZ_E$) and body-fixed (XYZ) reference frames in the horizontal plane

- The Earth-fixed frame, denoted as $X_EY_EZ_E$, is placed so that the X_EY_E plane coincides with the water surface, and the Z_E axis is positive downwards.

- The body-fixed frame, denoted as XYZ, is fixed to the vessel in such a way that the origin coincides with the centre of gravity, the X-axis is directed from aft to fore along the longitudinal axis of the hull, and the Y-axis is directed to the starboard.

The horizontal position and orientation of the vessel in the Earth-fixed coordinate system are defined by $\boldsymbol{\eta} = [x, y, \psi]$, where the first two variables describe the position and the last variable describes the heading angle. Correspondingly, the translational and rotational body-fixed velocities are defined by $\mathbf{v} = [u, v, r]$. The body-fixed general velocities are transformed to the Earth-fixed frame by

$$\dot{\boldsymbol{\eta}} = \mathbf{J}(\boldsymbol{\eta})\mathbf{v} \tag{2.1}$$

$$\mathbf{J}(\boldsymbol{\eta}) = \begin{bmatrix} c\psi & -s\psi & 0 \\ s\psi & c\psi & 0 \\ 0 & 0 & 1 \end{bmatrix} \tag{2.2}$$

where *c*, *s* are compact notations for cosine and sine, respectively.

The equation of motion is first expressed in the Earth-fixed coordinate system and then converted to the body-fixed coordinate system. Based on Newton's second law, the linear coupled differential equations of motion in the body-fixed coordinate can be written in the following form:

$$(\mathbf{M} + \mathbf{A})\ddot{\mathbf{r}}(t) + \mathbf{B}\dot{\mathbf{r}}(t) + \mathbf{C}\mathbf{r}(t) = \mathbf{F}_e(t) \tag{2.3}$$

$$\mathbf{F}_e(t) = \begin{bmatrix} R_{b1} \\ R_{b2} \\ R_{b6} \end{bmatrix} + \begin{bmatrix} R_{s1} \\ R_{s2} \\ R_{s6} \end{bmatrix} + \begin{bmatrix} R_{r1} \\ R_{r2} \\ R_{r6} \end{bmatrix} + \begin{bmatrix} F_{m1} \\ F_{m2} \\ F_{m6} \end{bmatrix} + \begin{bmatrix} F_{ow1} \\ F_{ow2} \\ F_{ow6} \end{bmatrix} + \begin{bmatrix} 0 \\ 0 \\ M_\psi \end{bmatrix} + \begin{bmatrix} mvr \\ -mur \\ 0 \end{bmatrix} \tag{2.4}$$

where $\dot{\mathbf{r}} = [u, v, r]$, the added mass matrix $\boldsymbol{A}$ in open water is calculated from a boundary element method routine, the damping term $\boldsymbol{B}$ is assumed to be zero in the stationkeeping mode, the hydrostatic restoring coefficient $\boldsymbol{C}$ is zero. The subscripts *1*, *2* and *6* refer to the directions of surge, sway, and yaw. The notation R_b is the ice-breaking force, which will be described in Section 3.1.The notation R_s is the ice submersion force,while the notation R_r denotes the ice force due to ice rubble accumulation. F_m is the restoring force due to the mooring system translated from the earth-fixed coordinate system to body-fixed coordinate system by the rotation matrix. The notation F_{ow} is the drag force due to the motion of the ship relative to the water. The notation M_Ψ represents the moment produced by the heading controller, which is zero if not used in the simulation. The last term in Eq. (4) is due to the translation from the earth-fixed coordinate system into the body-fixed coordinate system.

Newmark's method is used to solve the resulting equations of motion.

2.2.1 Ice force model

The ice loads acting on a moored ship in unbroken ice or large level ice floes depends significantly on the interaction process by which the hull breaks and displaces the ice. Once the ice contacts the hull, ice is being crushed. The crushing force then increases with increasing contact area until its vertical force component gets large enough to cause bending failure of the ice, after which the broken ice floes start to turn along the ship's hull until they are parallel to the hull. Finally, the floes submerge and slide along the hull as they are pushed by the next broken ice floes. With this concept in mind, an ice force model composed of an ice-breaking model and an ice rotating and sliding model is briefly described.

The numerical method to evaluate the ice loads that was introduced by Su et al. (2010), is extended to simulate the performance of a moored ship in the horizontal plane under more complex conditions. The basic geometric model for ice–hull interaction includes the full-size waterline of the ship and the edge of the ice. As shown in Fig.2.2, the waterline of the ship is discretized into a closed polygon and the edge of the ice is discretized into a poly line in the established simulation program. At each time step, the simulation program is set to detect the ice nodes which are inside the hull polygon. Then, each contact zone can be found. To check whether the ice node is inside the hull polygon, geometric tools from computer graphics are adopted. The detailed algorithm can be found in Schneider et al. (2002). At each contact zone shown in Fig.2.2, it is assumed that the contact surface between ice and hull is flat, and the contact area is simply determined by contact length and indentation depth. The contact length is calculated from the distance between adjacent hull nodes, and the indentation depth is calculated from the perpendicular distance from the cusp of ice nodes to the contact surface. More details are referred to Su et al. (2010).

a) Ice breaking force

The scenario of a ship advancing in level ice resembles that of a moored structure in drifting level ice with respect to the ice-breaking process. Thus, it is reasonable to apply the ice-breaking model described in Su et al. (2010) in the present model.

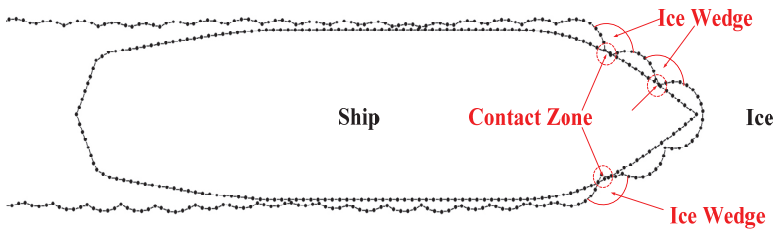

Fig.2.2 Discretization of the ship hull and the edge of the ice

The ice wedges formed in the ice breaking process were determined by bending cracks, which were idealized and described by a very important parameter, namely the icebreaking radius. The icebreaking radius R was derived from the expression given in Wang (2001) (based on information from Enkvist (1972) and Varsta (1983)):

$$R = C_l l \left(1.0 + C_v v^{rel}{}_n\right) \tag{2.5}$$

where $v^{rel}{}_n$ is the relative normal velocity between the ice and the hull node, C_l and C_v are two empirical parameters, C_l having a positive value and C_v is a negative value, l is the characteristic length of the ice:

$$l = \left(\frac{E h_i^3}{12(1-\nu^2)\rho_w g} \right)^{1/4} \tag{2.6}$$

Fig.2.3 shows that the ice wedge is determined by the interpolation of the icebreaking radius at the first and last contact nodes (i.e., R_f and R_l). The opening angle of the ice wedge is denoted as θ. In order to calculate the contact area A_c, the contact zone was discretized by a number of triangles (the triangles shown in Fig.2.3) based on the hull nodes that were in contact with ice sheet. Then A_c can be approximated by the sum of area of the triangles.

As mentioned above, in the first phase of contact only crushing takes place on the contact surface. The resultant crushing force F_{cr} is normal to the contact surface and is calculated as the product of the effective crushing strength σ_c and the contact area A_c, where the ice pressure on the contact surface is assumed to be uniform and equal to the effective crushing strength.

The frictional force is also taken into account in this model by using a coefficient of friction. When the vertical component of the crushing and frictional forces F_V exceeds the bending failure load P_f given in Eq. (2.7), the ice wedge will be formed by a bending crack and break off from the edge of the ice:

$$P_f = C_f \left(\frac{\theta}{\pi}\right)^2 \sigma_f h_i^2 \tag{2.7}$$

where θ is the opening angle of the idealized ice wedge shown in Fig.2.3, σ_f is the flexural strength of the ice, h_i is the thickness of the ice, and C_f is an empirical parameter.

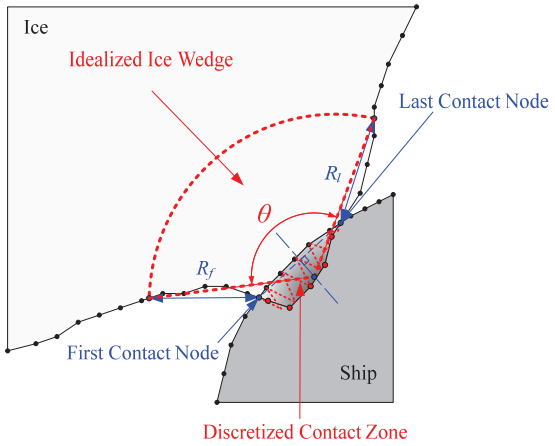

Fig.2.3 Idealized ice wedge and discretized contact zone

b) Ice submersion and friction force

Two models of calculating ice forces induced after the ice wedges are broken from the ice sheet are described in the thesis. The first model is based on the Lindqvist's ice resistance formula (Lindqvist, 1989). The second is based on the Croasdale 2D model (Croasdale, 1980).

Model I

An icebreaker is often moving forward against the ice, whereas a moored structure is often pushed by drifting level ice to move both forward and backward. When a moored vessel moves head on against the ice, the situation is similar to that of an advancing icebreaker; but if it moves sideways in the same direction of the drifting ice, the situation is different. In Paper 1, necessary modifications are introduced to satisfy the situation considered herein. It was assumed that if the structure moves forward, the bottom will be partially covered by ice and the bow area will be completely covered; if not, the bottom is assumed to be partially covered by ice and the stern area is assumed to be completely covered. Based on the ice resistance formula of Lindqvist (1989), the modified ice submersion resistance of a moored tanker due to loss of the potential energy of submerged ice floes and friction between the hull and ice floes is written as

$$R_s = \delta\rho g h_i \, s\,ign(v)(BT(B+T)/(B+2T) + \mu(A_f + pA_b)) \tag{2.8}$$

where $\delta\rho$ is the density difference between the water and ice, g is the acceleration of gravity, h_i is the ice thickness, B and T are the main dimensions of the hull, μ is the

friction coefficient between ice and hull, A_f and A_b are the areas of the bow or stern and of the flat bottom, respectively, and p is the ratio of the length of the ice covered area to the length of the ship's bottom. *sign(v)* depends on the velocity v of the ship in surge, defined as

$$sign(v) = \begin{cases} 1, & if\ v \geq 0 \\ -1, & else \end{cases} \tag{2.9}$$

In addition, the speed dependence of the submersion resistance is taken into consideration simply as follows (Lindqvist, 1989):

$$R_s(v_{rel}) = R_s(1 + 9.4 v_{rel} / \sqrt{gL}) \tag{2.10}$$

where v_{rel} is the relative velocity between the ship and the drifting level ice sheet, L is the length of the ship.

Model Π

When a structure is hitting an ice sheet, the structure will experience a time-varying ice force. The average of the ice force in the time domain is often defined as ice resistance. Lindqvist (1989) developed an empirical model to calculate the ice resistance on an icebreaker in straight line transit, where the ice-hull interaction process was divided into several phases pertaining to crushing at the stem, breaking by bending, rotating, and sliding with speed dependence. It is of great help in the early stage of designing an icebreaker. Valanto (2001) and Su et al. (2010) used the ice rotating and sliding model by Lindqvist and modified the breaking and crushing model in simulating the ice-hull interaction process. In this thesis, the method by Croasdale (1980) is used. The interaction between an ice sheet of thickness h_i and a structure sloping at angle α from the horizontal plane is shown in Fig. 2.4.

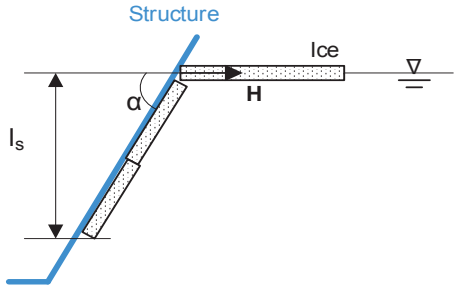

Fig. 2.4 Geometry for two-dimensional analysis of forces on a sloping structure

It is assumed that the broken ice floe from the intact ice sheet is continuously cleared around the structure by some other mechanism and does not contribute to ice pile up in front of the structure. Then the horizontal ice force during the ice rotation and sliding process on the sloped hull element per unit width H is written as

$$H = l_s \delta \rho h_i g(\sin\alpha + \mu\cos\alpha)\left(\frac{\sin\alpha + \mu\cos\alpha}{\cos\alpha - \mu\sin\alpha} + \frac{\cos\alpha}{\sin\alpha}\right) \tag{2.11}$$

where l_s is the vertical distance that ice is pushed down the slope, $\delta\rho$ is the density difference between water and ice, h_i is the ice thickness, g is the acceleration of gravity, and μ is the friction coefficient between the ice and the structure.

c) Ice accumulation force

According to some national and international classes such as ISO (2009) and API (1995), rubble accumulation is a main contribution to the total ice loads and must be included in the numerical simulation. There are some recommendations on the analytical models which can be used to model the interaction between a fixed structure with vertical and upward slope and incoming ice. For bending of level ice on an upward sloped structure with accumulation of rubble on the slope, ISO (2009) recommends using Croasdale model (Croasdale et al., 1994). Hidding et al. (2011), Bonnemaire et al. (2011) and Jensen et al. (2011) used this model to evaluate the response of a moored structure with inclined sides at the waterline in ice. By comparing the simulated responses of different types of structures to the measured responses with different ice conditions in basin tests, it was concluded that the Croasdale model (Croasdale et al., 1994) was the appropriate model for calculating ice loads and replicating the levels and characteristics of the response in all degrees of freedom.

For the Croasdale model, it is assumed the formation of ice rubble accumulation does not affect the ice breaking process so that the ice components from ice breaking and ice accumulation could be added. This assumption is reasonable for upward sloped structures. In model tests by Zhou et al. (2013), it was observed that the ice sheet contacted with the side of hull continuously and the bending failure of the ice sheet was not affected by the rubble formation beneath the intact ice sheet. It is also assumed that the porosity of ice rubble is constant without the compaction of rubble under compression or pore pressure in the rubble. It is based on the physical process. For upwards structures with wide necks and poor ice clearing capacity, Croasdale et al. (1994) described the process of ice rubble build-up as shown in Fig.2.5: (1) the ice fails in bending mode and starts riding up, (2) the ride-up continues up to the vertical shaft before the ice block falls down on the intact ice sheet, (3) a rubble pile forms in front of the structures, (4) the intact ice sheet continues to be pushed through the rubble to fail against the sloping structure. The sequence was then repeated. For a wide structure, the rubble does not clear away from the structure efficiently. Therefore, if a rubble field exists in front of the structure, additional forces affect the following load components: the load from breaking the intact ice sheet; the load component required to push the sheet ice through the ice rubble; the load to push the ice blocks up the slope through the ice rubble; the load required to lift the ice rubble on top of the advancing ice sheet prior to breaking it; the load to turn the ice block at the top of the slope.

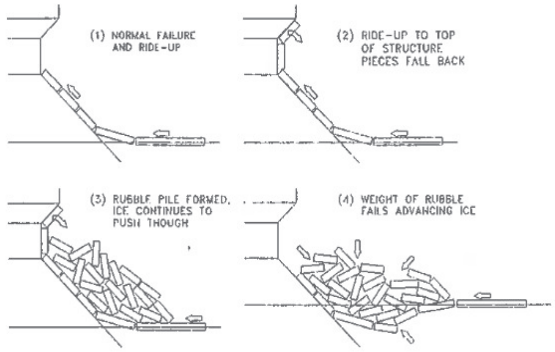

Fig.2.5 Sequence of ice rubble buildup (Croasdale, 1994)

During the ice rubble formation, the load components required to push the sheet ice through the ice rubble and to push the ice blocks up the slope through the ice rubble are assumed to be the main load contribution to the ice accumulation forces. The other load components are neglected in the simulation. The formulations of interest in ISO (2009) are given as

$$H = H_P + H_R + H_L, \tag{2.12}$$

$$H_P = A_1 \gamma \mu_i \tag{2.13}$$

$$H_R = \frac{(H_P \sin\alpha + A_2 \gamma \cos\alpha)(\mu_i + \mu)}{\cos\alpha - \mu \sin\alpha} + \xi l_R \delta \rho g h_i \tag{2.14}$$

$$H_L = \tfrac{1}{2} l_s^{\,2} \gamma \tan\varphi + l_s c \tag{2.15}$$

$$\gamma = \delta \rho g (1 - \eta) \tag{2.16}$$

$$\xi = (\sin\alpha + \mu \cos\alpha) / (\cos\alpha - \mu \sin\alpha) \tag{2.17}$$

where the force H_P represents the force needed to push the ice sheet horizontally through the rubble, the force H_R represents the force needed to push the ice blocks down the slope through the rubble, the force H_L represents the load required to lift the ice rubble on top of the advancing ice sheet prior to breaking it, φ is the angle of internal friction, c is the cohesion, η is the porosity of ice rubble,and μ_i is the friction coefficient between ice blocks. The other notations such as the areas A_1 and A_2 of the ice rubble, the length of ice rubble on the slop l_R, and the slope angle α are defined in Fig.2.6.

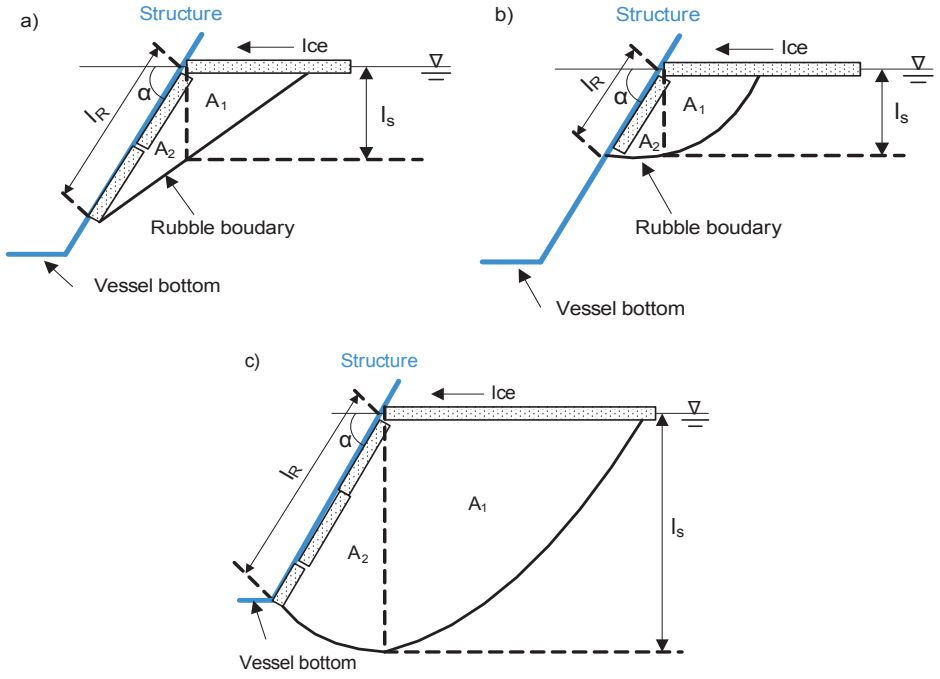

Fig.2.6 Bending of level ice – interaction geometries a) "Croasdale" model, b) Observed at initial stage c) Observed at steady state stage

As shown in Fig.2.6 a), the Croasdale model is based on an idealized geometry of the interaction which may not always model the actual interaction, but the Eqs (2.12-17) allow the modelling of a wider range of interaction geometries. The areas A_1, A_2 of the subsurface rubble and the rubble length on the slope l_R change as a function of time as the structure interacts with the ice sheet. Based on observations from underwater videos, the interaction geometries used in the simulation are presented as follows:

At the beginning of the interaction, the ice cusps broken against the structure will slide down along the structure sides, move eventually to the subsurface and accumulate beneath the surrounding ice sheet. The rubble piles will be pushed by the structure continuously and the ice rubble is rolling like a disc with increasing radius in cross sectional view from the underwater videos. The process is similar to pushing a snowball. Therefore, the total area of subsurface rubble (A_1+A_2) in the preliminary stage is simulated as a pie with the centre of a circle located at the intersection of waterline and the side of structure and the radius of the pie equal to l_R. The interaction geometry is shown in Fig 2.6 b). As the total area of rubble increases, the length l_R also increases until it reaches the maximum length of the slope. After that, the area A_2 and the length l_R are kept constant while the area A_1 still increases as time elapses, as shown in Fig 2.6c).

The ice load due to the sub-surface rubble depends significantly on the accumulation volume, the hull inclinations at the waterline, and the relative velocity between the ice and the hull. The 2D hull is discretized into a number of nodes at the waterline and the

ice loads on each hull element are calculated at each time step. Then the total ice loads acting on the hull are estimated as the sum of all local ice actions around the vessel hull in time domain. Thus, to properly simulate the local amount of rubble accumulation around the hull of varying profile is important.

2.2.2 Mooring system

Since changing heading is crucial for a vessel subjected to drifting ice in different directions, a turret mooring system is necessary. In addition, it must facilitate the operation of disconnecting and leaving the site quickly and reliably. The mooring system provides not only time-varying restoring forces but also damping forces, both of which should be taken into consideration in the vessel response analysis in the horizontal plane. A horizontal-plane turret mooring system model can be formulated as

$$\boldsymbol{\tau}_{mo} = -\mathbf{R}^{-1}(\psi)\mathbf{g}_{mo}(\boldsymbol{\eta}) - \mathbf{D}_{mo}(\mathbf{V}) \tag{2.18}$$

where $\mathbf{g}_{mo}(\boldsymbol{\eta})$ and $\mathbf{D}_{mo}(\mathbf{V})$ are the Earth- fixed restoring term and the additional damping, respectively. The nonlinear mooring line characteristics $\mathbf{g}_{mo}(\boldsymbol{\eta})$ can be found by dedicated software programs for slender marine structures, e.g. RIFLEX (2003) and others. The mooring damping term $\mathbf{D}_{mo}(\mathbf{V})$ could be obtained based on DNV (2004).

2.2.3 Heading control

As mentioned above, heading control plays a key role in keeping the bow of the vessel pointing into drifting ice. To design the heading control system based on a Kalman filter, some aspects need to be considered, including a control plant model, Kalman filter, reference generation, and thrust allocation.

a) Control plant model

The observer and controller are designed through a control plant model of the moored vessel. A process plant model for the vessel dynamics (Sørensen, 2005) in the horizontal plane can be expressed as

$$(\mathbf{M}_{RB} + \mathbf{M}_{A})\dot{\mathbf{V}} + \mathbf{C}_{RB}(\mathbf{V})\mathbf{V} + \mathbf{D}(\mathbf{V}_r) = \boldsymbol{\tau}_{ice} + \boldsymbol{\tau}_{mo} + \boldsymbol{\tau}_{th} \tag{2.19}$$

where $\mathbf{M}_{\mathrm{RB}}$ is the system inertia matrix and $\mathbf{M}_{\mathrm{A}}$ is the added mass; $\boldsymbol{\tau}_{\mathrm{ice}}$ is the level ice load vector in the body-fixed frame; $\boldsymbol{\tau}_{\mathrm{mo}}$ is the mooring force translated from the earth-fixed to body-fixed coordinate system by the rotation matrix; $\boldsymbol{\tau}_{\mathrm{th}}$ is the thruster vector consisting of forces and moments produced by the propulsion system; $\mathbf{C}_{RB}(\mathbf{V})$ is the skew-symmetric Coriolis-centripetal matrix.

It should be noted that only the yaw moment is considered. It is assumed that the nonlinear damping $C_{RB}(v)v$ in eq. (2.19) in yaw is small since the vessel's velocity is small in stationkeeping. The control plant model only considers 3-DOF. The resulting LF model of the yaw dynamics can be simplified as follows

$$\dot{\psi} = r \tag{2.20}$$

$$\dot{b}_{ice} = -T_{ice}^{-1} b_{ice} + E_i w_2 \tag{2.21}$$

$$m_{66}\dot{r} = \tau_{th} + b_{ice} + w_1 \tag{2.22}$$

$$y_m = r + v_y \tag{2.23}$$

where b_{ice} is the bias considering both slowly varying disturbances and unmodelled dynamics from ice disturbance; T_{ice} is a time constants for estimating the slowly varying yaw moment by the ice; E_i is the ice gain; m_{66} is the moment of inertia in yaw; w_1 and w_2 are the zero-mean white noises; y_m is the measured output; v_y is the measurement noise.

b) Kalman filter design

Based on the control plant model, the state-space model of a Kalman filter for heading control design can be expressed by Eqs. (2.20)-(2.23) as

$$\dot{x} = \mathbf{A}x + \mathbf{B}u + \mathbf{E}w \tag{2.24}$$

$$y_m = \mathbf{H}x + v_y \tag{2.25}$$

where $x = [\psi, r, b_{ice}]^{\mathrm{T}}$ is the state vector; $u = N_v$ is the control command to be defined; $w = [w_1, w_2]^{\mathrm{T}}$ represents the process noise vector, and

$$\mathbf{A} = \begin{bmatrix} 0 & 1 & 0 \\ 0 & 0 & m_{66}^{-1} \\ 0 & 0 & -T_{ice}^{-1} \end{bmatrix}, \mathbf{B} = \begin{bmatrix} 0 \\ m_{66}^{-1} \\ 0 \end{bmatrix} \tag{2.26}$$

$$\mathbf{E} = \begin{bmatrix} 0 & 0 \\ m_{66}^{-1} & 0 \\ 0 & E_i \end{bmatrix}, \mathbf{H} = \begin{bmatrix} 1 & 0 & 0 \end{bmatrix}. \tag{2.27}$$

The model given in Eq. (2.24) forms the basis of a Kalman filter design. In order to implement the filter on a computer, the model is discretized as

$$x(k+1) = \mathbf{\Phi}x(k) + \mathbf{\Delta}u(k) + \mathbf{\Gamma}w(k) \tag{2.28}$$

$$y_m(k) = \mathbf{H}x(k) + v_y(k) \tag{2.29}$$

$$\mathbf{\Phi} = \exp(\mathbf{A}h) \tag{2.30}$$

$$\mathbf{\Delta} = \mathbf{A}^{-1}(\mathbf{\Phi} - \mathbf{I})\mathbf{B} \tag{2.31}$$

$$\mathbf{\Gamma} = \mathbf{A}^{-1}(\mathbf{\Phi} - \mathbf{I})\mathbf{E} \tag{2.32}$$

where h is the sampling time, and the equivalent discrete-time noises $w(k)$ and v_y(k) are Gaussian and white noises with zero mean. For large offshore vessels and rigs, the sampling time is normally in the range of 100–500 ms (Fossen, 2009). The sampling time used in the following simulation is 100ms.

c) Reference Generation

A reference model based on a low-pass filter structure is used:

$$\frac{\psi_d(s)}{\psi_s(s)} = \frac{1}{T_m s + 1} \tag{2.33}$$

where s is the Laplace variable, ψ_s denotes the heading command, and ψ_d is the generated desired heading, and T_m is the time-constant. It should be noted that in order to obtain good tracking performance and stability, the bandwidth of the reference model must be lower than the vessel control system.

d) Heading control design

The heading control law for a moored vessel is proposed to be an output PID which is given as

$$N_\psi = -k_p \hat{\psi}_e - k_d \hat{r}_e - k_i \int_0^t \hat{\psi}_e dt \tag{2.34}$$

where $\hat{\psi}_e = \hat{\psi} - \psi_d$, $\hat{r}_e = \hat{r} - r_d$, $\hat{\psi}$ and $\hat{r}$ are the estimated heading and yaw rate by the Kalman filter, ψ_d and r_d are the desired heading and yaw rate from the reference model, and k_p, k_i, k_d are the PID controller gains. Integrator anti-windup should be implemented in order to avoid that the integrator integrates beyond the saturation limits of the actuators.

e) Thrust Allocation

Generally, dynamically positioned vessels use thrusters and main propellers to produce thrust, which can counteract environmental forces acting on the vessel in order to maintain its position and heading as closely as required to some desired position in the horizontal plane (Fossen, 2010). The function of the thruster allocation logic here is to derive the thrust and direction for each of the thrusters in order to satisfy the generalized force and moment demand from the control system subject to the minimization of energy demand (Fossen & Johansen, 2006).

A general relation between the control demand and the individual actuator demand thrusts is as follows

$$\tau_c = T_a T_{th} \tag{2.35}$$

where τ_c is the vector of thrust and moment command from the controller ; T_{th} is a vector of thruster demands in Cartesian coordinates, and T_a is the thruster arrangement matrix, defined as :

$$T_{th} = \begin{bmatrix} T_{1x} & T_{1y} & \cdots & T_{rx} & T_{ry} \end{bmatrix}^T \tag{2.36}$$

$$T_a = \begin{bmatrix} t_1 & \cdots & t_r \end{bmatrix} \tag{2.37}$$

where r is the number of thrusters. In 3 DOF (surge, sway, and yaw), the column vectors take the following form:

$$t_i = \begin{cases} \begin{bmatrix} 0 & 0 \\ 0 & 1 \\ 0 & l_{ix} \end{bmatrix} & \textit{tunnel thruster} \\ \begin{bmatrix} 1 & 0 \\ 0 & 0 \\ l_{iy} & 0 \end{bmatrix} & \textit{main propeller} \\ \begin{bmatrix} 1 & 0 \\ 0 & 1 \\ l_{iy} & l_{ix} \end{bmatrix} & \textit{azimuth thruster} \end{cases} \tag{2.38}$$

In general, Eq. (2.37) represents an underdetermined set of equations since the number of columns of the thruster arrangement matrix T_a is more than 3. There will be more variables describing the thruster settings than equations to solve (required forces and moment is solved in such a way to minimize the allocated power. One particular solution to the over-determined set of equations is the least-norm or minimum norm solution. The minimum norm solution of T_{th} could be achieved by finding the Moore-Penrose generalized inverse of T_a (Fossen, 2010). Then the solution can be expressed as:

$$T_{th} = T_a^{\dagger} \tau_c \tag{2.39}$$

$$T_a^{\dagger} = W^{-1} T_a^T (T_a W^{-1} T_a^T)^{-1} \tag{2.40}$$

$$W = \begin{bmatrix} w_{1x} & & & & 0 \\ & w_{1y} & & & \\ & & \ddots & & \\ & & & w_{rx} & \\ 0 & & & & w_{ry} \end{bmatrix} \tag{2.41}$$

where W is a weight matrix , in which the element w_{ix} is the cost to use the i_{th} thruster in the surge axis, and w_{iy} is the cost to use them in the sway axis. The higher the cost, the less thrust will be assigned to the thruster.

Then the solved thrust vector T_{th} can be converted to an azimuth angle command and thrust demand pair for each thruster unit:

$$T_{th} = \begin{bmatrix} \alpha_1 & T_1 & \dots & \alpha_r & T_r \end{bmatrix}^T \tag{2.42}$$

$$\alpha_i = \arctan \frac{T_{iy}}{T_{ix}} \tag{2.43}$$

$$T_i = \sqrt{T_{ix}^2 + T_{iy}^2} \tag{2.44}$$

If the solution for the thrust exceeds the thrust limit for any actuator, the solution of Eq.(2.40) using the pseudo-inverse technique in a least-squares sense will no longer hold and, hence, the desired thrust and moment demand will not be achieved.

The most important mode of control is to maintain the vessel's heading in the sense that the bow should be pointing into the prevailing weather in order to mitigate the ice forces acting on the vessel. If the vessel fails to maintain station with the bow oriented to minimize the loads, then it would certainly be unable to maintain the station for other more unfavorable heading angles. Therefore, thrust allocation with the heading priority scheme is of concern. The main procedure for the thrust allocation is therefore given as follows:

A. The first step should be to allocate thrusts as above, and examine the magnitudes of each demanded thrust. If any thruster is saturated, the demand vector for a heading priority control strategy should be modified, in which both the surge and sway demands are taken as zero and only the moment is allocated.

B. The magnitudes of each demand thrust should be rechecked for thruster saturation.

B1. If there is no saturated thruster after allocating the moment, which means that there is some reserve thrust capacity left in each thruster, but not enough to allocate the entire demand. It should be noticed that the azimuth angles and thrust levels are now optimum for meeting the prioritized yaw demand. With the azimuth angles fixed, the next step is to allocate the thrust required to satisfy the surge or sway. In addition, a ratio could be chosen between surge and sway, which reflects the relative importance between them.

B2. If all thrusters are saturated, there is no recourse except to give full thrusts.

B3. If there are still some thrusters saturated, a new method is necessary to meet the moment command to the best of the actuators' ability. If there are more than two thrusters unsaturated, then the thrust should be set to the maximum and the azimuth angle should be fixed for each saturated thruster. Then neglecting the saturated thrusters, the next step will allocate the remaining command for the unsaturated thrusters. The magnitudes of each demand thrust will be examined again. If no thruster is saturated, the allocation will terminate. Otherwise, the process is iterated until only one thruster is left unsaturated. The moment in the command vector is also taken as the most important element for allocation to the last unsaturated thruster. Surge or sway comes second, depending on the relative importance in the specific control task.

However, another problem is that the Moore-Penrose generalized inverse may not exist for certain azimuth angles due to singularity. The consequence is that no force is

produced in certain directions. Johansen et al. (2004) suggested a cost criterion with respect to the control forces, the azimuth angles, and the error between the commanded and achieved generalized force, which should be minimized. It is a non-convex nonlinear optimization problem. Two methods are attractive to solve the problem. Johansen et al. (2004) used a sequential quadratic programming approach to approximate the nonlinear program at each sample. If the singularities and azimuth rate limitations are not weighted in the cost function, a linear programming to the thrust allocation can be used (Webster&Sousa,1999; Lindfors, 1993).

Chapter 3

Ice Model Test

3.1 General

Many researchers have done simulation of ice-structure interaction. Wang (2001) developed a strategy to simulate the interaction between a moving level ice and a fixed conical structure. Nguyen et al. (2008) applied this ice failure model to simulate the behavior of a dynamic positioning vessel in level ice. Later, based on the similar ice failure model that was derived in Wang (2001), Su et al. (2010) refined the ice-ship contact procedure to simulate ship maneuvers in level ice. Aksnes (2010b) presented a numerical model for the interaction between a moored ship and a drifting level ice. However, this method is limited to one dimensional simulation with a moving ship in surge direction.

In Paper 1, the numerical method to calculate the ice loads due to ice breaking that was introduced by Su et al. (2010) is extended to simulate a moored ship motions and mooring performance in the horizontal plane under more complex i.e. level ice and pack ice conditions, where the ice breaking force can be calculated while the submersion and friction forces are taken into account based on Lindqvist (1989). But the Lindqvist model that was used previously is only valid for ice drift coming from forward of the ship. It is not clear how to consider the effects of ice submersion forces or forces due to ice accumulation on a vessel in level ice drift scenarios with different ice drift speeds and relative ice drift angles based on the extended numerical model. So a model test is desired to observe the ice loading process, especially the build-up processes of rubble-ice and measure the resulting ice forces. In this way, the extended numerical model is validated and modified. More details on the model test is found in Paper 4.

3.2 Experiment setup

The model tests were performed in the multifunctional ice basin of the Marine Technology Group in the Aalto University. The tank is 40 m long by 40 m wide and 2.8 m deep, installed with a carriage. The carriage could move in plane and reach any point of the surface. By varying the tank's air temperature, fine grained ice sheets can be generated and tempered.

MT Uikku is a double-hull icebreaking tanker that is owned by Neste Shipping and Kvaerner Masa-Yard's joint venture company, Nemarc. The dimensions of the tanker are reduced to model scale by a geometric scale factor λ. The scaling was performed using Froude and Cauchy scaling in that the inertial, gravitational, and crushing forces

are important in the ice model tests. A scaling factor of λ=31.6 is used for the present tests. The particulars of the model and full scale vessel are given in Table 3.1.

Table 3.1 Primary dimensions of MT Uikku (λ=31.6)

Item	Full Scale	Model Scale
Length [m]	150.0	4.75
Breadth moulded[m]	21.3	0.67
Tested Draft[m]	9.5	0.30
Bow waterline angle[deg]	21	
Bow stem angle[deg]	30	
Block coefficient	0.72	

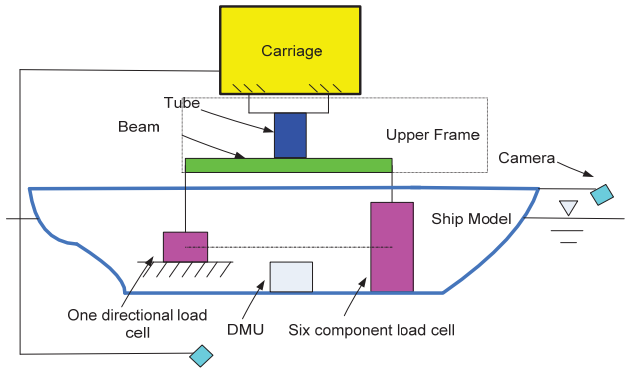

Fig.3.1 Side view illustration shoeing the components of the test system

The model was constrained in six degrees of freedom so that the six force components could be measured (Fig.3.1). An upper frame with a stiff tube and long beam was used to connect the towing carriage with the load measurement units rigidly, which are attached to the model. The following instrumentation was used in the tests.

- An LFX_A_3KN compact 6-component force transducer with built- in amplifier with 3 kN capacity measured the applied ice loads. It was mounted to the ship model to enable simultaneous measurement of 3 forces in 3 axial directions orthogonal to the transducer and 3 moments around the axes.

- A one-directional load cell with capacity 500 kN measured the applied force in yaw direction. The output from this load cell is proportional to the external yaw moment.

- A dynamic measurement unit (DMU) measured the translational and angular accelerations of ship model. The output is six fully conditioned analog signals, which can be connected directly to the data acquisition device without further buffering.

- Two cameras were used. One is fixed to the model at the bow area above water and orientated backwards to record the ice breaking process. The other is

installed underwater to give an impression on the subsurface ice transport process.

Impact tests in open water were conducted to define the dynamic characteristics of the model. In these tests, the model was subjected to an impact force in a known direction and then suddenly released so that it would experience free vibrations. The response of the model in water (without ice) was recorded. Frequency analysis was preformed based on the decaying time series from the results of the free vibration test. The calculated natural frequency of the model is 5.7 Hz in sway and 9.5Hz in surge. The calibration is presented in Appendix A.

3.3 Ice properties measurements

The fine grained ice sheet was generated by cooling, spraying, freezing and tempering. Two ice sheets were made for model tests. The thickness of the ice was adjusted by selecting an appropriate freezing time to produce the desired thickness. The strength of the ice was adjusted by altering the time allowed for warming-up the ice. The ice properties have been measured according to the recommended procedures of the ITTC. Due to the special dimensions of the ice basin, the properties vary as a function of the field length and width. The fine grained structure makes the model ice as such much more homogeneous and isotropic than natural sea ice, but some variations in the properties were still encountered, which reflects in the ice property measurements. The locations of measurements for the first ice sheet A and second ice sheet B are shown in Fig 3.2, respectively. The corresponding ice bending strengths, crushing strengths, elastic modulus's and ice thicknesses are presented in the Table 3.2, where X_i and Y_i are locations in the horizontal plane; h_i, σ_b, σ_c, E_i denotes the ice thickness, ice flexural strength, crushing strength, and elastic modulus, respectively.

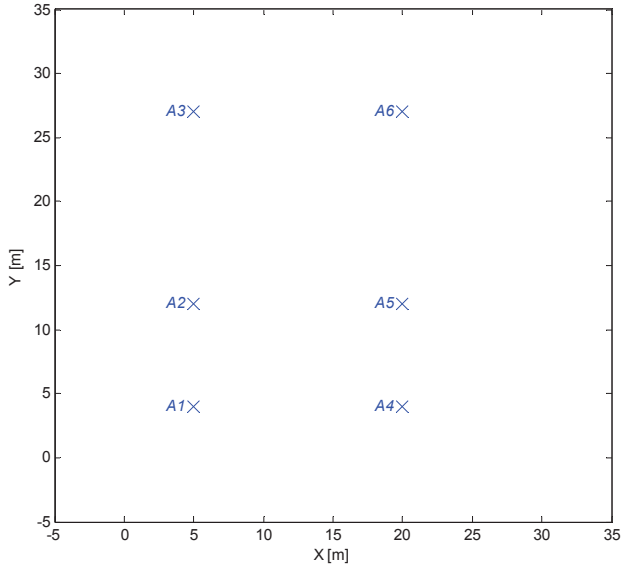

(a) Ice sheet A

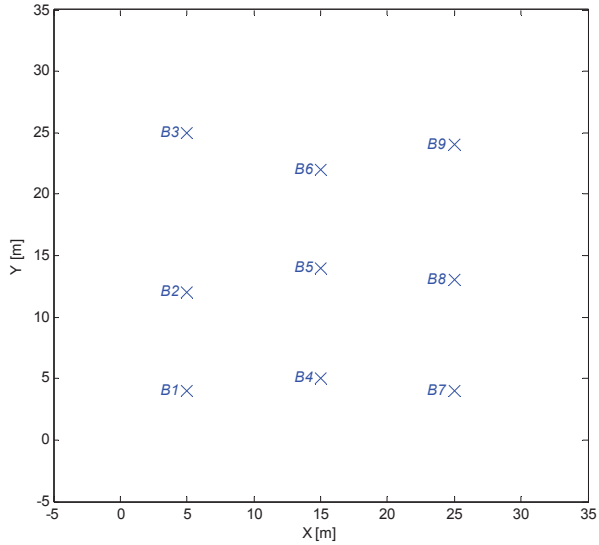

(b) Ice sheet B

Fig.3.2 Illustration of measurement locations for ice properties and ice thickness

Table 3.2 Ice properties and ice thickness

No.	X_i [m]	Y_i [m]	h_i [mm]	σ_b [kPa]	σ_c [kPa]	E_i [MPa]
A1	5	4	24	25	73	35
A2	5	12	24	28	65	33
A3	5	27	25	30	66	25
A4	20	4	24	27	90	24
A5	20	12	24	27	51	34
A6	20	27	25	19	60	25
B1	5	4	32	27	64	33
B2	5	12	32	33	62	60
B3	5	25	33	38	58	36
B4	15	5	31	28	60	39
B5	15	14	30	31	56	68
B6	15	22	30	27	62	40
B7	25	4	31	39	60	35
B8	25	13	33	39	57	56
B9	25	24	33	35	53	38

3.4 Test Matrix

An earth-fixed right-handed reference frame $X_EY_EZ_E$ and a vessel-fixed right-handed reference frame XYZ are defined. Let the heading (yaw) ψ of the vessel be the angle between the X-axis and the X_E-axis, as illustrated in Fig.3.3.The positive Z direction is upwards.

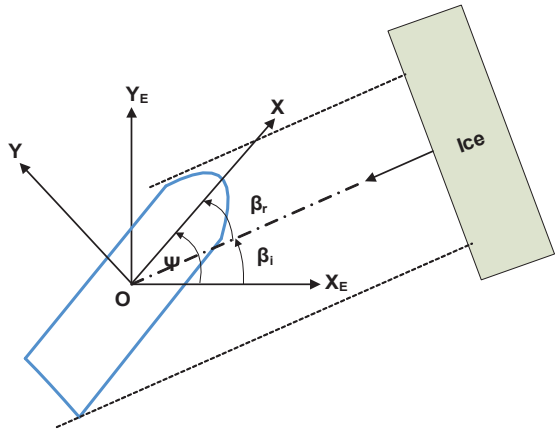

Fig.3.3 Definitions of earth-fixed reference frame $X_EY_EZ_E$, body-fixed reference frame XYZ, vessel heading ψ, ice drift direction β_i and relative ice drift direction β_r.

The absolute ice drift direction β_i is defined in the $X_EY_EZ_E$ system and the relative ice drift direction is defined as $\beta_r = \psi - \beta_i$, as shown in Fig.3.3. In the model tests, the ice drift angle was constant at zero degree and three different constant heading angles, namely 0, 45, and 90 degrees, were tested. The test program is presented in Table 3.3 and the associated ice properties could be found in Table 3.2. The test number in Table 3.3 is synonymic to the corresponding ice sheet number.

Table 3.3 Test program matrix with the model speed, V_i, and the heading, ψ

Test No.	V_i [m/s]	ψ [deg]	Measured parameters
101	0.0365	90	Ice force, accelerations, dimension of ice pile
102	0.089	90	Ice force, accelerations, dimension of ice pile
103	0.0365	0	Ice force, accelerations
104	0.089	0	Ice force, accelerations, size of ice cusp
105	0.0365	45	Ice force, accelerations, dimension of ice pile
201	0.0365	90	Ice force, accelerations, dimension of ice pile
202	0.089	90	Ice force, accelerations, dimension of ice pile
203	0.0365	45	Ice force, accelerations, dimension of ice pile
204	0.089	45	Ice force, accelerations, dimension of ice pile
205	0.0365	0	Ice force, accelerations, size of ice cusp
206	0.089	0	Ice force, accelerations, size of ice cusp

A data acquisition system (DAS) was applied to record the analog signals from the instrumentation. The data were sampled at a rate of 107 Hz. Offset values were taken for all instrumentation before each test with everything held stationary. When this was completed, the DAS was started, and the carriage towed the ship model with a certain heading through the ice at the desired speed. With this approach, there were very low loads at the initial portion of each time series, which represent the loads during the time before the ship model encounters the ice sheet. It should be noted that since the data acquisition system was always started before the hull was towed at a certain speed, segments of the time series were extracted from the full time series to represent

conditions when the hull was in full contact with level ice. The force–time series presented in this paper are all extracted from longer data records. After the carriage had travelled the appropriate length of the ice tank for the test, it stopped along with the DAS system. Following this, the entire process was repeated for the next test. During each test run, the underwater video camera monitored the transport of broken ice under the hull. Another video camera above water was directed towards the stern and wake of the vessel monitoring the breaking performance of the ship model. Further, visual observations were continuously made and some photos were taken when appropriate.

3.5 Model test results

The qualitative results and analysis have been addressed in Paper 4. Parts of quantitative results were presented in Paper 5 as compared to the numerically simulated results. The measured forces were recorded in the time domain with the mean value and standard deviation at steady state given in Table 3.4. The time series of ice forces are shown in Appendix B.

Table 3.4 Results of level ice tests (mean ± standard deviation)

Test No.	F_x (N)	F_y (N)	F_z (N)	M_x (N.m)	M_y (N.m)	M_z (N.m)
101	-0.7± 5.9	463± 99	224±60	-14±8.6	128 ±40	-7.9 ± 69
102	4.7 ± 8.9	332 ± 106	164 ±76	-17±12	106 ±54	22± 86
103	-18 ± 3.8	1.8 ± 17.4	26±20	0.0±2.6	-51 ±20	-4.8 ± 23
104	-18 ± 4.0	18 ± 26	67±33	-2.4±4.1	3.3±32	-12 ± 34
105	-7.7 ± 6.0	290 ± 76	117±42	-13±5.9	73±39	-61 ± 53
201	-3.4 ± 12	632 ± 210	314±117	-31±17	217±78	-17 ± 135
202	-8.4 ± 12	638± 217	332±134	-40±23	212±105	42.4 ± 178
203	-26 ± 12	623 ± 166	275±93	-37±14	170±78	-127 ± 129
204	-42 ± 11	672 ± 189	331±115	-45±18	196±94	-110 ± 170
205	-21 ± 7.0	51 ± 31	63±25	-3.3±3.8	-25±27	3.5 ± 35
206	-23 ± 6.2	56 ± 42	55±45	-3.4±6.2	-25±48	6.3 ± 40

Chapter 4

Numerical Model Validation

4.1 General

As described in Chapter 2, the ice force model is composed of the ice breaking model and the ice submersion model or ice accumulation. The ice breaking model is based on the physical ice breaking process, considering initial interaction between ice and structure. Once the ice cusp is fragmented from the intact ice sheet, it will rotate and submerge. Then the ice cusp may clear away from the structure or accumulate in front of the structure, depending on many factors. This means the two scenarios occurred to the submerged ice blocks. One is that a few ice blocks cover part of the structure surface. The other is that massive ice floes pile up in front of the structure. Therefore, both ice submersion models considering the first scenario and the ice accumulation model considering the second scenario are used in simulations. The simulated results with conical and ship-shaped structures are compared with full scale and model scale measurements. Paper 1 and Paper 5 are associated with the following sections. Two ice submersion models are compared in a numerical way. Finally, relative contribution of different force components is presented and discussed through numerical simulation of the ice breaking tanker MT Uikku.

4.2 Model validation

Numerically simulated ice forces on a conical structure and ship-shaped structure are compared with field measurements and model test data.

4.2.1 Kulluk

In Paper 1, the simulation results obtained with the model are validated against full scale measurements and experimental data from model tests of the Kulluk platform. The ice breaking model and ice submersion model I (based on the Lindqvist model) are used to calculate the dynamic ice forces exposed to the Kulluk in the horizontal plane. As a wide moored conical structure, the Kulluk deployed in the Beaufort Sea during the 1980s is modelled and simulated. It had a downward sloping circular hull near the waterline, which failed the oncoming ice in flexure mainly and an outward flare near the bottom to clear the broken ice cusps away from the moon pool and mooring lines. The mooring system of Kulluk is radially symmetric and consists of 12 lines. The main dimensions and hydrostatics of the Kulluk are given in Table 4.1. The ice characteristics used in the simulation resemble those mentioned in Wright (1999), given in Table 4.2. The initial ice boundary is shown in Fig.4.1.

Table 4.1 Primary dimensions and hydrostatics of the Kulluk

Items	value	unit
Overall beam	81	m
Waterline beam	67.9	m
Bottom beam	62	m
Draught	11.5	m
Displacement	$2.8 \cdot 10^7$	kg
Vertical Centre of Gravity	13.2	m
Mass Moment of Inertia(Pitch)	9.0•109	kg.m2
Mass Moment of Inertia(Roll)	1.0•1010	kg.m2

Table 4.2 Ice characteristics

Parameter	Symbol	Value	Unit
Density	ρ_i	880	kg/m3
Young's modulus	E	5400	MPa
Poisson ratio	γ	0.33	
Crushing strenght	σ_c	2.3	MPa
Flexural strength	σ_f	0.5	MPa
Frictional	μ_i	0.15	

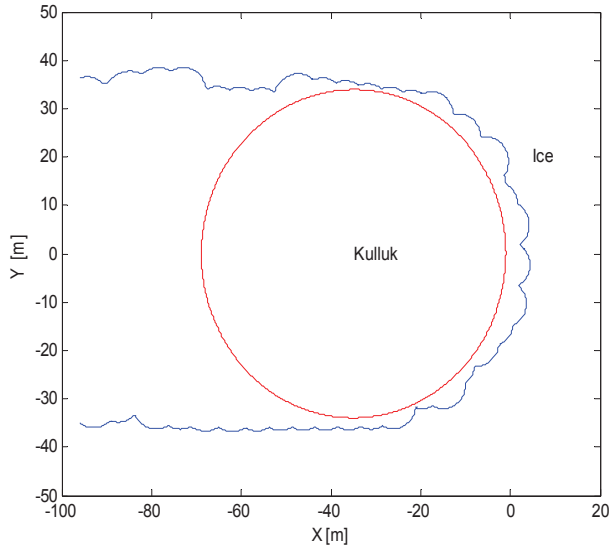

Fig.4.1 Initial ice boundary for the Kulluk simulation in Earth-fixed frame

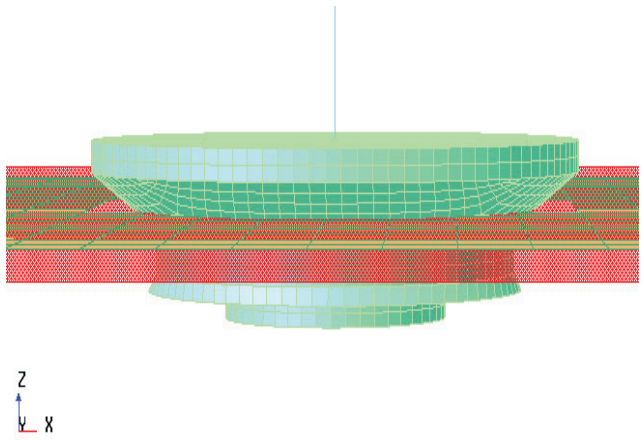

a) Side view

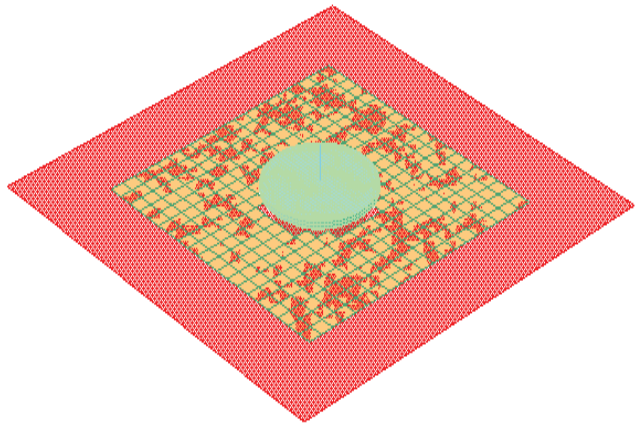

b) Top view

Fig.4.2 Hydrodynamic panel model of the Kulluk Model

The added mass, damping term, and hydrostatic restoring coefficients are calculated using the software SESAM. The panel model for hydrodynamic calculation of the Kulluk is shown in the Fig 4.2. The calculated added mass is used in the simulation. The damping term is neglected. The hydrostatic restoring coefficient is zero.More parameter setup in the simulation can be found in Paper 1.

An example of the main time series from the simulation case using ice driftvelocity of 0.6m/s and ice thickness of 1.0m is given in Fig 4.3, where the ice forces are given in body-fixed coordinates while the global mooring forces and displacements of the Kulluk are given in earth-fixed coordinates. Fig 4.4 shows an episode of the ice force in surge from Fig.4.3.

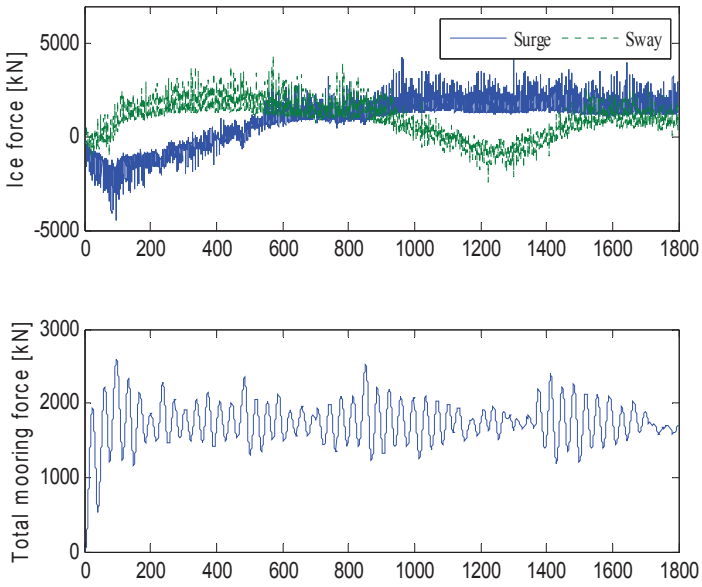

Fig.4.3 Simulated time series of ice and mooring forces on the Kulluk

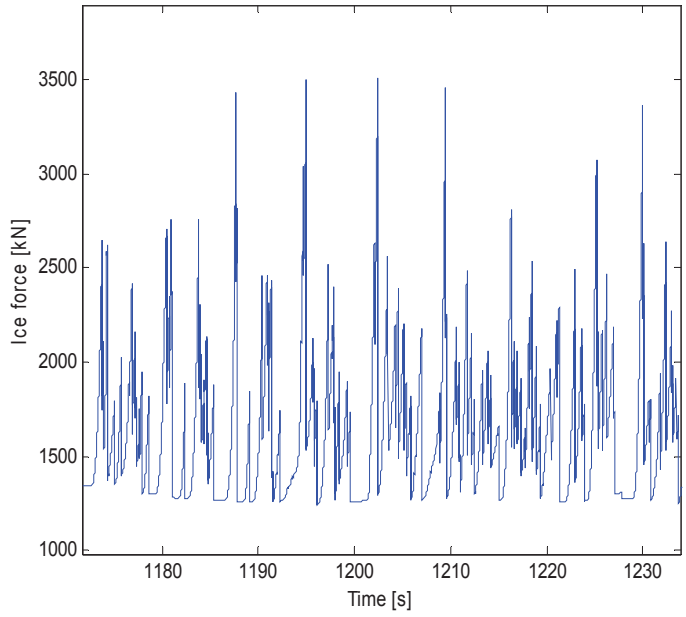

Fig.4.4 An episode of ice force in surge from Fig.4.3

The derived mean, standard deviation, and maximum of mooring forces versus the ice thickness are plotted in Fig.4.5. The full scale data and the model tests data of the Kulluk were also shown in this figure for comparison in terms of the mooring forces. Fig.4.5 shows that the simulated loads show fairly good agreement with the full scale

measurements, although some scatter exists in the full scale data. The mean mooring force increases monotonically with the ice thickness. The HSVA test results agree well with the full scale loads, but they are somewhat high for thicker ice. The IIHR tests measure slightly high, especially at the ice thickness of 1.1 m. The possible reasons have been presented in Paper 1.

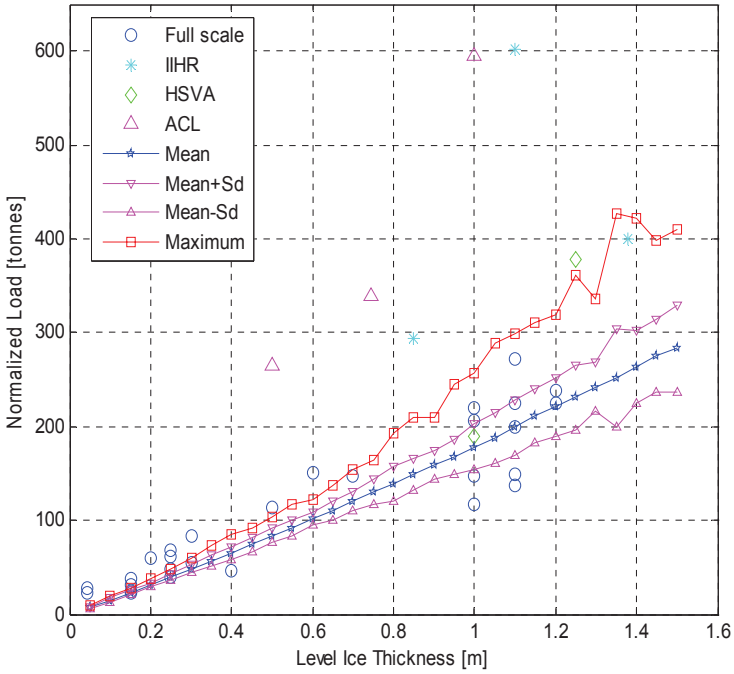

Fig.4.5 Comparison of ice loads from the simulation, full scale, and model scale measurements (ACL-ARCTEC Canada Limited; HSVA -Hamburg Ship Model Basin; IIHR Iowa Institute of Hydraulic Research)

In addition, Wright (1999) presented a load versus ice drift speed scatter plot. To compare this with calculations, ten simulation runs were made where the ice thickness was set to be constant at 1 m and the ice drift speed ranged from 0.025 m/s to 0.6 m/s, being the same conditions as those normalised in Wright (1999). The calculated loads of interest are plotted against those obtained from Wright (1999) in Fig.4.6. The field data show no obvious effect of ice drift speed on the ice load level on the Kulluk in level ice. The simulated loads coincide with the measurements very closely. The mean mooring forces do not change much as the ice drift speed varies, but they tend to increase monotonically as the ice drift speed increases when the speed is above 0.3 m/s. In the simulated cases, the dynamics of the Kulluk are more pronounced at low ice drift speeds than under high drift speed conditions. When the ice drift speed is approximately 0.2 m/s, the maximum mooring force to mean mooring force ratio is up to 2.5, which indicates a large oscillation. Notably, there is a difference between the full scale results and the numerical maximum for velocities from 0.1 to 0.2 m/s. The possible reasons have been explained in Paper 1.

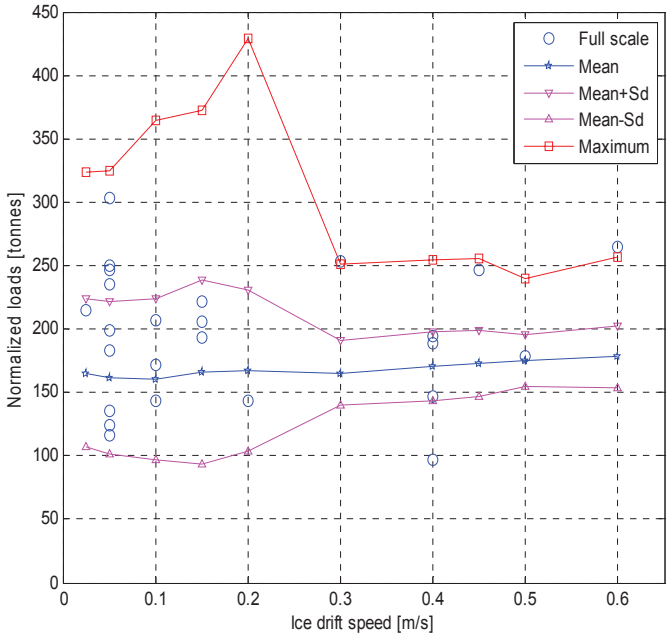

Fig.4.6. Simulated and Full scale loads of Kulluk in level ice versus ice drifting speed

Comparing Fig.4.5 with Fig.4.6, it shows that the maximum mooring loads on the Kulluk with ice thickness of 1.0 m and drift speed of 0.2 m/s are close to those with ice thickness 1.4 m and drift speed 0.6 m/s, which clearly shows the effect of low ice drift speed on the peak mooring forces. Although there are some uncertainties in the validation, this numerical model is suitable for studying and simulating the dynamics of moored structures and ice forces judging from a comparison of the simulated data with field data from the Kulluk.

Moreover, Fig.4.7 shows the ratio of the maximum offset of the Kulluk to the water depth versus level ice thickness. The Kulluk mooring system was originally designed to withstand the loads from 1.2m of level unbroken ice when there is no ice management support. The mooring system was expected to resist the global loads up to 750 tonnes in a drilling mode within an offset envelop of 5% of water depth. The water depth is 50 m. In reality, the mooring system capability of the Kulluk was much less than intended. From the present simulation, it is seen that even if the practical global mooring stiffness is much lower than the designed, the Kulluk could still withstand the loads from the level ice up to 1.12m within the operational limit provided that ice drift speed is kept at 0.6 m/s. This simulated ice thickness of 1.12 m is close to the target 1.2m.

Fig 4.8 shows the ratio of the maximum offset of the Kullk to the water depth versus ice drift speed with ice thickness constant at 1.0m. It is also found that the Kulluk experiences a large offset in the low ice drift speed conditions. When the speed is below 0.27m/s, the maximum offset of the Kulluk is beyond operational limit. The behavior coincides with the fact that the Kulluk normally worked in managed ice conditions although it occasionally operated in moving unbroken ice conditions with ice thicknesses up to 0.6 m (Wright, 1998). It should also be noted that the damping due to

the hull and mooring system is not taken into consideration, which may lead to a higher maximum mooring force. However, to evaluate the damping of moored structures in ice is complicated. More research about the damping is needed, especially for reliability analysis of moored structure operating in ice-infested areas.

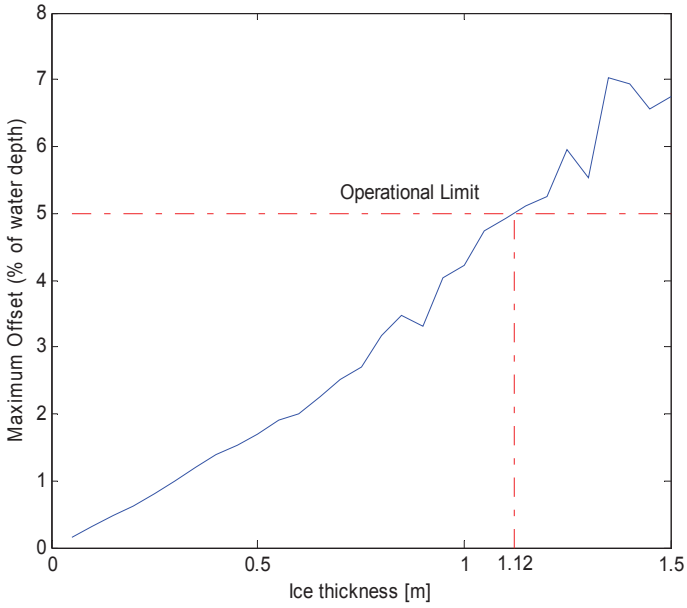

Fig.4.7 Simulated maximum offset versus ice thickness with ice speed at 0.6m/s

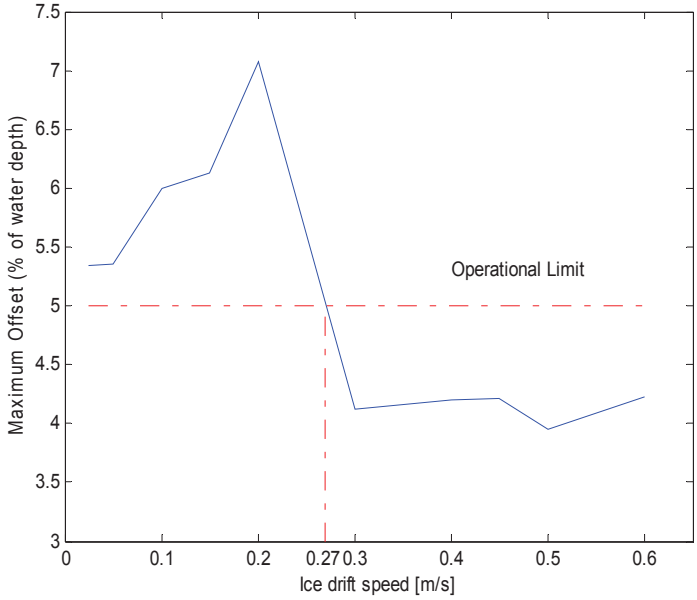

Fig.4.8 Simulated maximum offset versus ice drift speed with an ice thickness 1.0 m

4.2.2 MT Uikku

As a ship-shaped structure, a model of the icebreaking tanker MT Uikku was used for ice model tests in the ice tank of the Marine Technology Group in the Aalto University. The ship model was mounted rigidly to the main carriage and towed through the unbroken ice sheet to simulate the interaction process. The resulting ice loads including ice-rubble loads against the hull in the horizontal plane were measured and are presented in Paper 4. The numerical simulation is also performed to calculate the ice loads with the same parameter setups as obtained from the model tests. The simulated results are compared with measured data.

In Paper 5, the ice breaking model is used to calculate dynamic ice forces during ice breaking process. In addition, the ice submersion model Π (based on Croasdale 2D solution) or the ice accumulation model (based on Croasdale 3D solution) is used to consider the effect of submerged ice floes on a structure, depending on occurrence of ice accumulation. If ice pile-up occurred in some tests, the ice accumulation model would be used. Otherwise, the ice submersion model would be used.

The measured ice properties as well as the model speed and heading setup in full scale are listed in the Table 4.3. The main parameters include ice thickness, h_i, bending strength, σ_b, compressive strength, σ_c, elastic modulus, E_i, model speed, V_i and heading, ψ. Two ice sheets were made, where 11 tests with two towing speeds at three heading angle settings of the hull were conducted.

Table 4.3 Ice properties as well as model speed and heading used in the simulations

Ice sheet	Test No.	h_i[m]	σ_b [kPa]	σ_c[kPa]	E_i[MPa]	V_i [m/s]	ψ [deg]
	101	0.76	828	2176	1042	0.2	90
	102	0.77	914	2075	914	0.5	90
I	103	0.77	724	1748	929	0.2	0
	104	0.76	844	2192	984	0.5	0
	105	0.76	852	2209	915	0.2	45
	201	1.01	940	1991	1466	0.2	90
	202	1.03	1117	1889	1520	0.5	90
	203	1.01	1231	1862	1420	0.2	0
II	204	1.04	1168	1736	1483	0.5	0
	205	0.96	920	1840	1685	0.2	45
	206	0.95	912	1862	1701	0.5	45

In Paper 5, the results are shown in three groups according to the heading settings (0, 45, 90 degree) in the model test. For each group, the typical time histories of the ice forces in the horizontal plane from both model test and numerical simulation are presented and compared. The presented time signals are filtered with a low cut-off frequency to show the general evolution of ice forces in the time domain.

For cases with 90 degrees heading, it comprise tests 101,102,201,202 as shown in Table 2. Since there is a strong ice drift speed effect on the ice accumulation phenomenon from observation in the model tests, the time series of ice forces from tests 101 (low drift speed), and 102 (high drift speed) are shown in Figs. 4.9 and 4.10. From Fig.4.9, it is found that the smoothed ice forces on the horizontal plane from simulation approaches those from the experiment. From Fig.4.10, it is clear that the magnitudes of

the amplitudes for both ice forces time series are at the same level. As time goes, the simulated ice forces in surge and sway get close to those from the experiment while the simulated yaw moment is very close to the measured one over all simulated duration. For cases with other headings, reference is made to Paper 5.

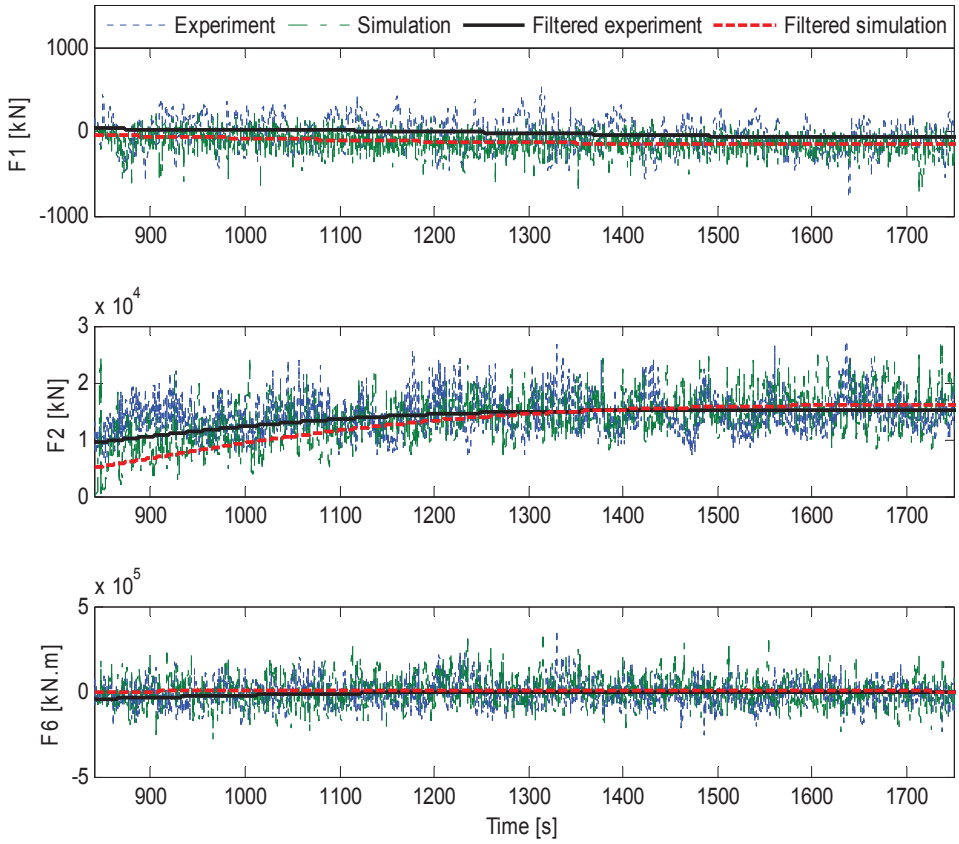

Fig. 4.9 The time history of ice forces on the hull for test 101 after 840 s

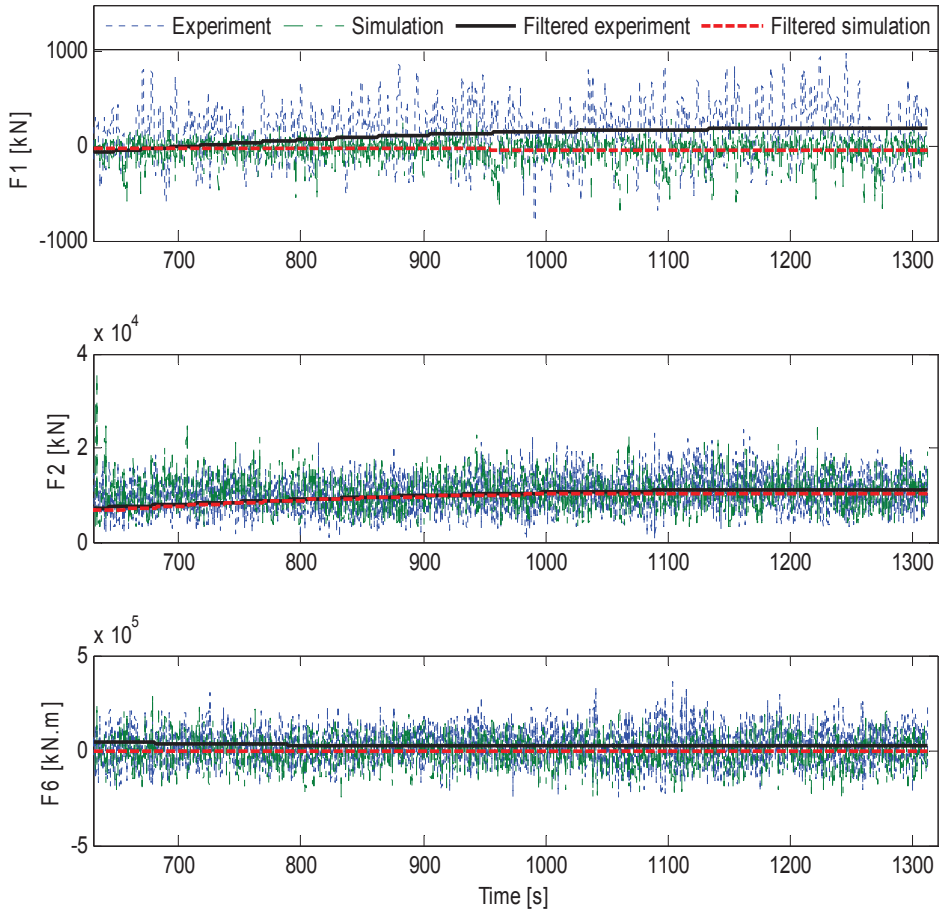

Fig. 4.10 The time history of ice forces on the hull for test 102 after 630 s

The mean value and standard deviation of the ice forces at steady state for all 11 tests, in terms of simulation and experiment are shown in Table 4.4 for different headings.

For the cases with 90 degrees heading, it is seen that a good agreement is achieved with respect to the standard deviation of the ice forces from the simulations. The calculated mean ice forces in surge and sway agree well with those from the model test, but the predicted ice yaw moments deviate from the measured ones.

For the cases with 45 degrees heading, it is seen that a good agreement is achieved with respect to the mean value and standard deviation of the ice forces from simulations. The mean level of the calculated forces in sway and yaw directions is very close to the corresponding measured forces. In x-direction, both the mean ice force and standard deviation are over predicted to some extent for all three tests.

For the cases with 0 degree heading, it is seen that a good agreement is achieved for the mean values in x-direction in spite of the overestimated standard deviation. However, the transverse forces and yaw moments due to ice are not well predicted.

Table 4.4 Experimental and simulated level ice forces (mean values ± standard deviation)

Heading	Case No.	Model test			Numerical simulation		
		F_1(kN)	F_2 (kN)	F_6 (kN.m)	F_1 (kN)	F_2 (kN)	F_6 (kN.m)
90	101	-23 ± 182	14200± 3100	-9600± 65700	-126 ±107	13800± 4200	-525 ± 76000
	102	40 ± 296	10200 ± 3200	20700 ± 81900	-38 ± 103	10200 ± 3400	-9700 ± 75000
	201	-107 ± 391	19900± 6600	-16600 ± 134000	-189± 185	19500± 5400	-15800± 120000
	202	-264 ± 383	19800 ± 6800	39500 ± 173000	-68 ± 258	18300 ± 7100	-46400± 171000
45	105	-241 ± 190	9100 ± 2400	-60000 ± 52500	-669 ± 224	9900 ± 2500	-57600 ± 66500
	203	-820 ± 367	19600 ± 5200	-126000 ± 128000	-1230 ± 584	18500 ± 5500	-125000 ± 144000
	204	-1320 ± 355	21100 ± 5900	-109000 ± 169000	-1320 ± 611	19200 ± 6100	-100000 ± 162000
0	103	-465 ± 121	58 ± 546	-4700 ± 22600	-440 ± 191	-5 ± 324	33± 14912
	104	-563 ± 124	573 ± 814	11900 ± 33700	-528 ± 229	27 ± 944	1300 ± 37200
	205	-667 ± 224	1600 ± 978	3400 ± 34400	-634 ± 292	-45 ± 291	-1300 ± 13800
	206	-723 ± 196	1800 ± 1300	6200 ± 39300	-692 ± 315	2 ± 600	370 ± 27900

4.3 Comparison between the two ice submersion models

In numerical simulation of tests with 0 degree heading, the submersion model Π (based on Croasdale 2D solution) is used to calculate the ice load due to submerged ice floes on the MT Uikku. In order to compare the difference between the two ice submersion models, ice submersion model I (based on Lindqvist), in addition to the ice breaking model is also used to calculate mean ice resistance on the hull for cases with 0 degree heading.

The corresponding calculated ice resistances by the different models and the measured ice resistance are presented in Fig. 4.11. It is shown from Fig. 4.11 that the simulated ice resistance with the submersion model Π (based on Croasdale 2D solution) coincides well with the measured value, but the submersion model I from Lindqvist underestimates the ice resistance specific to the measured data in the model tests to some extent.

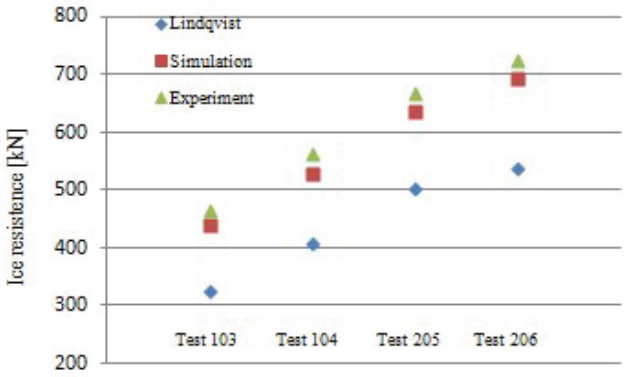

Fig. 4.11 Comparison of ice resistances from simulation and model tests

4.4 Relative contribution of different force components

It is assumed that the calculations of the ice breaking force and the ice submersion or accumulation force are independent in the numerical simulation. It implies that the forces obtained from the ice breaking model and ice submersion or accumulation model are added to give the total ice forces. The relative contribution of the mean of the ice breaking force and the ice submersion or accumulation force of the total forces for all simulated 11 cases is presented in this section. By relative contribution, we mean the ratios $R_b/(R_b+R_s)$ and $R_s/(R_b+R_s)$, or $R_b/(R_b+R_r)$ and $R_r/(R_b+R_r)$, where the notations R_b ,R_s and R_r are defined in Eq.(2.4).

The ice forces in the horizontal plane are simulated, including longitudinal force, transverse force, and yaw moment, of which the transverse force is dominant for cases with 90 and 45 degrees heading and the longitudinal force is dominant for cases with 0 degree heading. Thus, only the relative contribution of each component of the transverse force for cases with 90 and 45 degrees heading and the longitudinal force for cases with 0 degrees heading are concerned. The relative contribution of the mean of ice breaking force and ice accumulation or submersion of the total transverse ice force for cases with 90 and 45 degrees heading is given in Table 1. The relative contribution of the mean of ice breaking force and ice submersion of the total longitudinal ice force for cases with 0 degree heading is given in Table 4.6.

It is found from both Table 4.5 and 4.6 that the ice breaking component generally contributes to 50–73% of the total ice force, and the submersion or accumulation term 27–50%. The ice breaking force is dominant in most simulated cases. The ice accumulation occurs when the ice drift speed is low. For cases with 90 degrees heading, the ice accumulation component gives higher contribution than the ice submersion component.

It is also seen from both Tables 4.5 and 4.6 that the ice drift speed has effects on the relative contribution of the ice breaking component. For tests with the same ice thickness and heading angle, the contribution of the breaking component increases and

the contribution of the submersion or accumulation component decreases as the ice drift speed increases.

Table 4.5 Relative contribution of the mean of the different terms of the transverse ice force for cases with 90 and 45 degrees heading

Heading	Case No.	Ice breaking component	Ice accumulation or submersion component
90	101	55%	45%
	102	70%	30%
	201	50%	50%
	202	71%	29%
45	105	73%	27%
	203	55%	45%
	204	68%	32%

Table 4.6 Relative contribution of the mean of the different terms of the longitudinal ice force for cases with 0 degree heading

Heading	Case No.	Ice breaking component	Ice submersion component
0	103	52%	48%
	104	62%	38%
	205	55%	45%
	206	61%	39%

For tests with the same heading angle and ice drift speeds, the relative contribution of the breaking component and the ice accumulation or submersion component on ice thickness does not change too much as the ice thickness increases. In other words, the dependency of relative contribution of each component on ice thickness is minor. |

Chapter 5

Simulation Results with Heading Control

5.1 General

A moored icebreaking tanker, MT Uikku, is used in a case study. Paper 1, Paper 2, and Paper 3 are associated with this chapter. In Paper 1, a simple heading controller is designed, which keeps the moored tanker aligned with the drift ice direction. Based on the heading controller, the effects of ice thickness, ice drift speed, and global mooring stiffness on mooring forces and responses of the moored vessel are studied. In Paper 2, a heading controller based on a Kalman filter is designed. Moreover, a thrust allocation method is developed to go with the heading controller. In Paper 3, the performance of the moored tanker with heading control is simulated in time domain to estimate the stationkeeping capability of the tanker in level ice.

5.2 Parameter sensitivity analysis

Sensitivity studies are carried out with respect to the effects of ice thickness, ice drift speed and mooring stiffness on the dynamics of the moored tanker with heading control. The main dimensions of MT Uikku are presented in Table 3.1. The level ice used in the following simulations is assumed to have the constant properties shown in Table 4.2.

The first set of simulation was done to study the influence of ice thickness on the behavior of moored tanker. The initial heading of the vessel is zero. The ice drifting speed is assumed to be constant at 0.6 m/s. The selected ice thickness in the simulation ranges from 0.05 m to 0.7 m with an interval of 0.05 m. The resultant time histories of the mooring forces are of most importance and thus presented in the Fig. 5.1 while the other time series are not given. The resulting ice resistance as a function of ice thickness is plotted in Fig. 5.2.

From Fig. 5.2, there is a clear trend of increasing load with increasing ice thickness, although the simulated ice resistance does not increase with ice thickness monotonically. For instance, the simulated loads did not vary much when the ice thickness was changed from 0.5 m to 0.6 m. This may be attributable to the different icebreaking patterns formed in the interaction between the hull and the two types of ice sheet (Su et al, 2010).

The second set of simulation was done to study the effect of the ice drifting speed on the horizontal response of moored tanker. The ice thickness is constant at 0.6 m. The selected ice drift speeds in the simulation were 0.1, 0.2, 0.3, 0.4, 0.5, 0.6, and 0.8 m/s. The response of the system in surge is mainly taken into consideration. The resultant time histories of the mooring forces, surge offsets, and velocities in the surge direction

are shown in the Fig 5.3. The mooring forces as a function of ice drift speed are plotted in Fig 5.4.

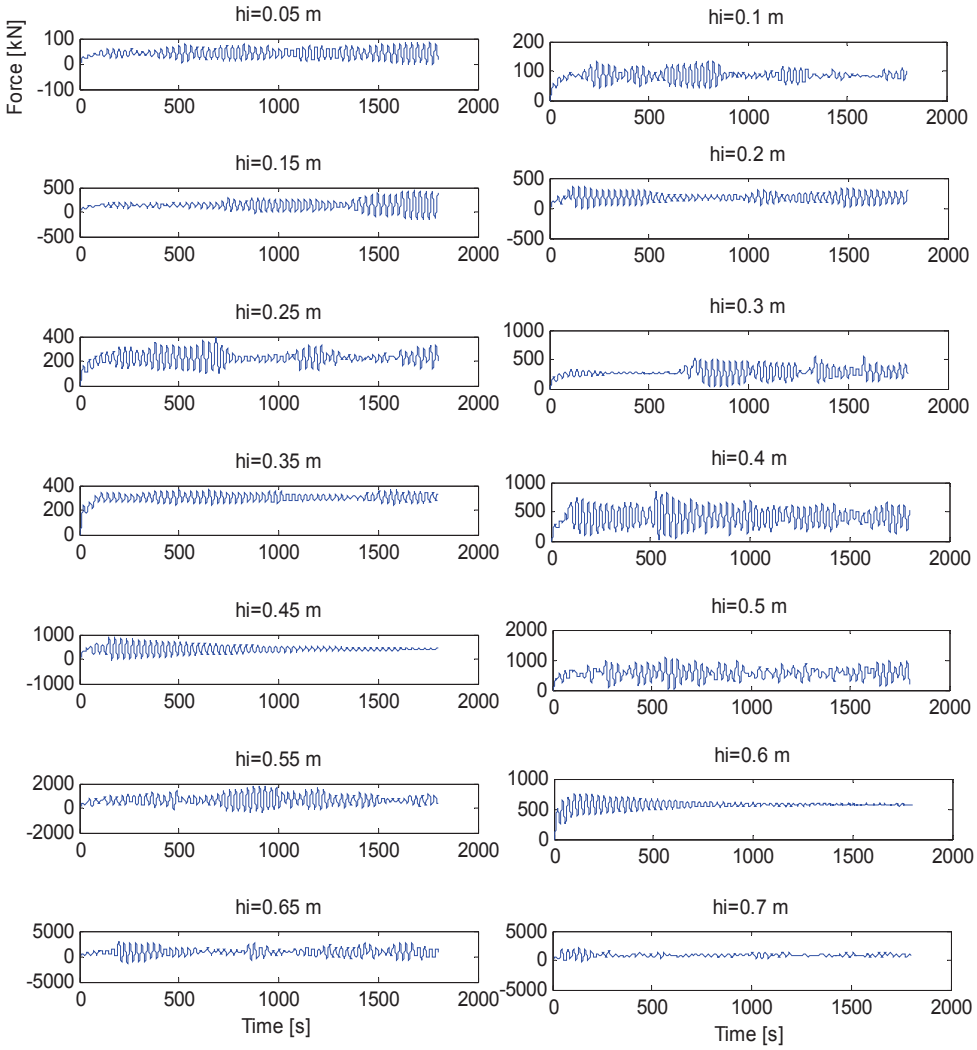

Fig.5.1 Simulated time histories of mooring forces with different ice thickness

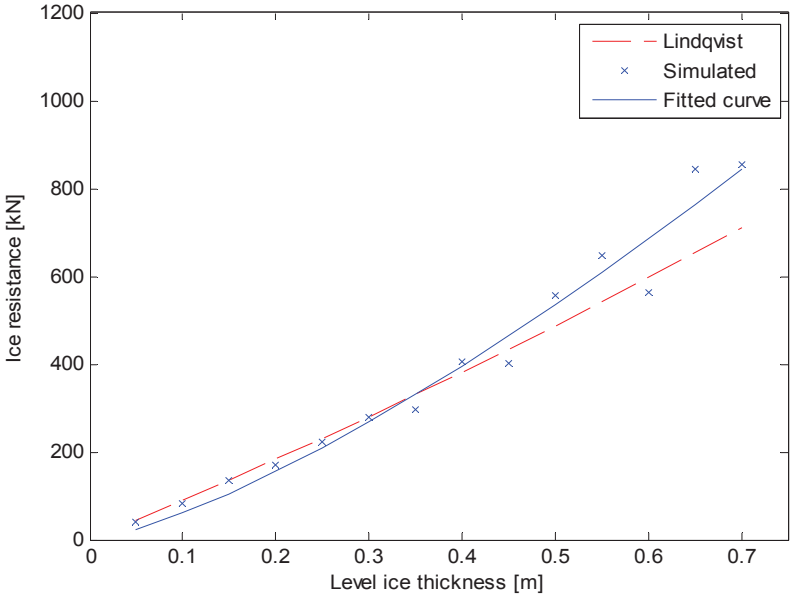

Fig.5.2 Simulated ice resistance versus ice thickness

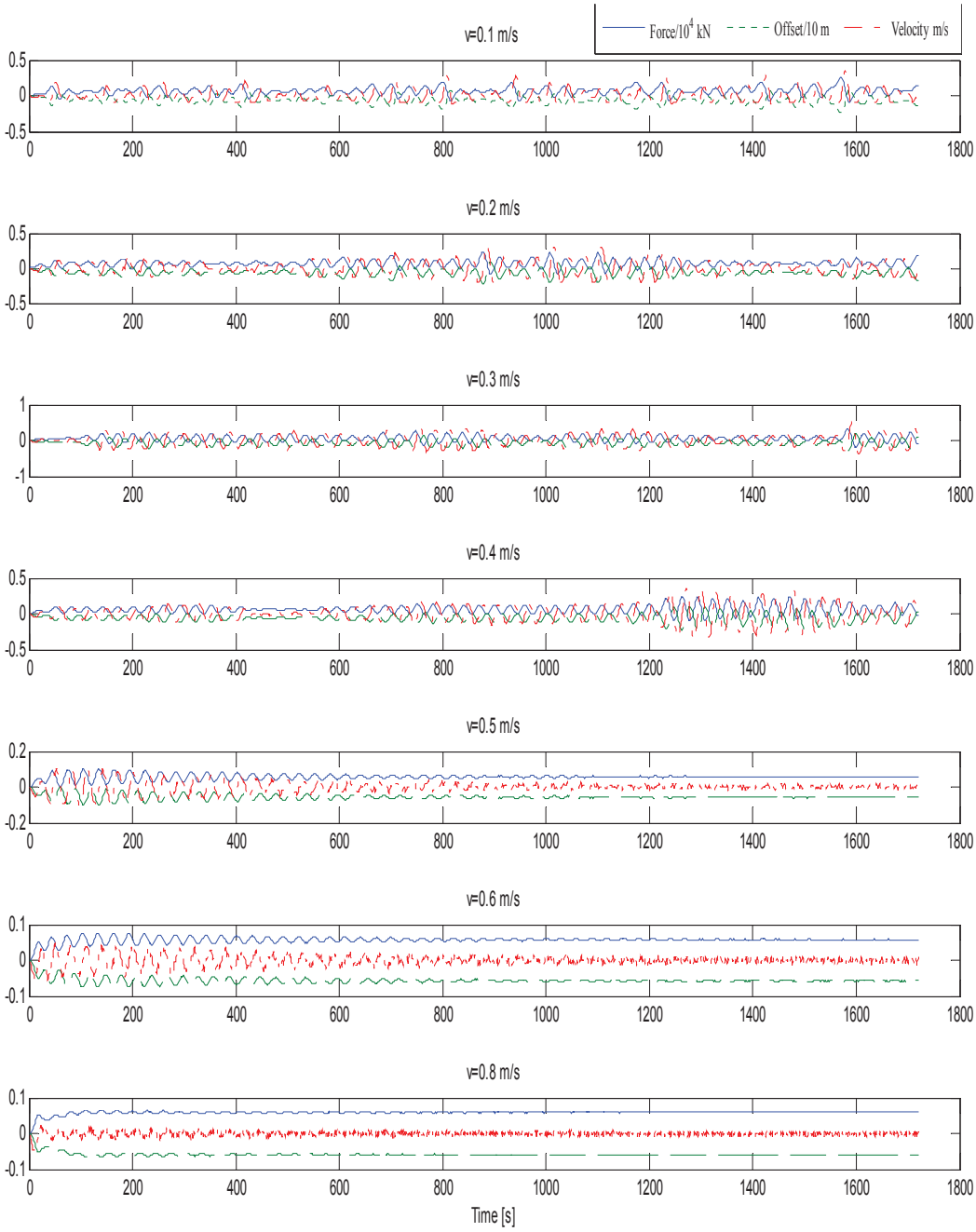

Fig.5.3 Time histories of the simulated mooring forces, offsets,and velocities with varying ice drift speed

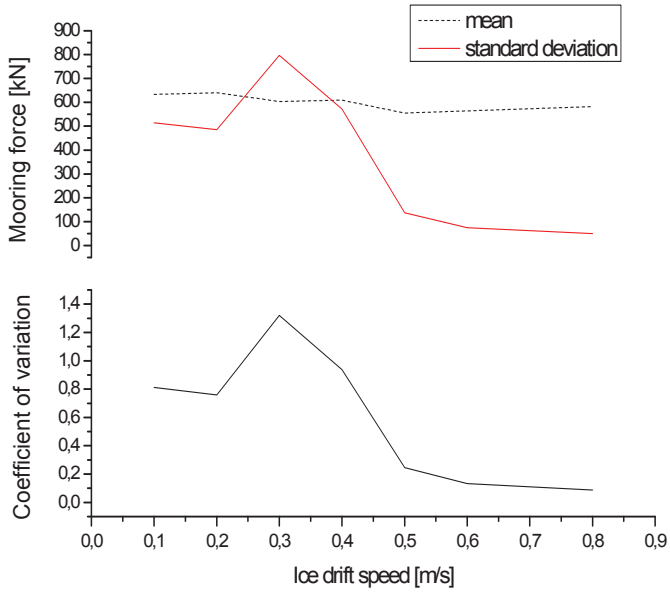

Fig.5.4 The mean and standard deviation of the mooring forces vs speed (neglecting the first 200 s of the simulated time series)

From Fig. 5.4, the effect of the drift velocity varies depending on its range. There is no obvious velocity effect on the mooring force deviation when the ice drift speed is relatively low. When ice drift speed increases from 0.2 m/s to 0.3 m/s, there is an increase in the maximum offset and velocity of the vessel in surge. Then, the amount of maximum offset and velocity of the vessel in surge drops down quickly and tends to approach zero asymptotically as the ice drift speed continues to increase. On the whole, the tanker experiences higher mooring force variance in the plane with lower drift speeds (below 0.4 m/s) compared to that with higher drift speeds.

The third set of simulation was done to study the effect of the mooring stiffness on the horizontal response of the moored tanker. The ice thickness is constant at 0.6 m while the ice drifting speed is set to be 0.6 m/s. The mooring stiffness is assumed to be linear and six different mooring stiffnesses are used: 300, 500, 1000, 2000, and 3000 kN/m. The time series of mooring forces are given in the Fig. 5.5. The resulting mooring force as a function of mooring stiffness is plotted in Fig. 5.6.

From Fig. 5.6, it is found that the mooring stiffness has an effect on the standard deviation and maximum of the mooring forces and the turret offset. The standard deviation and maximum of the mooring force increase non-monotonically with increasing mooring stiffness. The amplitude of the oscillations decreases with increasing mooring stiffness.

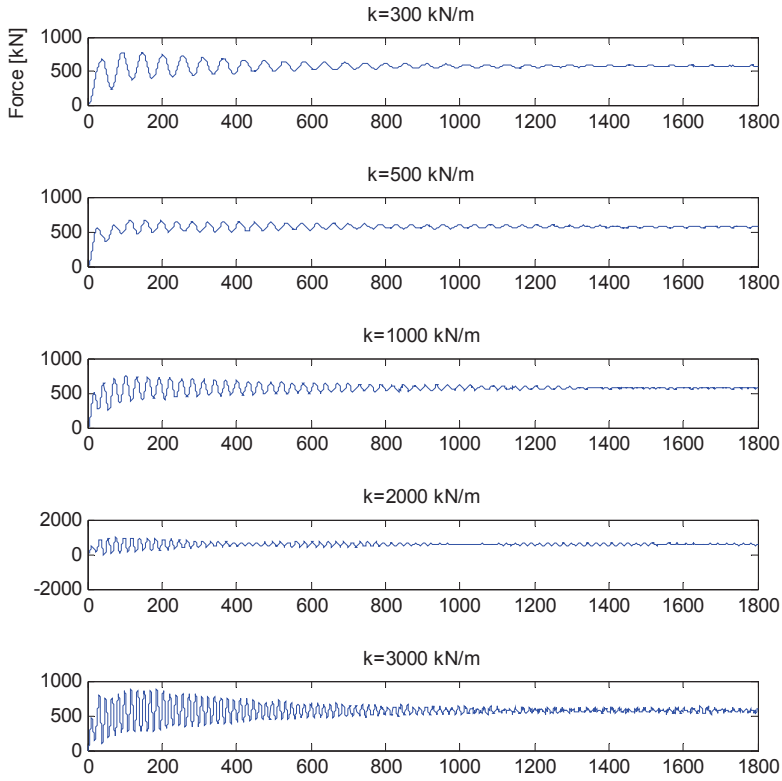

Fig. 5.5 Time histories of mooring forces with different mooring line stiffness

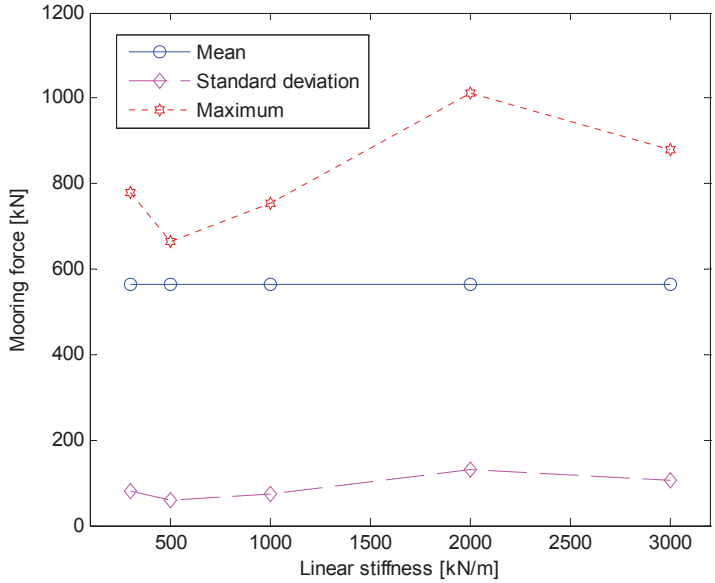

Fig. 5.6 Mooring force in surge versus linear stiffness

5.3 Stationkeeping capability

Stationkeeping capability is a key consideration to evaluate the floating structure performance in level ice. It is closely related to the availability and feasibility of various operations with stationkeeping modes. The capability plot, often presented as a polar diagram with a number of envelops, is used to establish the vessel's capability to keep position in a certain environment with a certain combination of thrusters. The environmental forces and moments are increased until they are exactly balanced by the maximum available thrust offered by the thruster configuration (Gonsholt and Nygård, 2002). Since ice loads dominate the environmental loads in level ice waters, the capability of a moored vessel assisted with heading control is characterized by the maximum ice thickness that the vessel could resist at a certain relative ice drift angle.

The limiting ice thicknesses at different ice drift angles that the moored tanker with and without heading control could resist are shown in Fig.5.7 as a function of relative ice drift angle.

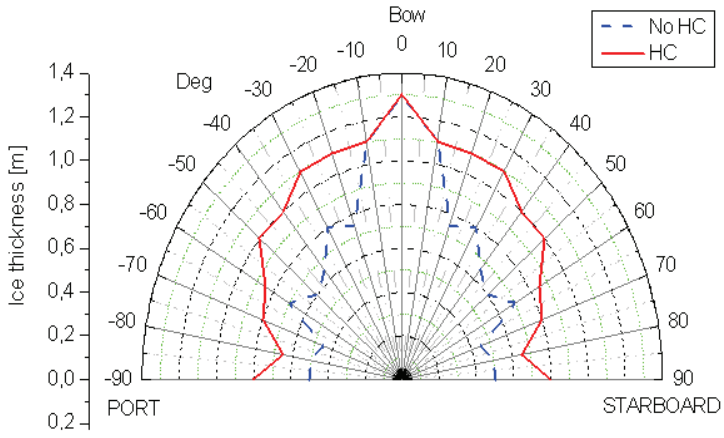

Fig.5.7 Capability plot for moored tanker MT Uikku without heading control (No HC) and with heading control (HC)

From Fig. 5.7, it is interesting to see some special findings as follows:

- The maximum limiting ice thickness is 1.3 meters at 0 degree. The lowest limiting ice thickness is 0.45 meter at 70 degrees for the moored tanker without HC and 0.65 meter at 80 degrees for the moored tanker with HC. In general, the limiting ice thickness decreases as the ice drift angle increases in both cases, but not monotonously. This may be attributed to the dynamics of vessel introduced by the drifting ice with different angles.

- Using heading control to assist a moored tanker enhances the stationkeeping capability significantly except for cases with ice drift angle at 0 and 10 degrees. Although the heading control setting is the same for all HC cases, the commanded force by the controller is different on a case by case basis, depending on the heading error between the ice drift angle and the present

heading. This means that when heading control is used, the calculated forces from the control system in cases with ice drift angle at 0 and 10 degrees are less than those in other cases. The effort made by the heading control system is less and thus it does not make significant influence on the stationkeeping ability of the tanker.

To sum up, using heading control to assist the moored tanker could enhance the stationkeeping capability significantly except for cases with ice drift angle at 0 to 10 degrees. The main outcome of the paper shows that the limiting ice thickness for a moored ship can be increased by using heading control, and, hence, offers an extension of the operating season for moored ships.

Chapter 6

Conclusions and Recommendations for Future Work

6.1 General

This thesis deals with both numerical and experimental study on the stationkeeping of floating structures in level ice. The numerical model was shown to reproduce phenomena of continuous icebreaking during the ice-structure interaction observed in the fields and in model tests. In the simulation, the thickness and strength properties of the ice encountered by the ship are assumed to be constant or predefined based on the statistical data. The interdependence between the ice load and the ship's motion was taken into account, and the three degree-of-freedom rigid body equations of surge, sway, and yaw were solved by numerical integration. The resulting global ice loads on marine structures can thus be obtained in a deterministic way. The research work comprises three main aspects, namely: numerical model, heading control, and model tests.

First, a 2D numerical model for the interaction between drifting level ice and a moored structure in the horizontal plane was developed. The floating structure is treated as a rigid body kept on station by a mooring system or mooring combined with a dynamic position (i.e., heading control) system. The ice-breaking process was modelled using a geometrical method that characterizes the contact zones between the hull of moored structure and the ice sheet. Ice rotation and sliding processes were modelled semi-empirically using ship ice resistance formulations. The initial numerical model does not account for ice accumulation. The numerical model predicts the time history of both the ice forces and the global mooring forces as well as the dynamics of the floating structure. The simulation results obtained with this model were compared with full scale measurements and experimental data from model tests on the Kulluk platform conducted in the Beaufort Sea during the 1980s. The results show good agreement between the field measurements and the model tests. In this respect, the numerical model can give reasonable predictions of global ice loads and performance of structures with stationkeeping operation in level ice.

The model was extended by adding an ice accumulation model to the original numerical model. The updated numerical model combines the ice actions in the vicinity of the waterline caused by breaking of intact ice with submersion of broken ice floes below the waterline, which pertains to ice rotation, sliding, and ice accumulation. This model was validated by comparing with model tests. In these simulations the ship model was moored by artificially high stiffness to the carriage to resemble the ice tank setup as closely as possible and towed through an intact ice sheet. The measured and numerically calculated ice loads were compared by varying the ice drift speed, the relative ice drift angles, and the ice properties. Good agreement was achieved in terms of mean value,

standard deviation, maximum and extreme force distributions, although there were some deviations between predicted and measured results for certain cases. In a way, the numerical model can be applied to predict the ice loads on moored or dynamically positioned structures in stationkeeping operations in level ice with constant drift direction, and it can be extended to variable relative ice drift direction.

Second, heading control of a position-moored vessel operating in a level ice regime was simulated. The heading control system based on a Kalman filter was designed to ensure that the vessel is kept at an appropriate position within safe limits. Using this control strategy, the desired control force is computed to counteract the environmental disturbances. A thrust allocation method was also developed to go with the heading controller. A case study was conducted with ice drift angle 0° and 15°, and the results show that the proposed control system performs satisfactory for a moored vessel in level ice. Besides, the capability of this stationkeeping strategy was studied and could be used to extend the operating season for moored ships.

Third, a series of ice model tests have been carried out to investigate the key ice load issues on an icebreaking tanker. A model of the ice going tanker Uikku was mounted rigidly to the main carriage and towed through the unbroken ice sheet to test the interaction process in the ice tank of the Marine Technology Group in the Aalto University. Ice rubble accumulation on the upstream side of the hull beneath the ice sheet was observed in some runs. The formations and build-up processes of rubble-ice in front of the hull are important and the accompanying ice loads were measured. Those data are useful for modifying the numerical model and including an ice force component caused by ice rubble accumulation.

6.2 Summary of main contributions

The main contributions of this thesis are summarized as follows:

1) Developed a numerical model for simulating the interaction between drifting level ice and a moored structure with and without heading control;

2) Investigated the effects of ice thickness, ice drift speed, and global mooring stiffness on the mooring forces and responses of the vessel;

3) Investigated the influence of turret position on the directional stability of ship shaped structure under typical varying ice drift speeds and directions;

4) Proposed an approach to keep the structure operating in level ice and designed a heading control system based on a Kalman filter for moored ship-shaped structures and developed a thrust allocation method to go with the heading control in ice;

5) Estimated the stationkeeping capability of a moored ship with heading control by considering the interconnection between the vessel motions and the ice dynamics;

6) Carried out a model test with a moored icebreaking tanker to observe the process of ice loading on the towing hull and measured the resulting ice forces as well as identified the main factors that affect the ice load levels;

7) Described how the formation and build-up of rubble-ice under the intact ice sheet in front of the hull are significantly influenced by towing speed and heading angle;

8) Developed an ice force model by accounting for the ice accumulation and modified the rotation and sliding model for the numerical model based on numerous observations and measured data from model tests;

9) Carried out a comparative study between the numerical model and experimental results for a tanker in model scale and a cylindrical structure in model and full scale in the time domain.

6.3 Recommendations for future work

The following interesting and important issues relating to the topic of this thesis are identified as possible topics for further research.

1) The present research mainly focuses on constant ice conditions. Structures operating in the ice covered area may encounter different ice conditions. Therefore, a randomly varying ice condition should be considered in the numerical simulation of ice-hull interaction. The thickness and strength properties of the ice encountered by the ship should be predefined based on the statistical data and use of the Monte Carlo method.

2) The ice breaking pattern has been assumed to be 'fixed' in the present study. According to the observation and measurement in model tests, it may vary significantly. Therefore, a probabilistic distribution of parameters describing the ice breaking pattern could be established based on data from model tests or field observations, and used in simulations.

3) The present numerical model is based on a uniform crushing of a constant ice pressure on the contact surface between ice and hull. The pressure–area relationship could be used to refine the ice loading process. Moreover, the ice breaking model is based on simplified elastic theory. Further studies on other models would be beneficial to possibly improve the simulation of the ice–hull interaction process.

4) The contribution of ventilation and slamming during ice cusp rotation to the total ice loads on the structures should be investigated, especially under the condition of high relative ice speed.

5) The present numerical model can be applied to predict the dynamic ice loads on a moored or dynamically positioned structure in stationkeeping operations in level ice with constant drift direction. It can also be extended to variable relative ice drift direction.

6) The simulation of the structure motion is limited to the horizontal plane (i.e., surge, sway, and yaw) without considering heave, roll, and pitch motions of the structure in the present simulation. The model could be extended to 6 DOF.

7) Heading control assisted mooring system is used to keep the position of ship-shaped vessels in level ice. An alternative approach could be to use a pure DP combined with ice management (icebreaker assistance) to limit ice loads. One to three ice breakers might then be needed to break the intact ice sheet into small ice blocks on the upstream of the DP vessel. In this case, more effort should be made on studying broken ice loads on the DP vessel and control strategy.

8) The thruster or propulsion efficiency concerning interaction between ice blocks and propellers are not discussed in the present thesis. These issues remain for further study.

References

Aksnes, V., 2010. A panel method for modeling Level Ice Actions on Moored Ships. Part1: Local Ice Force Formulation. Cold Regions Science and Technology, Vol. 63, pp. 29-39.

API "American Petroleum Institute Recommended Practice for Planning, Designing, and Constructing Structures and Pipelines for Arctic Conditions", 2nd Edition, API Publications, 1220 L Street N.W., Washington, DC 20005, 1995.

Bonnemaire, B., Lundamo, T., Evers, K.U., Løset, S., Jensen, A., 2008. Model testing of the Arctic Tandem Offloading Terminal –Mooring Ice Ridge Loads. Proceedings of the 19th IAHR International Symposium on Ice. Vancouver, British Columbia, Canada.

Bonnemaire, B., Lundamo, T., Serré, N., Fredriksen, A., 2011. Numerical simulations of moored structures in ice: influence of varying ice parameters. Proceedings of the 21st International Conference on Port and Ocean Engineering under Arctic Conditions (POAC), Montréal, Canada.

Bruun, P.K., Løset, S., Gürtner, A., Kuiper, G., Kokkinis, T., Sigurdsen, A., Hannus, H., 2011.Ice model testing of structures with a downward breaking cone at the water line JIP; presentation, set-up & objectives. Proceedings of the 30th International Conference on Ocean, Offshore and Arctic Engineering (OMAE), Rotterdam, The Netherlands.

Croasdale, K.R., 1980. Ice forces on fixed, rigid structures. In: CRREL Special Report 80-26, Working Group on ice forces on structures. A State-of-the-Art Report. Int. Association for Hydraulic Research, Section on ice problems. U.S. Army CRREL, Hanover, NH, USA, pp. 34-103.

Croasdale, K.R., Cammaert, A.B., Metge, M., 1994. A Method for the Calculation of Sheet Ice Loads on Sloping Structures. Proceedings of the 12th International Symposium on Ice, Trondheim, Norway, Vol. 2, pp. 874–875.

Deter, D., Doelling, W., Lembke-Jene, L., Wegener, A., 2009. Stationkeeping in Solid Drift Ice. DYNAMIC POSITIONING CONFERENCE, Houston, USA.

DNV–Det Norske Veritas, 2004. Positioning mooring. Offshore Standard DNV-OS-E301.

Enkvist, E., 1972. On the ice resistance encountered by ships operating in the continuous mode of ice breaking. Technical report, The Swedish Academy of Engineering Sciences in Finland.

Enkvist, E., Varsta, P., Riska, K., 1979. The Ship-Ice Interaction, vol. 2. The International Conference on Port and Ocean Engineering under Arctic Conditions (POAC), Trondheim, pp. 977–1002.

Fossen, T.I., 2010. Guidance and Control of Marine Craft. Marine Cybernetics, Trondheim, Norway.

Fossen, T.I., Johansen T.A., 2006. A survey of control allocation methods for ships and underwater vehicles. In: IEEE Conference on Control and Automation, IEEE, pp. 1–6.

Gonsholt, A., Nygård, B., 2002. DP design studies. Dynamic Positioning Conference, Houston, USA.

Hidding, W., Bonnaffoux, G., Naciri, M., 2011. Advanced weathervaning in ice. Proceeding of the 30th international Conference on Offshore Mechanics and Arctic Engineering (OMAE), Rotterdam, The Netherlands.

ISO/DIS 19906 Draft International Standard 2009.

Jeffries, M.G., Wright, W.H., 1988. Dynamic response of Molikpaq to ice-structure interaction. Proceedings of the International Conference on Offshore Mechanics and Arctic Engineering (OMAE), pp. 201-220.

Jensen, A., Bonnemaire, B., Lundamo, T., Ravndal, O., 2011. Efficient combination of numerical simulations and ice basin testing in the design process of moored structures in ice. Offshore Technology Conference (OTC), Houston, Texas, USA.

Johansen, T.A., Fossen, T.I., Berge, S.P., 2004. Constraint Nonlinear Control Allocation with Singularity Avoidance using Sequential Quadratic Programming. IEEE Transactions on Control Systems Technology, vol. TCST-12, pp. 211–216.

Keinonen, A., Wells, H., Dunderdale, P., Pilkington, R., Miller. G., Brovin, A., 2000. Dynamic positioning operation in ice, offshore sakhalin, may – june 1999. Proceedings of the 10th International Offshore and Polar Engineering Conference (ISOPE), Seattle, USA.

Kjerstad, N., 2011. Ice Navigation. Tapir Academic Press, Trondheim.

Kuehnlein, W.L., 2009. Philosophies for dynamic positioning in ice-covered waters. Offshore Technology Conference (OTC), Houston, Texas, USA.

Lewis, J.W., Debord, F.W., Bulat, V.A., 1982. Resistance and propulsion of ice-worthy ships. Transactions of Society of Naval Architects and Marine Engineers (SNAME), Vol. 90, pp. 249-276.

Lindfors, I., 1993. Thrust Allocation Method for the Dynamic Positioning System. 10th International Ship Control Systems Symposium (SCSS'93), Ottawa, Canada, pp. 3.93–3.106.

Lindqvist, G., 1989. A Straightforward Method for Calculation of Ice Resistance of Ships. Proceedings of International Conference on Port and Ocean Engineering under Arctic Conditions (POAC), pp.722–735.

Liu, J.C., Lau, M., Williams, F.M., 2006. Mathematical modeling of ice–hull interaction for ship maneuvering in ice simulations. Proceedings of 7th International Conference

and Exhibition on Performance of Ships and Structures in Ice (ICETECH), Banff, Alberta, Canada.

Løset, S., Aarsnes, J.V., 2009. Icebreaking Buoy in Arctic Waters. The 9th International Conference and Exhibition for Oil and Gas Resources Development of the Russian Arctic and CIS Continental Shelf RAO/CIS Offshore 2009, St. Petersburg, Vol. 1, pp. 138-143.

Løset, S., Grøsland, R., Jensen, A., 2003. Model testing of a single anchor moored ship in the wake of a buoy in level ice and pressure ridges. Proceedings of the 17th International Conference on Port and Ocean Engineering under Arctic Conditions (POAC), Trondheim, Vol. 1, pp. 393-405.

Løset, S., Ø. Kanestrøm, Pytte, T., 1998. Model tests of a submerged turret loading concept in level ice, broken ice and pressure ridges. Cold Regions Science and Technology, Vol. 27, pp. 57-73.

Lubbad, R., Løset, S., 2011. A numerical model for real-time simulation of ship–ice interaction. Cold Regions Science and Technology, Vol. 65, pp. 111–127.

Martio, J., 2007. Numerical simulation of vessel's maneuvering performance in uniform ice. Report No. M-301, Ship Laboratory, Helsinki University of Technology, Finland.

Moran, K., Backman, J., Farrell, J.W., 2006. Deepwater drilling in the Arctic Ocean's permanent sea ice. The Proceedings of the Integrated Ocean Drilling Program (IODP), Vol. 302.

Nguyen, D.T., Sørbø, A.H., Sørensen, A.J., 2009. Modeling and control for dynamic positioned vessels in level ice. Proceedings of the 8th Conference on Manoeuvring and Control of Marine Craft, Guarujá, Brazil.

Sawamura, J., Tsuchiya, H., Tachibana, T., Osawa, N., 2010. Numerical modeling for ship maneuvering in level ice. Proceedings of the 20th International Symposium on Ice (IAHR), Lahti, Finland.

Schneider, P.J., Eberly, D.H., 2002. Geometric Tools for Computer Graphics. Morgan Kaufmann Publishers, San Francisco, USA.

Sørensen, A.J., 2005. Marine cybernetics: modelling and control. In Lecture notes (5th ed.).UK-05-76. Trondheim,Norway:Department of MarineTechnology, NTNU.

Strand., J.P., Sørensen, A.J., Fossen, T.I., 1998. Design of automatic thruster assisted position mooring systems for ships. Modelling, Identification and Control, Vol. 19, No. 2, pp.65-71.

Su, B., Riska, K., Moan, T., 2010. A Numerical Method for the Prediction of Ship Performance in Level Ice. Cold Regions Science and Technology, Vol. 60, pp. 177–188.

Timco, G.W., Johnston, M.E., 2002. Caisson Structures in the Beaufort Sea 1982-1990: Characteristics, Instrumentation and Ice Loads. Technical Report CHC-TR-003, Ottawa, Canada.

User's Manual Riflex, version 3.2.3, 2003. MARINTEK Report No.519619.

Valanto, P., 2001. The resistance of ships in level ice. SNAME Transactions 109, pp. 53–83.

Varsta, P., 1983. On the mechanics of ice load on ships in level ice in the Baltic Sea. Publications 11, Technical Research Centre of Finland, Espoo, Finland.

Wang, S., 2001. A Dynamic model for Breaking Pattern of Level Ice by Conical Structures. Ph.D. Thesis, Department of Mechanical Engineering, Helsinki University of Technology, Finland.

Webster, W.C., Sousa, J., 1999. Optimum Allocation for Multiple Thrusters. Proc. of the Int. Society of Offshore and Polar Engineers Conference (ISOPE'99), Brest, France.

Wilkman, G., Suojanen, R.A., Saarinen, S., Mattsson, T., Leiviskä, T., 2009. DP in iIce Conditions – Challenges and Opportunities. DYNAMIC POSITIONING CONFERENCE, Houston, USA.

Wright, B., 1999. Evaluation of Full Scale Data for Moored Vessel Stationkeeping in Pack Ice. PERD/CHC Report 26–200, Ottawa, Canada.

Wright, B., Associates Ltd. Canatec Consultants Ltd. AKAC Inc, 1998, Moored Vessel Stationkeeping in Grand Banks Pack Ice Conditions, PERD/CHC Report 26-189, submitted to The National Research Council of Canada.

Yue, Q.J., Li, L., 2003. Ice Problems in Bohai Sea Oil Exploitation. Proceedings of the 17th International Conference on Port and Ocean Engineering under Arctic Conditions (POAC), Vol. I, pp. 151-163.

Zhou, L., Moan, T., Riska, K., Su, B., 2011b. Heading control for turret-moored vessel in level ice based on Kalman filter with thrust allocation. Submitted to journal for review.

Zhou, L., Riska, K., Moan, T., 2012b. Station Keeping Capacity of a Moored Structure with Heading Control in Level Ice. Proceedings of the 21st IAHR International Symposium on Ice, Dalian, China.

Zhou, L., Riska, K., Moan, T., Su, B., 2012c. Numerical modeling of ice load on an icebreaking tanker: comparing simulations with model tests. Submitted to journal for review.

Zhou, L., Riska, K., von Bock und Polach, R., Moan, T., Su, B., 2013. Experiments on level ice loading on an icebreaking tanker with different ice drift angles. Cold Regions Science and Technology, Vol. 85, pp. 79-93.

Zhou, L., Su, B., Riska, K., Moan, T., 2011a. Numerical Simulation Of Moored Ship in Level Ice. Proceeding of the 30th international Conference on Offshore Mechanics and Arctic Engineering (OMAE), Rotterdam, The Netherlands.

Zhou, L., Su, B., Riska, K., Moan, T., 2012a. Numerical simulation of moored structure station keeping in level ice. Cold Regions Science and Technology, Vol. 71, pp. 54-66.

Appendix A

Model test calibration

The calibration of instrumentation was done at the beginning of the test program to ensure reliable and accurate performance. The dynamic measurement unit was calibrated by inclining them at specific angles with respect to the earth's gravitational field prior to installation in the model. The calibration of 6-component force transducer and one directional load cell are combined since some force components are coupled each other. The model was fixed to the carriage in the water before the calibration process started.

The series of tests used to determine the calibration matrix were carried out as follows. This was done by applying an increasing load in six degrees of freedom and measuring the resulting analog signals from the force transducer and load cell. For this particular calibration, information on 5 (except yaw moment) of the possible 6 degrees of freedom from force transducer and one degree of freedom (yaw moment) from load cell was recorded. External known loads were applied in one direction at a time.

The first loading case was an applied force in the negative x-direction. The setup for this case can be seen in Fig.A.1. The signal due to zero loading was recorded. Then, the applied weight was placed on the tray quickly and smoothly and briefly stopped from oscillating. This helps achieve a higher accuracy because oscillations create variations in the readings. A final zero reading was taken until the program stops recording. If an external force or disturbance was affecting the measurements more tests were conducted to obtain accurate results. For this case, additional moment about the y-axis was introduced since the loading point is not located at the center of gravity in the Z-direction.

The second loading case was an applied force in the positive y-direction. Fig.A.2 demonstrates the setup for this case. The setup for the force in the y-direction is slightly different from that of the force in the x-direction. Due to limited space in the cave to fix the pulley bracket, the ship model needs to turn 90◦. The loading process in the y-direction is similar to that applied in the y-direction. Likewise, moment about the x-axis was introduced.

To produce a moment about the z-axis, weights were placed on the tray, which is located some distance away from the center of gravity in the x-direction. This applied a direct moment about the z-axis with negative force in the y-direction and also moment about the x-axis. Fig.A.3 shows the setup used to apply a moment about the z-axis. The procedure as described for applying a force aforementioned was also applied here. The fourth loading case was an applied moment about the y-axis. This was achieved by

placing the weights directly on the hull at the center line, as shown in Fig.A.4 for this case. This setup would also introduce a negative force in the z-direction.

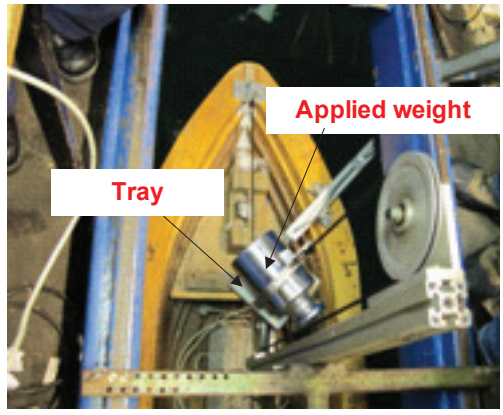

Fig.A.1 Setup for Load Case 1 – Force in Negative X-axis

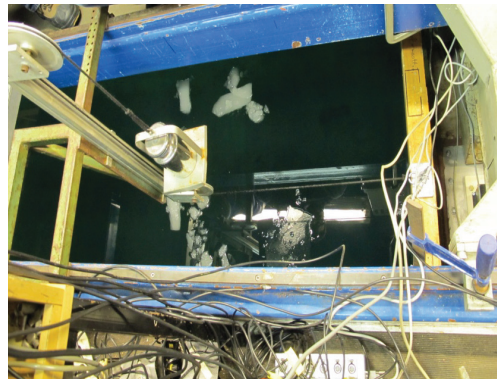

Fig.A.2 Setup for Load Case 2 – Force in Y-axis

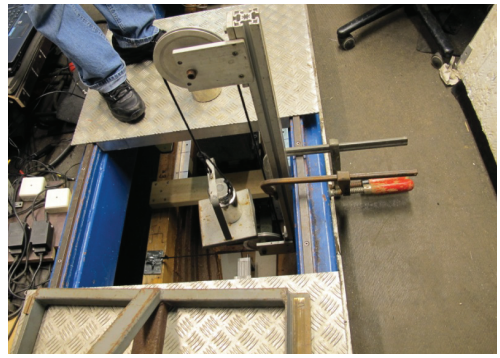

Fig.A.3 Setup for Load Case 3 – Moment about Z-axis

Fig.A.4 Setup for Load Case 4 – Moment about y-axis

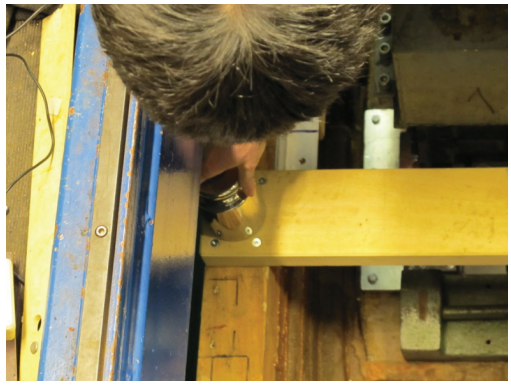

Fig.A.5 Setup for Load Case 6 – Force in Z-axis

The fifth loading case was an applied moment about the x-axis. This was achieved by placing the weights directly on the side of hull. This setup would also introduce a negative force in the z-direction. The final setup for applying a force in the negative z-direction is shown in Fig.A.5. This would introduce two moments about the x-axis and y-axis, respectively.

The six independent load directions (Fx, Fy, Fz, Mx, My,Mz) were used in order to calculate the 6x6 calibration matrix. The applied forces and moments are presented in Table A.1. The zero load cases are excluded from this table as they do not apply a load to the transducer. Calibration matrix $[K]_{LSF}$ is calculated from the results obtained from the measurements. (LSF represents Least Square Fitting method). The error $\{r\}_i$ between the applied load vector $\{f\}_i$ and the load vector $[K]_{LSF}\{v\}_i$ calculated from the measured voltage values is

$$\{r\}_i=\{f\}_i-[K]_{LSF}\{v\}_i \tag{A.1}$$

where i is the number of the measurement. The zero measurements were excluded from the total number of measurements. Then the matrix K is derived as:

$$K = 1000 * \begin{bmatrix} 0.02 & -2.11 & -0.02 & 0.54 & 0.02 & 5.17 \\ 1.80 & 0.03 & -0.04 & 0.06 & 0.50 & -245 \\ 1.44 & -0.91 & -1.95 & 2.66 & 0.46 & -13.9 \\ -0.10 & 0.06 & -0.02 & -0.17 & -0.11 & 5.58 \\ 1.36 & -1.01 & 1.93 & 2.58 & 0.43 & -11.9 \\ 1.71 & 0.07 & -0.01 & -0.07 & 0.47 & 226 \end{bmatrix}$$

Table A.1 Loads per each load case.

Direction	Weight [kg]	Fx [N]	Fy [N]	Fz [N]	Mx [Nm]	My [Nm]	Mz [Nm]
	5	-49.05	0	0	0	-13.22	0
Fx	10	-98.10	0	0	0	-26.44	0
	20	-196.2	0	0	0	-52.88	0
	5	0	49.05	0	-13.22	0	0
Fy	10	0	98.10	0	-26.44	0	0
	20	0	196.2	0	-52.88	0	0
	5	0	-49.05	0	13.28	0	69.90
Mz	10	0	-98.10	0	26.44	0	139.79
	15	0	-147.15	0	39.66	0	209.69
	5	0	0	-49.05	0	90.64	0
My	10	0	0	-98.10	0	181.29	0
	20	0	0	-196.2	0	362.58	0
	5	0	0	-49.05	15.45	0	0
Mx	10	0	0	-98.10	30.90	0	0
	10	0	0	-98.10	30.90	0	0
	5	0	-49.05	-14.96	-54.74	0	0
Fz	10	0	-98.10	-29.92	-109.48	0	0
	20	0	-196.2	-59.84	-218.96	0	0

Appendix B

Time histories of measured forces

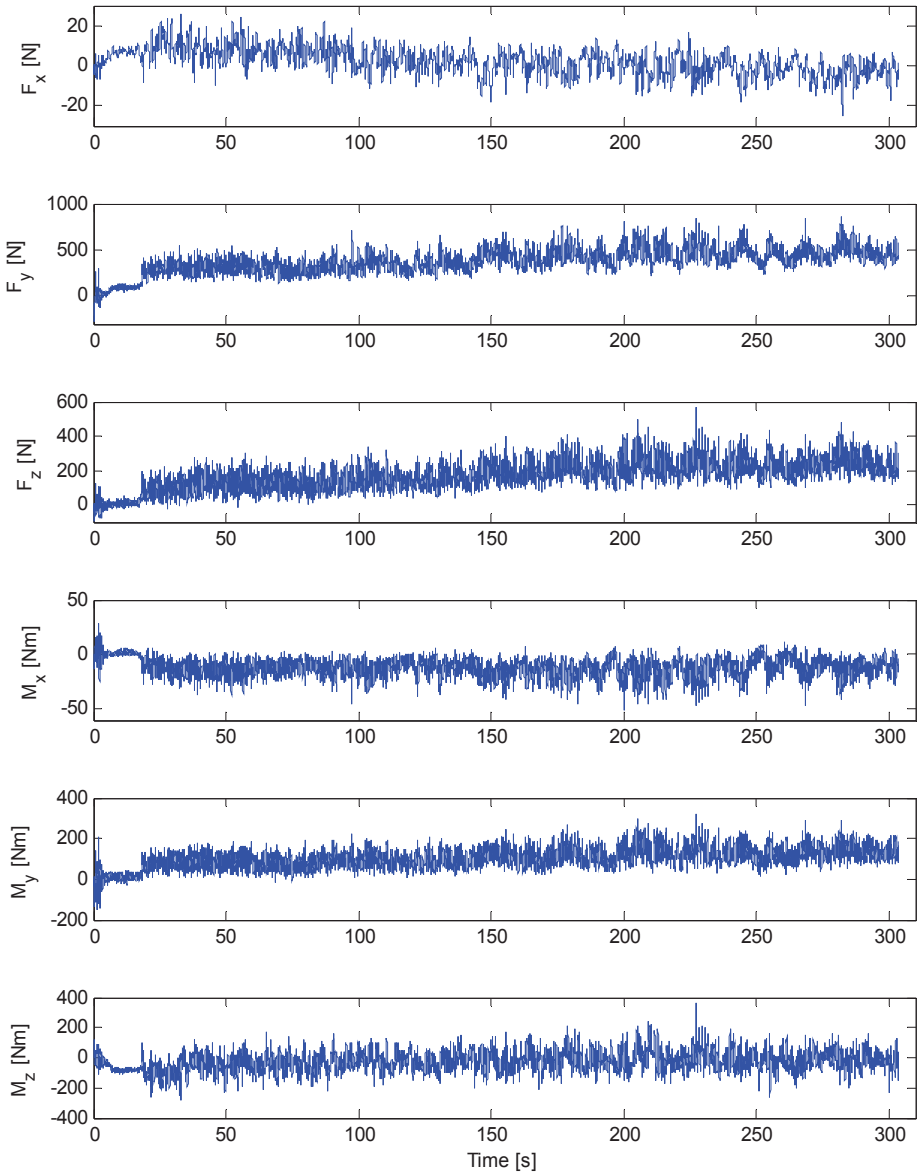

Fig.B.1 Measured ice forces in test 101

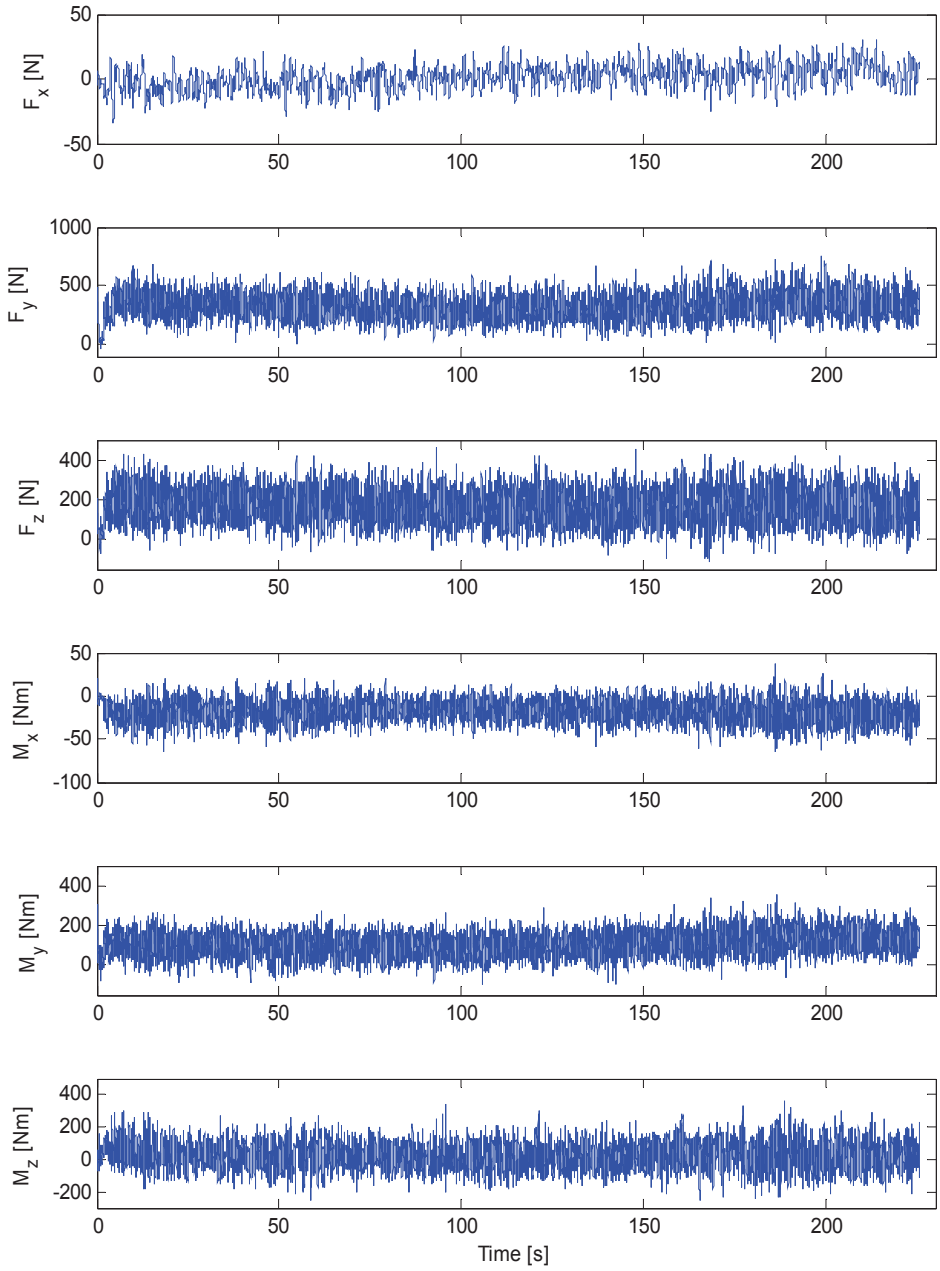

Fig.B.2 Measured ice forces in test 102

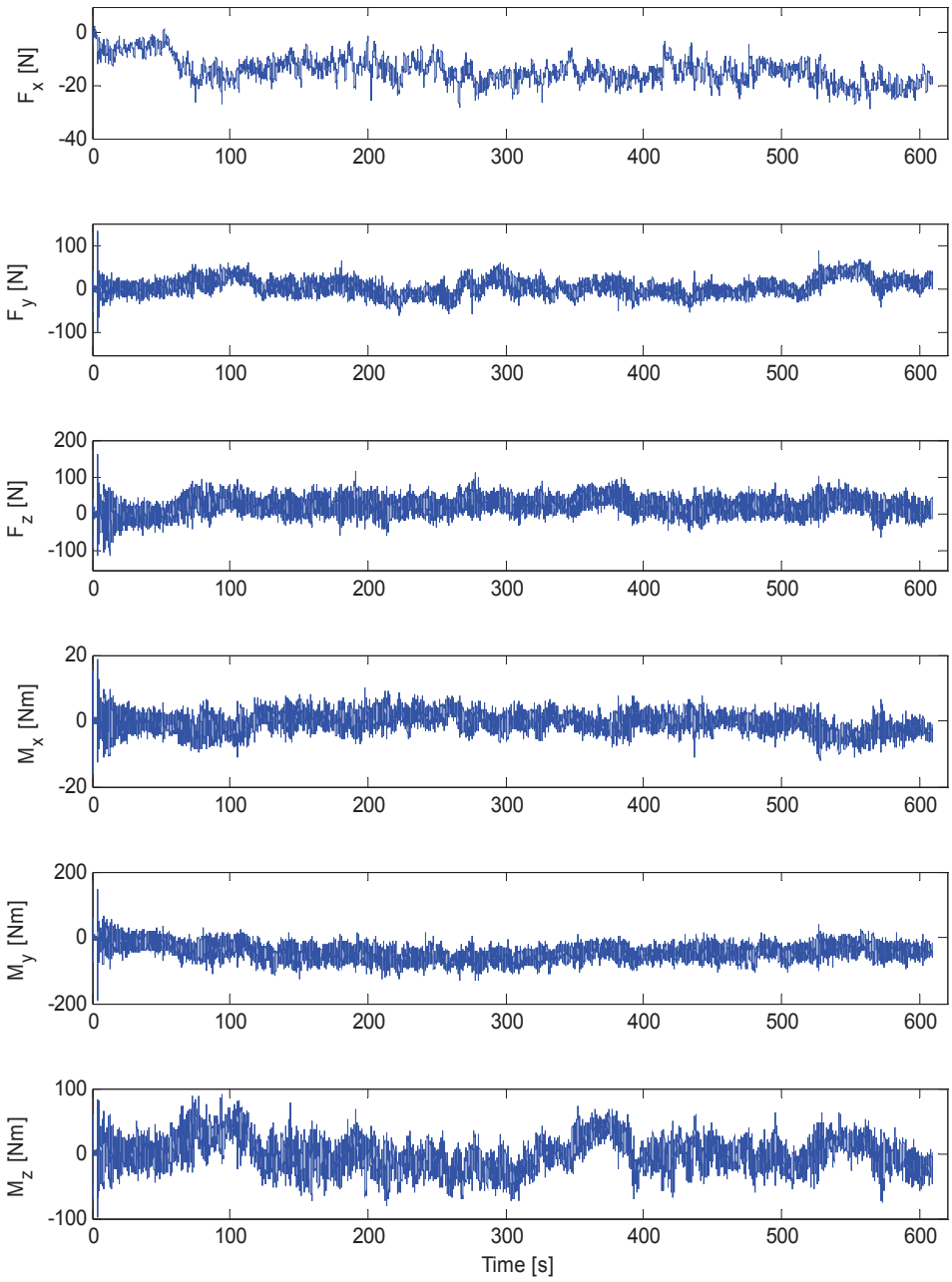

Fig.B.3 Measured ice forces in test 103

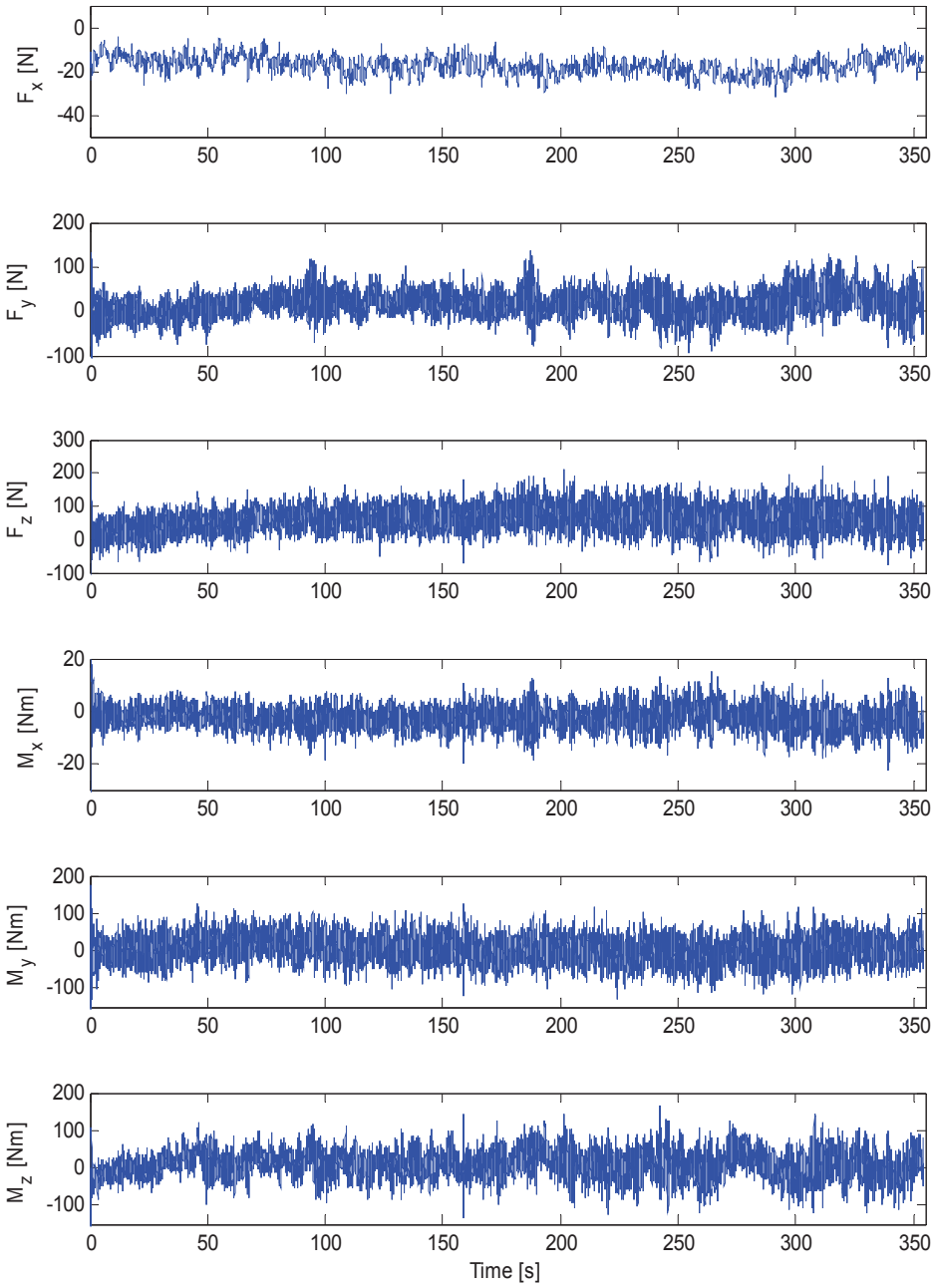

Fig.B.4 Measured ice forces in test 104

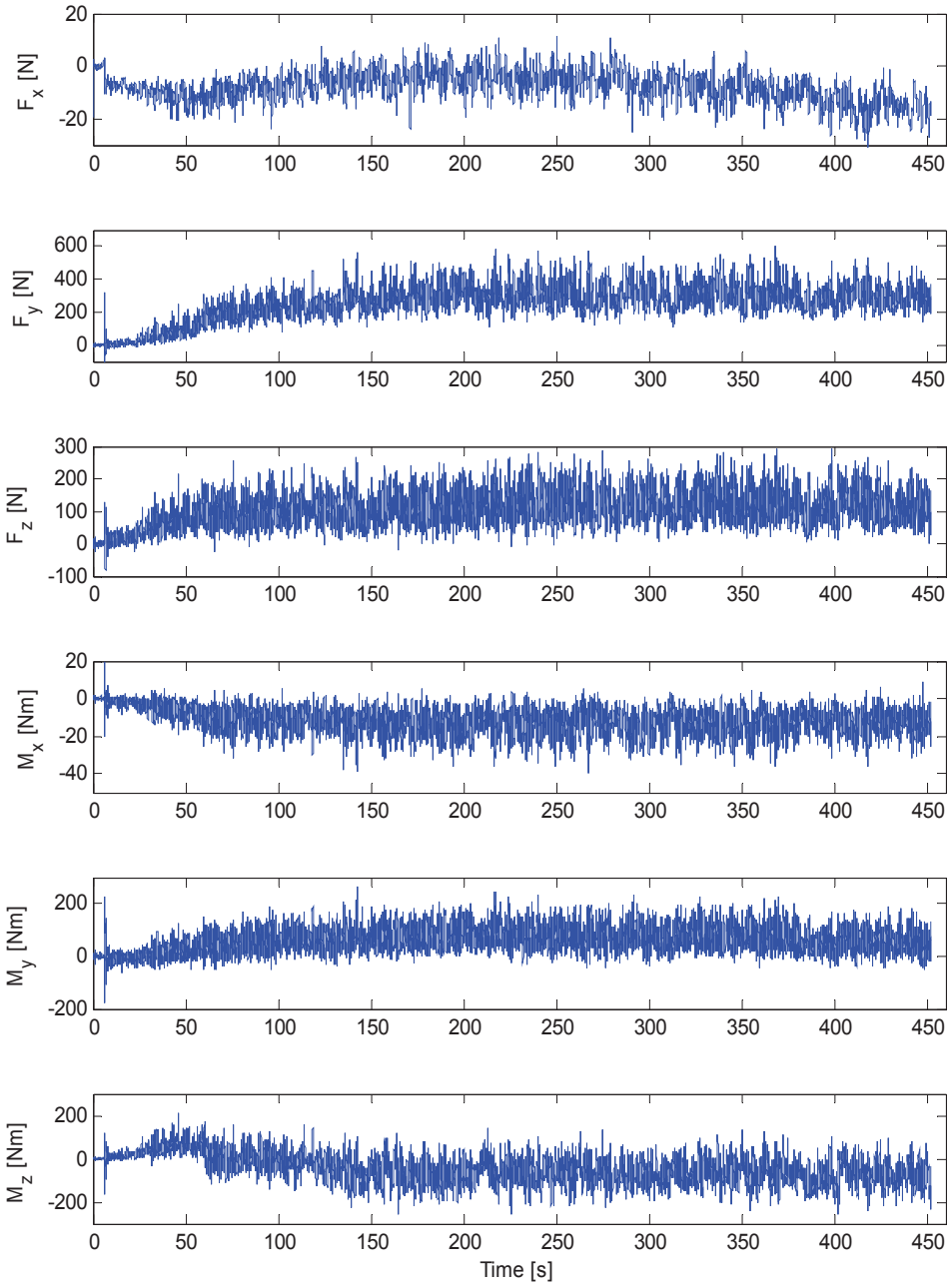

Fig.B.5 Measured ice forces in test 105

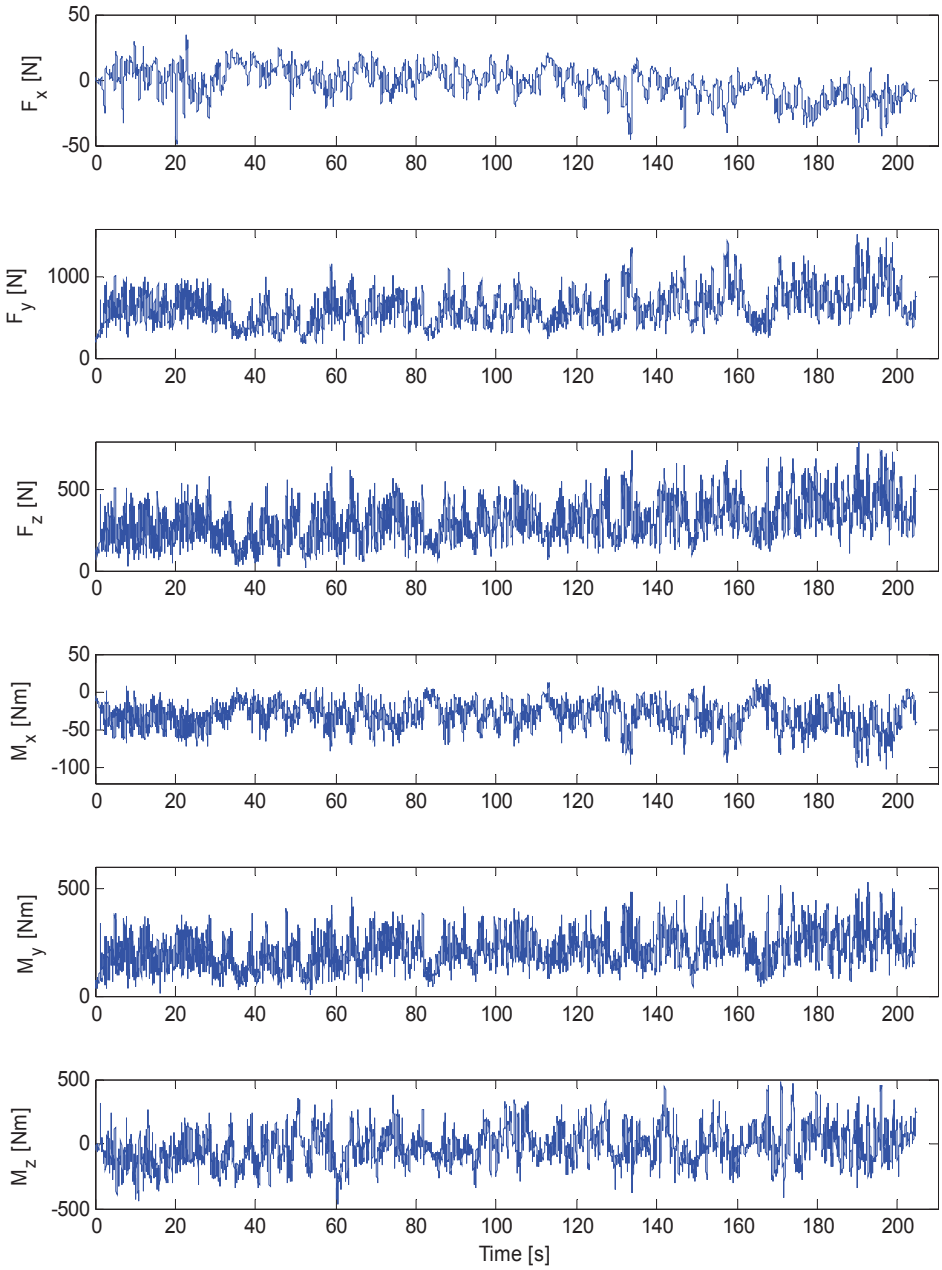

Fig.B.6 Measured ice forces in test 201

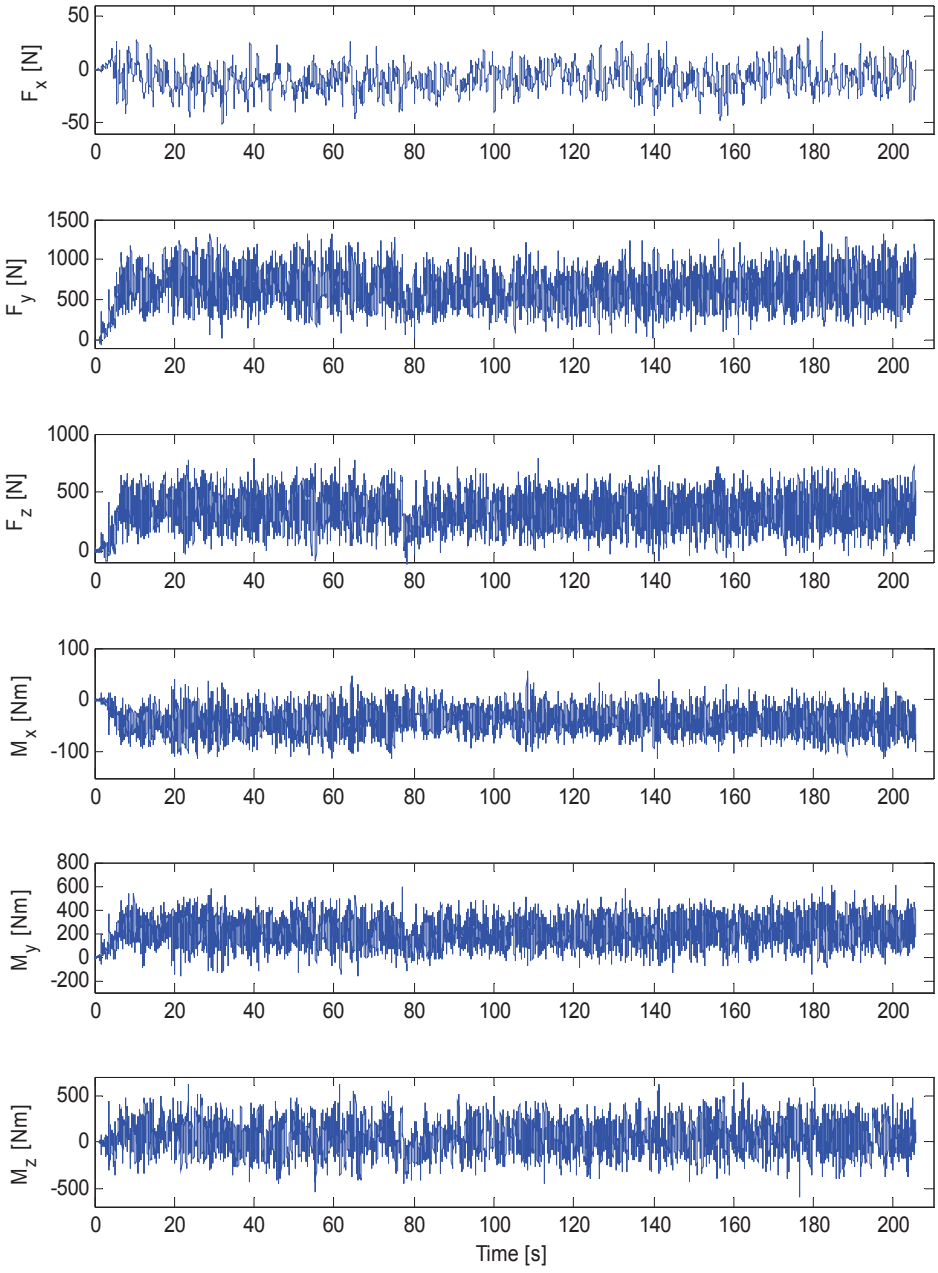

Fig.B.7 Measured ice forces in test 202

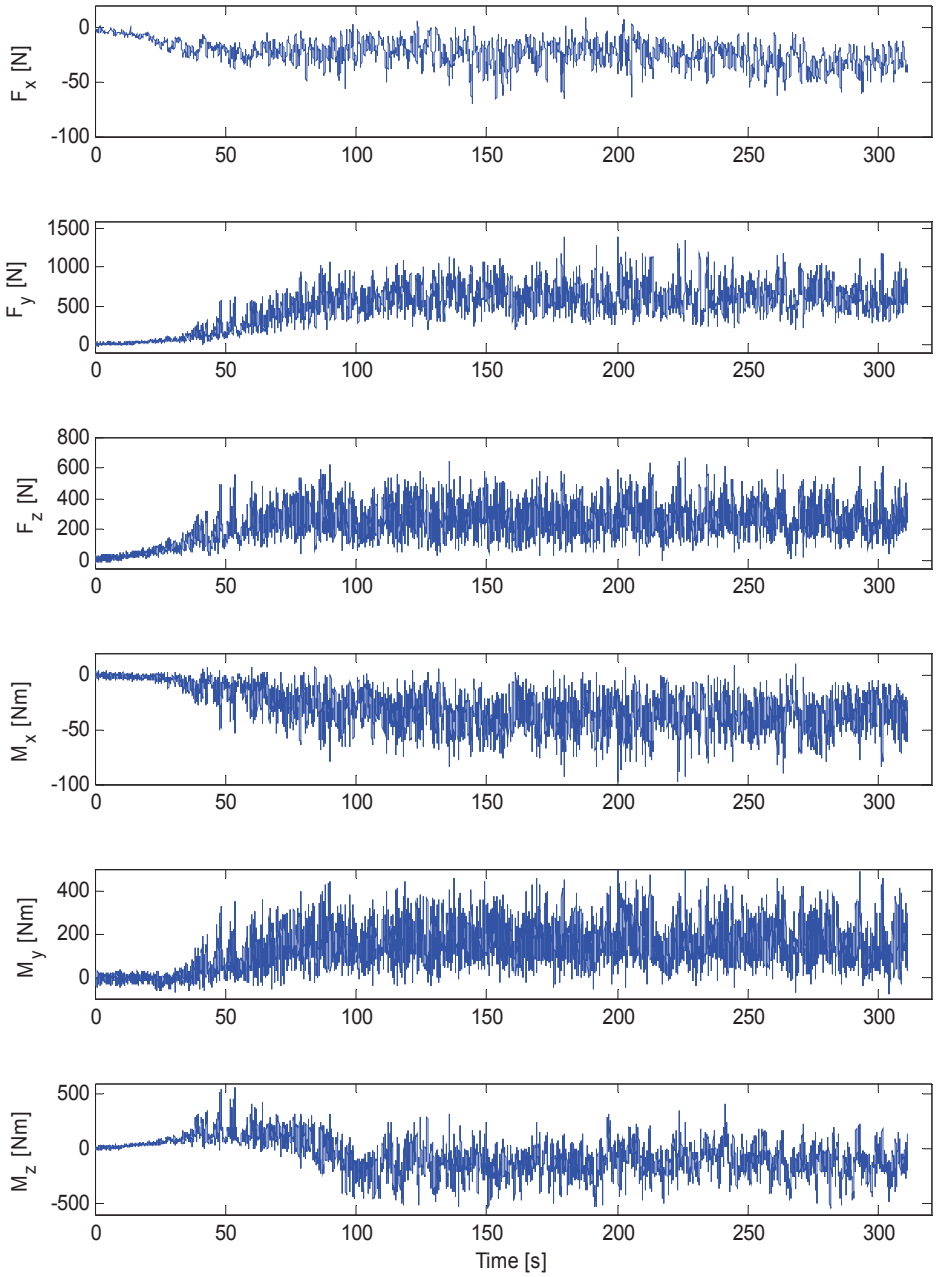

Fig.B.8 Measured ice forces in test 203

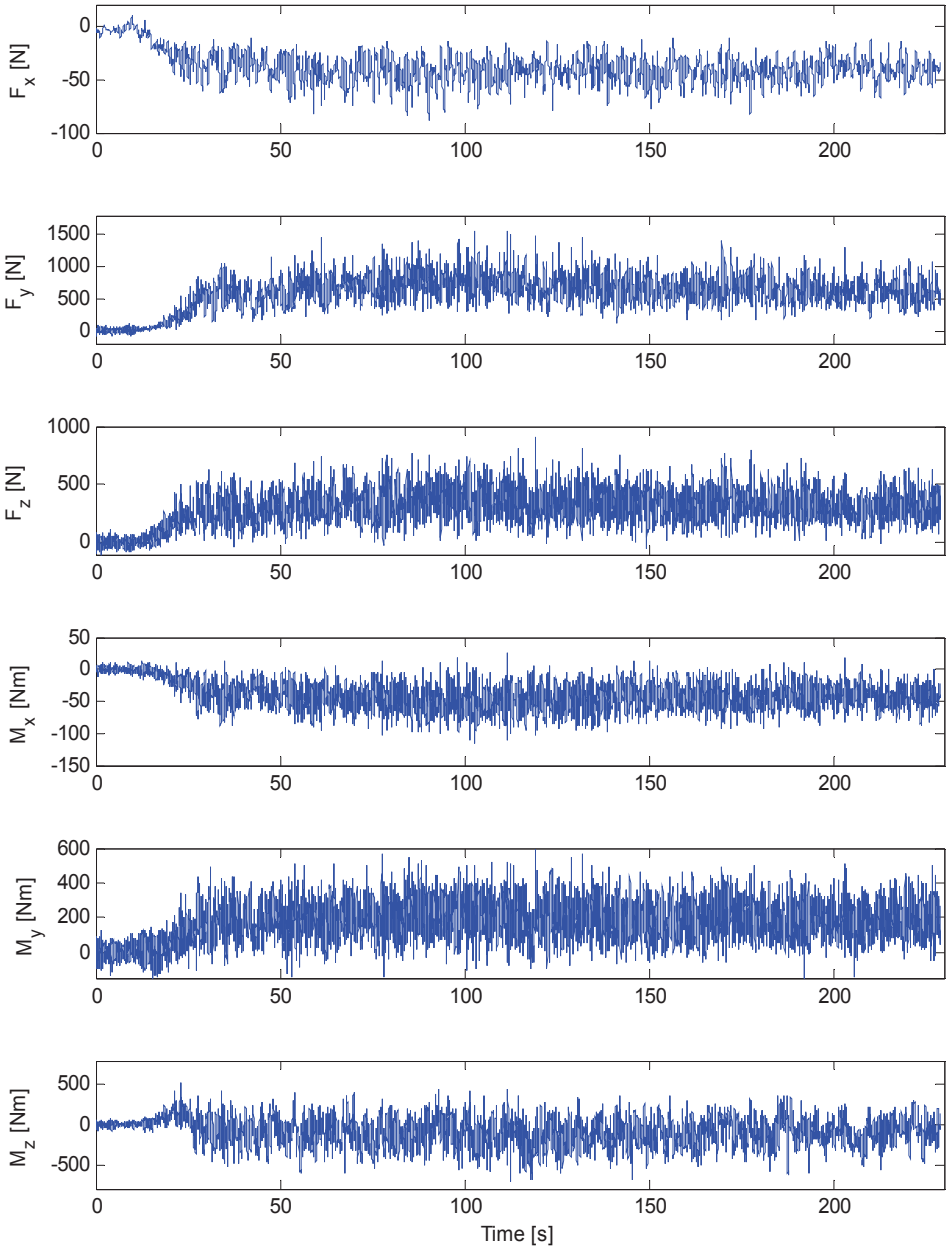

Fig.B.9 Measured ice forces in test 204

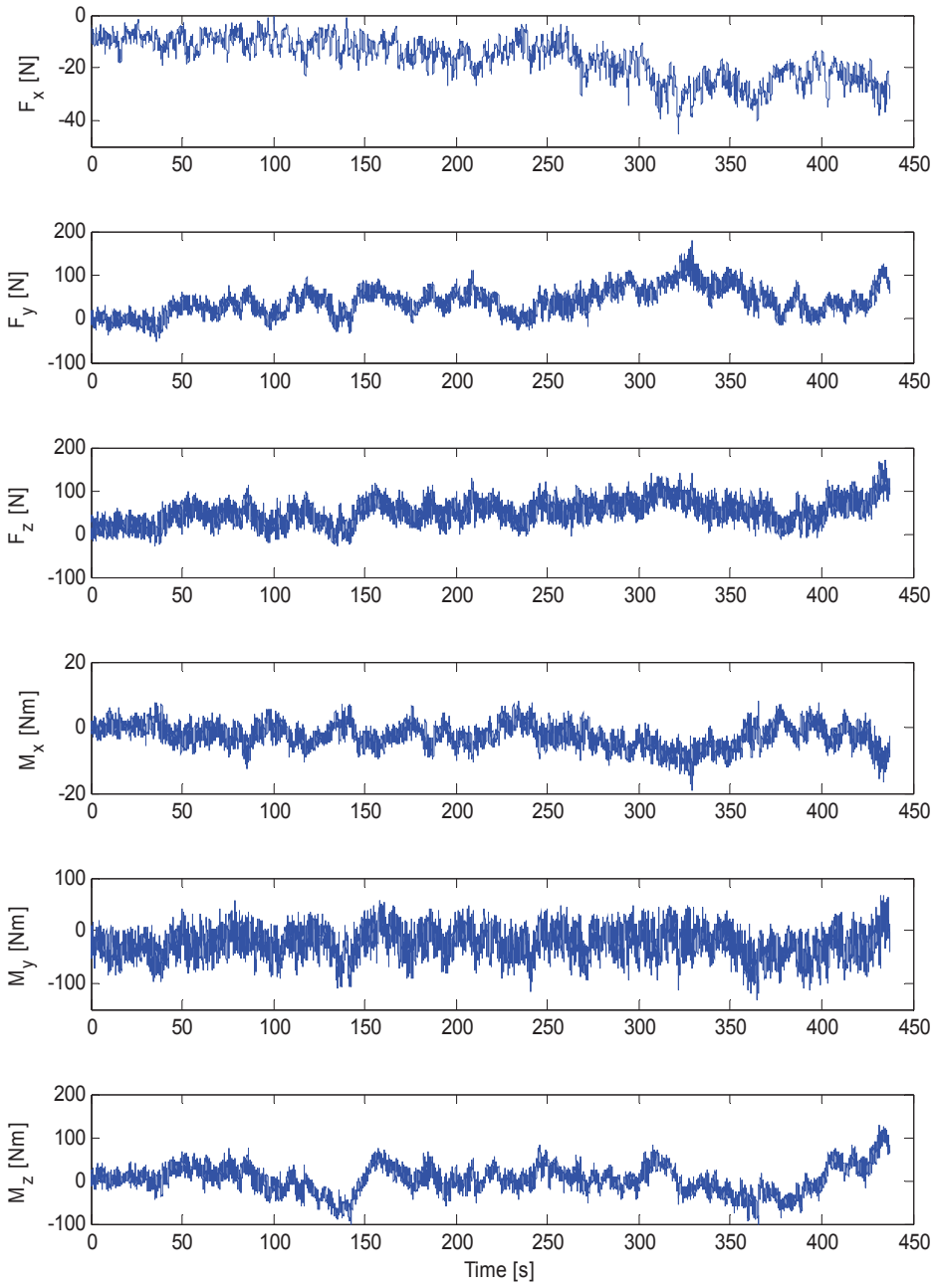

Fig.B.10 Measured ice forces in test 205

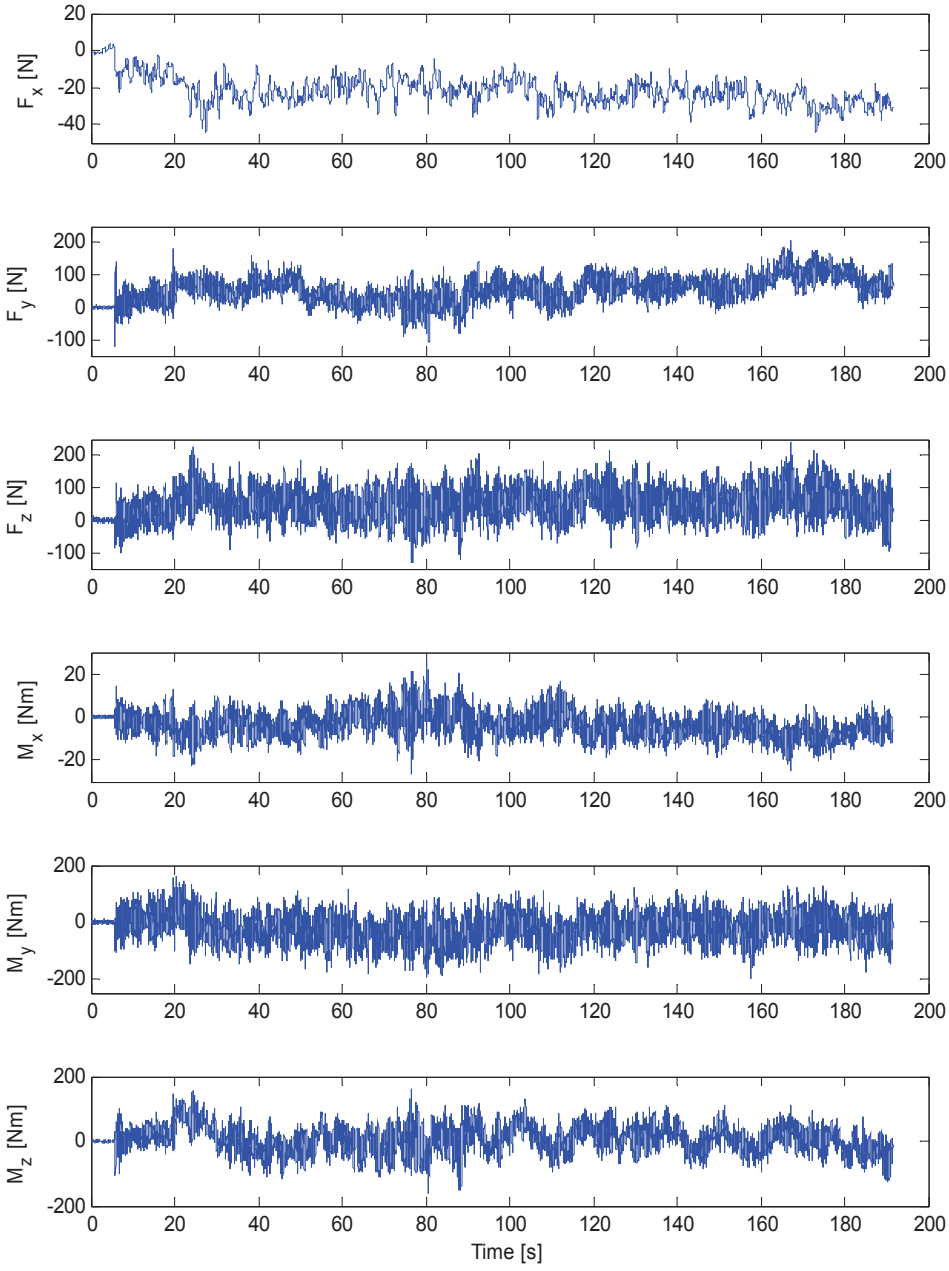

Fig.B.11 Measured ice forces in test 206

Appendix C

Appended Papers

Paper 1:

Numerical simulation of moored structure station keeping in level ice

Paper 2:

Heading control for turret-moored vessel in level ice based on Kalman filter with thrust allocation

Paper 3:

Station keeping capacity of a moored structure with heading control in level ice

Paper 4:

Experiments on level ice loading on an icebreaking tanker with different ice drift angles

Paper 5:

Numerical modeling of ice load on an icebreaking tanker: comparing simulations with model tests

Paper 1

Numerical simulation of moored structure station keeping in level ice

Li Zhou, Biao Su, Kaj Riska and Torgeir Moan

Published in Cold Regions Science and Technology 71 (2012), 54-66

Cold Regions Science and Technology 71 (2012) 54–66

Contents lists available at SciVerse ScienceDirect

Cold Regions Science and Technology

journal homepage: www.elsevier.com/locate/coldregions

Numerical simulation of moored structure station keeping in level ice

Li Zhou [a,*], Biao Su [a], Kaj Riska [a,b], Torgeir Moan [a]

[a] Centre for Ships and Ocean Structures, Norwegian University of Science and Technology, Trondheim, Norway
[b] ILS Oy, Helsinki, Finland

ARTICLE INFO

Article history:
Received 3 May 2011
Accepted 17 October 2011

Keywords:
Numerical simulation
Moored structure
Dynamic ice loads
Planar stability
Heading controller

ABSTRACT

This paper describes a 2D numerical model for the interaction between drifting level ice and a moored structure. The floating structure is treated as a rigid body kept on station by a mooring system, and it can only move in the horizontal plane. The ice-breaking process is modelled using a geometrical method that characterises the contact zones between the hull of moored structure and the ice sheet. Ice rotating and sliding processes are modelled semi-empirically using ship ice resistance formulations. The numerical model predicts the time history of both the ice forces and the global mooring forces as well as the dynamics of the floating structure. The proposed model is validated by comparison with field data. The simulation results obtained with this model are compared with full scale measurements and experimental data from model tests on the Kulluk platform conducted in the Beaufort Sea during the 1980s. The results show good agreement between the field measurements and the model tests. This model is also used to study the influence of turret position on the stability of a moored icebreaking tanker (MT Uikku) under typical varying ice drift speeds and directions. Based on the heading controller, which keeps the hull aligned with the drift ice direction, the effects of ice thickness, ice drift speed and global mooring stiffness on mooring forces and responses of the moored vessel are studied.

1. Introduction

The study of moored structures in ice-covered waters is of interest to oil exploration and exploitation. Although model tests are deemed at present to be the best method of studying the action of ice on moored ships, numerical tools should be developed for initial studies to assist the model tests and the actual design and operation of marine structures in ice-infested areas.

Level ice is a basic component in all ice interactions. For instance, consolidated layers of ice ridges, broken or managed ice when the floes are relatively large can be modelled with level ice methodology. Thus, the investigation of numerical simulations of station keeping in ice begins with level ice.

Many researchers have conducted a great deal of work on the level ice–structure interaction process. Enkvist et al. (1979) discussed the main phenomena in the level ice-breaking process. Kotras et al. (1983) predicted ship performance in level ice. Keinonen et al. (1996) Lindqvist (1989), and Riska et al. (2001) developed semi-analytical and empirical performance models that are of great help in the early stage of designing an icebreaker. Valanto (2001) divided the ice-hull interaction process into four phases: breaking, rotating, sliding and clearing. Wang (2001) also developed a method for simulating the interaction between moving level ice and a fixed conical structure. Based on an ice failure model similar to that derived by Wang (2001), Su et al. (2010) refined the ice-ship contact procedure to simulate ship manoeuvres in level ice. The numerical analysis was validated by comparing simulations with ship performance data from the ice trails of icebreaker AHTS/IB Tor Viking II. Lubbad and Løset (2011) described a numerical model that simulates ship–ice interactions in real time based on the commercial routine PhysX, which was initially developed for computer gaming.

To study moored structures in ice, Sayed and Barker (2011) applied the Particle-In-Cell method based on a hybrid Lagrangian–Eulerian formulation to simulate the interaction between broken pack ice and a moored Kulluk platform. Moreover, (Aksnes, 2010b; Aksnes and Bonnemaire, 2009a) presented a semi-empirical method incorporating probabilistic models based on the model test results. However, this model is limited to one-dimensional simulations in the surge direction only. Moored structures in ice conditions may be subjected to ice drift from different directions depending on variations in currents and wind. The contact geometry and thus ice failure is influenced by the different incident angles between the hull and ice motion. Therefore, more degrees of freedom need to be included in the numerical model. Zhou et al. (2011) presented a 2D method in the horizontal plane for simulating level ice-hull interaction process. It is a basic study of moored ship in ice, and validation was conducted through a standardised scaling up technique of Wright (1999). However, Valkonen et al. (2008) showed a limitation of this scaling up

* Corresponding author. Tel.: +47 41340189; fax: +47 73595528.
E-mail address: li.zhou@ntnu.no (L. Zhou).

0165-232X/$ – see front matter.
doi:10.1016/j.coldregions.2011.10.008

method by comparing field measurements from the icebreaker KV Svalbard and the Kulluk platform and declared that applying the technique to large and wide ships may be unreasonable.

Zhou et al. (2011) compared measurements from the Kulluk with simulated results and dealt with the standardisation procedure. As an extension of that study, the present paper shows a simulation of direct level ice action on the Kulluk to validate the simplified numerical model. Also, the effects of turret position, ice drift speed, ice thickness and global mooring stiffness on moored structure dynamics are studied because these factors play a vital role in predicting level ice–structure interactions.

2. Station-keeping in ice

Floating structure station keeping can be accomplished by three methods: a mooring system; a dynamic positioning system; or a combination of the first and second methods. The pure mooring method is relatively popular. Relevant industrial experience with moored structures has been obtained from drilling operations in the Beaufort Sea (Wright, 1999). Turret moored drill ships that operated in the Beaufort Sea include CanMar's drill ship in the 1970s and 1980s and the conical Kulluk unit in the 1990s. More information about moored structures came from a number of model tests conducted by Comfort et al. (1982), Evers et al. (1983) and Nixon and Ettema (1988). Comfort et al. (1999) assembled an extensive set of ice model test data for floating and moored structures and presented the data in a common format to identify overall trends, and the Kulluk is also included as a typical structure. Recently, Aksnes et al. (2008) and Bonnemaire et al. (2008) carried out ice model tests of an arctic tandem offloading terminal with a focus on mooring forces in level and ridged ice. Later, Aksnes et al. (2010a) and Bonnemaire et al. (2010) conducted ice basin tests on a moored offloading icebreaker in variable ice drifting directions.

3. Overview of the numerical method

In the developed 2D model, only level ice with uniform ice properties is considered. The action of drifting level ice on a moored object is complex, and several ice failure patterns occur, primarily crushing and bending. The resulting broken ice pieces from intact ice may rotate, collide, accumulate, slide along the surface of the structure, and be pushed away from the structure. Nonlinear interactions among the water, structure and ice floes such as ventilation and slamming can arise during this process, especially when the relative speed between the ice and the structure is high. Therefore some assumptions have to be made to simplify the problem.

It is assumed that the ice drift speed is low and thus ventilation and slamming are neglected. Only the local crushing between the structure and the ice and the bending failure that occurs at a distance from the crushing region are involved. A breaking phase dominates the dynamic response of the structure and the other phases mainly determine quasi-static effects. The structure is also assumed to have good ice clearing capacity so that neither does ice pile up nor does the ice rubble accumulate.

Two reference frames are used, see Fig. 1.

- The Earth-fixed frame, denoted as $X_EY_EZ_E$, is placed so that the X_EY_E plane coincides with the water surface, and the Z_E axis is positive downwards.
- The body-fixed frame, denoted as XYZ, is fixed to the vessel in such a way that the origin coincides with the centre of gravity, the X-axis is directed from aft to fore along the longitudinal axis of the hull, and the Y-axis is directed to the larboard.

The horizontal position and orientation of the vessel in the Earth-fixed coordinate system are defined by $\boldsymbol{\eta} \triangleq [x, y, \psi]$, where the first two variables describe the position and the last one describes the angle.

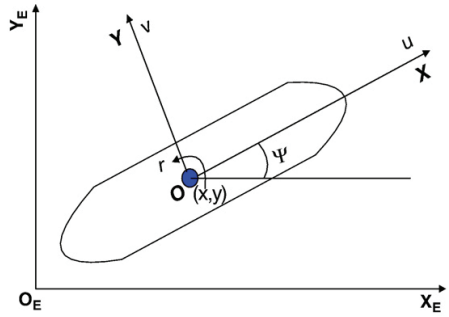

Fig. 1. Earth-fixed ($X_EY_EZ_E$) and body-fixed (XYZ) reference frames in the horizontal plane.

Correspondingly, the translational and rotational body-fixed velocities are defined by $\mathbf{v} \triangleq [u, v, r]$. The body-fixed general velocities are transformed to the Earth-fixed frame by

$$\dot{\boldsymbol{\eta}} = \mathbf{J}(\boldsymbol{\eta})\mathbf{v} \tag{1}$$

where

$$\mathbf{J}(\boldsymbol{\eta}) = \begin{bmatrix} c\psi & -s\psi & 0 \\ s\psi & c\psi & 0 \\ 0 & 0 & 1 \end{bmatrix} \tag{2}$$

where c, s are compact notations for cosine and sine, respectively.

The equation of motion is first expressed in the Earth-fixed coordinate system and then converted to the body-fixed coordinate system. Based on Newton's second law, the linear coupled differential equations of motion in the body-fixed coordinate can be written in the following form:

$$(\mathbf{M} + \mathbf{A})\mathbf{r}(\mathbf{t}) + \mathbf{B}\dot{\mathbf{r}}(\mathbf{t}) + \mathbf{C}\mathbf{r}(\mathbf{t}) = \mathbf{F}_e(\mathbf{t}) \tag{3}$$

where

$$\mathbf{F}_e(\mathbf{t}) = \begin{bmatrix} R_{b1} \\ R_{b2} \\ R_{b6} \end{bmatrix} + \begin{bmatrix} R_{s1} \\ R_{s2} \\ R_{s6} \end{bmatrix} + \begin{bmatrix} F_{m1} \\ F_{m2} \\ F_{m6} \end{bmatrix} + \begin{bmatrix} F_{ow1} \\ F_{ow2} \\ F_{ow6} \end{bmatrix} + \begin{bmatrix} 0 \\ 0 \\ M_\psi \end{bmatrix} + \begin{bmatrix} mvr \\ -mur \\ 0 \end{bmatrix} \tag{4}$$

where $\dot{\mathbf{r}} \triangleq [u, v, r]$. Added mass A is calculated from a boundary element method routine. The damping term **B** is assumed to be zero in the station-keeping mode. The hydrostatic restoring coefficient **C** is zero. The subscripts 1, 2 and 6 refer to the directions of surge, sway and yaw. R_b is the ice-breaking force, which will be described in Section 3.1. R_s is the ice submersion force. Fm is the restoring force due to the mooring system translated from the earth-fixed coordinate system to body-fixed coordinate system by the rotational matrix described in Eq. (2). F_{ow} is the drag force due to the motion of the ship relative to the water. M_Ψ represents the moment produced by heading controller, which is zero if not used in the simulation. The last term in Eq. (4) is due to the translation from the earth-fixed coordinate system into the ship coordinate system.

To numerically solve the equations of motion that were established above, Newmark's method was deployed.

3.1. Ice force model

The ice load acting on a moored ship in unbroken ice or large level ice floes depends significantly on the interaction process by which the hull breaks and displaces the ice. Once the ice contacts the hull, ice is being crushed. The crushing force then increases with increasing contact area until its vertical force component gets large enough to cause

bending failure of the ice, after which the broken ice floes start to turn along the ship's hull until they are parallel to the hull. Finally, the floes submerge and slide along the hull as they are pushed by the next broken ice floes. With this concept in mind, an ice force model composed of an ice-breaking model and an ice rotating and sliding model is briefly described.

The scenario of a ship advancing in level ice resembles that of a moored structure in drifting level ice with respect to the ice-breaking process. Thus, it is reasonable to apply the ice-breaking model described in Su et al. (2010a) in the present model. As for the ice submersion processes, these might be somewhat different. An icebreaker is often moving forward against the ice, whereas a moored structure is often pushed by drifting level ice to move both forward and backward. When a moored vessel moves head on against the ice, the situation is similar to that of an advancing icebreaker; but what if it moves sideways in the same direction of the drifting ice? Thus, modifications need to be made to satisfy the situation considered herein. It was assumed that if the structure moves forward, the bottom will be partially covered by ice and the bow area will be completely covered; if not, the bottom is assumed to be partially covered by ice and the stern area is assumed to be completely covered.

Based on the ice resistance formula of Lindqvist (1989), the modified ice submersion resistance of a moored tanker due to loss of the potential energy of submerged ice floes and friction between the hull and ice floes is written as

$$R_s = \delta\rho g h_i sign(v)\left(BT(B+T)/(B+2T) + \mu\left(A_f + pA_b\right)\right) \tag{5}$$

where $\delta\rho$ is the density difference between water and ice., g is the acceleration of gravity, h_i is the ice thickness, B and T are the main dimensions of the hull, μ is the friction coefficient between ice and hull, A_f and A_b is the area of the bow or stern and of the flat bottom, p is the ratio of the length of the ice covered area to the length of the ship's bottom. *Sign* (v) depends on the velocity of ship v in surge, defined as

$$sign(v) = \begin{cases} 1, \textit{ if } v \geq 0 \\ -1, \textit{ else} \end{cases} \tag{6}$$

In addition, the speed dependence of the submersion resistance is taken into consideration simply as follows:

$$R_s(v_{rel}) = R_s\left(1 + 9.4 v_{rel}/\sqrt{gL}\right) \tag{7}$$

where v_{rel} is the relative velocity between the ship and the drifting level ice sheet, L is the length of the ship.

3.2. Mooring system

An internal turret mooring system is usually applied for the station keeping of offshore structures. The vessel is allowed to rotate around the turret. The internal turret is placed within the ship's hull. It is desirable to utilise turret systems because it is important to be able to disconnect and leave the site quickly and reliably.

The motions of a moored ship in ice conditions are significantly influenced by the mooring lines. Furthermore, mooring systems provide not only time-varying restoring forces but also damping forces, both of which should be taken into consideration in vessel response analysis in the horizontal plane. Mooring line damping is excluded in the following simulation. Only the restoring force due to the mooring system is included herein. RIFLEX (2003) is used to derive the restoring force curves due to the mooring system for various turret offsets. Then, the relation between the restoring forces and the offsets can be pre-calculated and approximated by a curve before the simulation in ice.

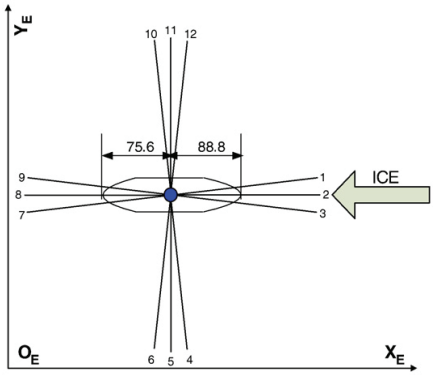

Fig. 2. Horizontal projection of the mooring system.

The mooring system used in the simulations consists of twelve identical mooring lines with three lines in each group as shown in Fig. 2. Each mooring line has an identical chain–wire–chain configuration. The angle between adjacent mooring lines at each corner is 10°. The main characteristics of the selected chain and wire components of each mooring line are listed in Table 1.

The offset-restoring force relationship of the mooring system of the selected set-up in surge and sway is shown in Fig. 3. It is represented by a polynomial function as shown with a solid line.

The coupling effects between deviations in surge and sway are neglected because the mooring arrangement is symmetric about the X–Z plane. If the tanker does not move far away from the equilibrium position, then the mooring restoring force and the offset exhibits an approximately linear relationship with the stiffness of the mooring system equal to approximately 1000 kN/m. The corresponding natural surge and sway frequency is approximately 0.21 rad/s.

3.3. Heading controller

Control actions of the dynamic positioning system are undertaken based on the deviation of the present position measured on-time and the desired input position. Generally speaking, three kinds of control actions are usually used: proportional, derivative and integral control. Proportional control produces a force and moment that is proportional to the difference between the desired state (for instance, the heading is considered as the state herein) and the actual state. Derivative control gives a force and moment that are proportional to the rate of the difference. Integral control gives a force and moment that are proportional to the integral of the difference. In other words, control force proportional to speed is provided by a derivative controller, whereas force proportional to displacement from equilibrium is provided by a proportional controller. These forces are similar to damping and stiffness forces in that they are proportional to velocity (or

Table 1
Characteristics of chain and wire components.

Characteristics	*Chain*	*Wire*	
Nominal diameter (mm)	125	136	
Weight in water (kN/m)	2.67	0.80	
Axial stiffness, EA (kN)	1.03E6	1.64E6	
Non-dimensional normal drag coefficient	2.73	2.33	
Non-dimensional longitudinal drag coefficient	0.30	0.17	
Length of component	upper	lower	125
	25	350	
Total length (m)	500		
Water depth (m)	150		

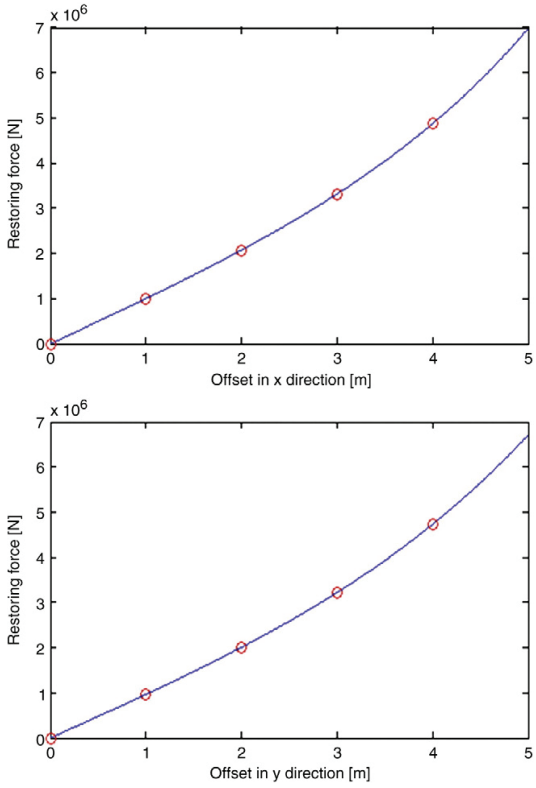

Fig. 3. Offset-restoring force curves of mooring lines.

displacement). If the heading deviates from the desired direction, the controller initiates the actuators to drive the vessel into the desired heading. The control strategy is important for reducing the fuel consumption of the mooring positioning system. The heading controller chosen here is a proportional and derivative control law

$$M_\psi = -k_p\tilde{\psi} - k_d\dot{\tilde{\psi}} \tag{8}$$

where M_ψ is the yaw moment necessary for the propulsion system to counteract the disturbance of external excitation. k_p denotes the proportional gain. k_d is the derivative gain. $\tilde{\psi} \triangleq \psi - \psi_d$ where ψ_d is the desired heading.

In general, the proportional gain is selected so that the natural period of the slowly oscillating ship in yaw is from 30 to 80 s. The derivative gain is set to approximately 50% of the critical damping. Reference is made to Fossen (2002).

4. Model validation

In this section, a wide, moored conical structure (the Kulluk) deployed in the Beaufort Sea during the 1980s is modelled and simulated. The simulation results obtained with the model are validated against full scale measurements and experimental data from model tests of the Kulluk.

Wright (1999) presented a review of operational experience from the Kulluk. It has a downward sloping circular hull near the waterline that breaks the oncoming ice mainly in flexure, and it has an outward flare near the bottom that clears the broken ice cusps away from the moonpool and mooring lines. A photograph of the Kulluk is shown in Fig. 4. The mooring system of the Kulluk is radially symmetric and consists of 12 lines. A linear global stiffness of 1.191 MN/m is assumed for the simulation. The ice characteristics used in the simulation are close to those mentioned in Wright (1999) and are shown in Table 2. The water depth is 50 m.

Fig. 4. A photograph of the Kulluk (Sayed and Barker, 2011).

The underwater hull was taken as a circular conical structure when calculating the drag force F_{ow} in Eq. (4). The heading controller is not necessary at all because the Kulluk has a circular section on the waterline plane. The position at which the turret projects from the waterline plane is located at the centre of the circle. The yaw moment is not of interest in the simulation because the heading does not affect the ice-breaking process. It should be noted that only the bow area is taken into consideration when calculating the ice sliding and rotating forces because almost no broken ice floes go under the bottom due to the outward flare. Half of the surface of the bow area of the Kulluk underwater is considered. The added mass $\boldsymbol{A}$ is calculated using the software SESAM.

An example of a time series from the simulation using an ice drift velocity of 0.6 m/s and ice thickness of 1.0 m is given in Fig. 5, where ice forces and translational velocities of the Kulluk are given in body-fixed coordinates and global mooring forces and displacements of the Kulluk are given in earth-fixed coordinates. Fig. 6 shows a part of the ice force in surge from Fig. 5.

Thirty cases with ice drift velocity of 0.6 m/s and ice thicknesses ranging from 0.05 m to 1.5 m are simulated. The derived mean, standard deviation, and maximum mooring force versus ice thickness are plotted in Fig. 7. The full scale data and model test data from the Kulluk are also shown in Fig. 7 for comparison.

Table 2
Ice characteristics.

Parameter	*Symbol*	*Value*	*Unit*
Density	ρ_i	880	kg/m^3
Young's modulus	E	5400	MPa
Poisson ratio	γ	0.33	
Crushing strength	σ_c	2.3	MPa
Flexural strength	σ_f	0.5	MPa
Frictional coefficient	μ_i	0.15	

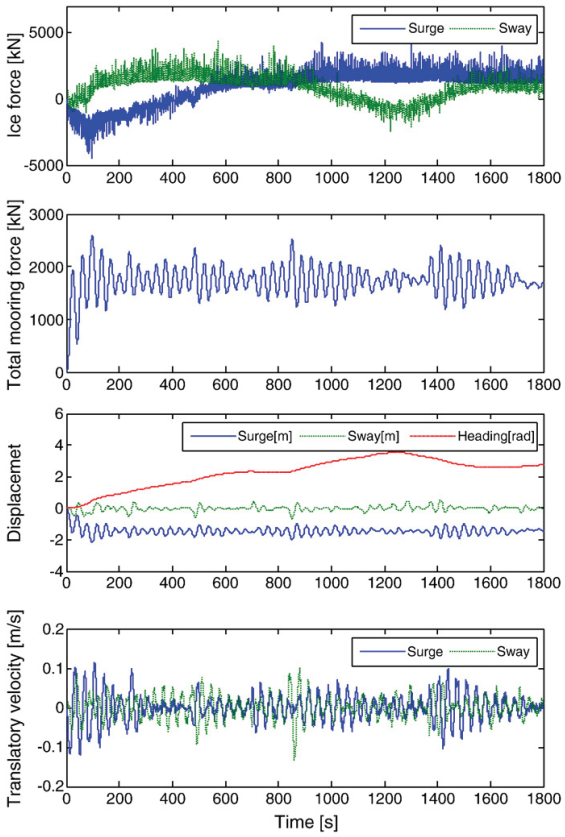

Fig. 5. Simulated time series of ice forces, mooring forces and responses of the Kulluk.

Fig. 7 shows that the simulated loads show fairly good agreement with the full scale measurements, although some scatter exists in the full scale data. The mean mooring force increases monotonically with ice thickness. The HSVA test results agree well with the full scale loads, but they are somewhat high for thicker ice. The IIHR tests measure slightly high, especially at the ice thickness of 1.1 m. This increased reading may be attributable to higher ice flexural strengths in the model tests. The ice sheets in the ACL tests were made from

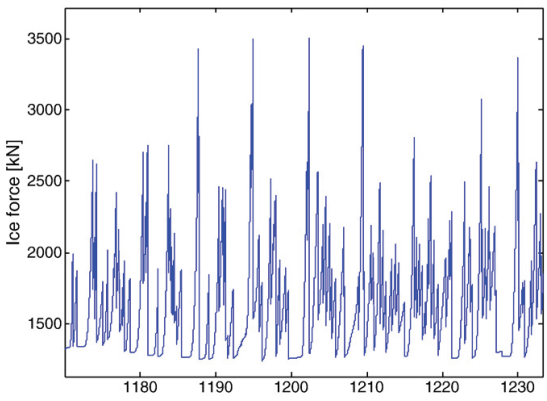

Fig. 6. An episode of ice force in surge from Fig.5.

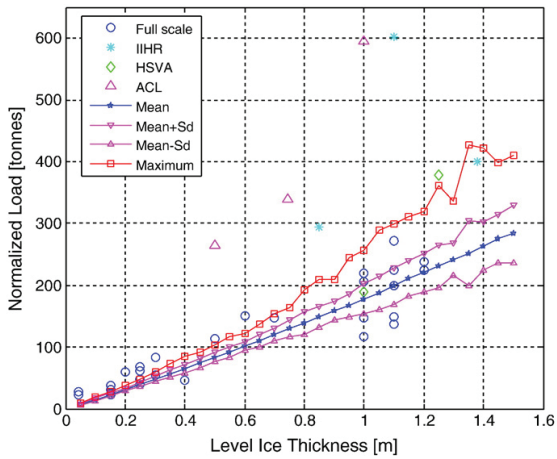

Fig. 7. Comparison of simulated Kulluk loads, full scale loads and model tests in level unbroken ice.

wax, which results in a relatively high friction coefficient between the hull and the level ice.

Some deviations remain between the simulation results and the full scale data. There are many reasons for these deviations. One reason may be a lack of necessary information on the density, friction coefficient and drift speed of the ice, which is required in the simulations. Sensitivity studies assessing these factors need to be carried out. Another reason for the differences may derive from the fact that the original measurements involved ice interactions at different times of the year and in different years. Resulting variations in ice strength and ice friction are normalised based on a vessel resistance prediction formula (Keinonen et al., 1996). However, according to Valkonen et al. (2008) this normalisation approach is controversial when applied to large and wide ships, a category to which the Kulluk belongs.

In addition, Wright (1999) presented a load versus ice drift speed scatter plot. To compare this with calculations, ten simulation runs were made where the ice thickness was set to be constant at 1 m and the ice drift speed ranged from 0.025 m/s to 0.6 m/s, being the same conditions as those normalised in Wright (1999).

The calculated loads of interest are plotted against those obtained from Wright (1999) in Fig. 8. The field data show no obvious effect of ice drift speed on the ice load level on the Kulluk in level ice. The simulated loads coincide with the measurements very closely. The mean mooring forces do not change much as the ice drift speed varies, but they tend to increase monotonically as the ice drift speed increases when the speed is above 0.3 m/s. In the simulated cases, the dynamics of the Kulluk are more pronounced at low ice drift speeds than under high drift speed conditions.

When the ice drift speed is approximately 0.2 m/s, the maximum mooring force to mean mooring force ratio is up to 2.5, which indicates a large oscillation. Notably, there is a difference between the full scale results and the numerical maximum for velocities from 0.1 to 0.2 m/s. There are three main reasons for this difference. One reason is that the frequency range where the main ice force energy concentrates is close to the natural frequency of the Kulluk. This factor will be explained in more detail in Section 5.5.3. The second reason may be that damping from the hull of the Kulluk and the mooring system, which affects the amplitude of oscillation, is not taken into consideration. However, evaluating the damping of moored structures in ice is complicated. More results about damping should be available especially for the reliability analysis of moored structures operating in ice-infested areas. The third reason for the scatter in the results

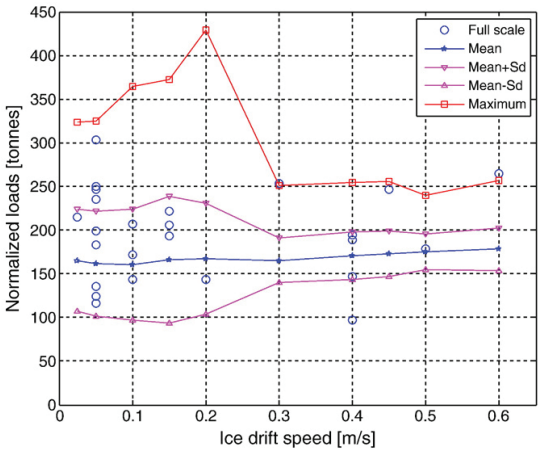

Fig. 8. Simulated loads and full scale loads of the Kulluk in level ice versus ice drift speed.

at low speeds is that the mooring load data obtained at 0.1 to 0.2 m/s may not capture the dynamic characteristics of the Kulluk.

Comparing Fig. 7 with Fig. 8 shows that the maximum mooring loads on the Kulluk with ice thickness of 1.0 m and drift speed of 0.2 m/s are close to those with ice thickness 1.4 m and drift speed 0.6 m/s, which clearly shows the effect of low ice drift speed on the peak mooring forces.

Although there are some uncertainties in the validation, this numerical model is suitable for studying and simulating the dynamics of moored structures and ice forces judging from a comparison of the simulated data with field data from the Kulluk.

5. Analysis of mooring in level ice

5.1. Setup of numerical implementation

Station-keeping is simulated with primarily ice load taken into consideration because of its greater influence on the behaviour of moored vessels compared to other environmental loads. In this section, an icebreaking tanker named MT Uikku is moored in level ice. The response of the moored ship in the horizontal plan is derived in drifting ice at a constant speed. The level ice used in the following simulations is assumed to have the constant properties shown in Table 2.

MT Uikku is a double-hull icebreaking motor tanker that was constructed to meet the standards of the highest Finnish-Swedish Ice Class, IA Super. The primary dimensions of MT Uikku are given in Table 3. A 3D ship geometry model of MT Uikku was developed to calculate the hydrodynamic coefficients, which are required for the calculation of the ship's motions.

The basic geometrical model includes the waterline of the ship and the edge of the ice, both of which are discretised, as shown in Fig. 9. The ice nodes are defined with horizontal positions (x, y) and a normal downward frame angle (φ), whereas the hull nodes are defined with horizontal positions (x, y) and ice thickness (h_i).

Table 3
Primary dimensions of MT Uikku.

Primary dimension	*value*	*unit*
Length over all	164.4	m
Length between perpendiculars	150.0	m
Breadth moulded	22.2	m
Draught	12	m
Displacement	22,600	ton
Deadweight	15,750	ton
Block coefficient	0.72	

5.2. Examples of time series

Turret position and ice drifting angle are defined in Fig. 10, where *Lct* denotes the distance between the vessel's centre of gravity and the location of the turret in body-fixed coordinates, and the ice-drift angle is the angle between direction of the incoming ice and the longitudinal axis of the vessel.

The vessel is supposed to rotate freely due to excitation from ice without using heading control. The distance Lct is selected as Lpp/3 and the drift angle is zero. The ice thickness is constant at 0.6 m. Time histories of ice forces, the total mooring forces and turret offset are presented in Figs. 11, 12 and 13.

As shown in Fig. 11, the submersion process in surge varies slowly while the icebreaking process is of short duration and acts on the structures as impulse peaks. This does not mean the icebreaking force is trivial compared to other ice force components. Lubbad and Løset (2011) pointed out that the contribution of the ice-breaking force to the total ice force varies with the interaction speed from approximately 55% at low speeds to approximately 25% at high speeds. How the ice-breaking force influences the dynamics of a moored structure mainly depends on the ice thickness, the ice drift speed, the global mooring stiffness and the mass of the structures. Therefore, parameter sensitivity analysis for moored floaters in ice is necessary.

Fig. 12 gives the resultant time-varying mooring forces in surge and sway. Although it is difficult to compare these with model test results directly at present, their plausibility can still be assessed. Aksnes and Bonnemaire (2009a, 2009b) performed model tests of a moored ship in variable level ice drifts and measured maximal mooring forces between 1.9 and 2.6 MN in straight ice drift. Considering the differences in ice thickness, ice properties and bow shapes between the model tests and

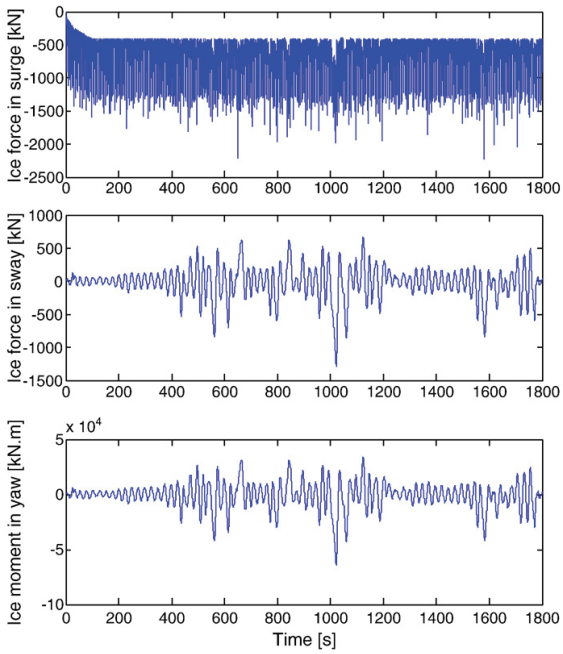

Fig. 9. Discretisation of the ship hull and ice edge.

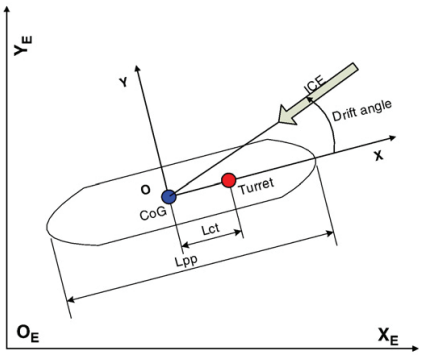

Fig. 10. Definition of turret location and drifting angle.

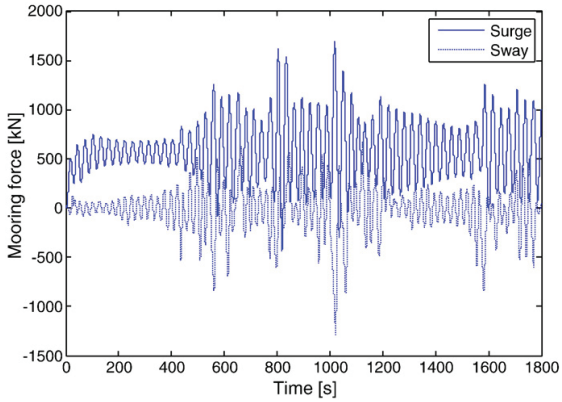

Fig. 12. Time series of total mooring forces in surge and sway.

the simulation, the load level of the numerical model (approximately 2.0 MN) is reasonable.

Fig.13 shows that the turret offset oscillates around a certain value, and the heading appears to be stable at 0 angle with maximum deviation less than 0.03 rad.

5.3. Analysis of stability without heading control

In the previous section, the simulations were carried out with Lct fixed. The effect of Lct on the stability of a moored tanker without heading control is investigated in this section. Lct ranges from 0 to Lpp/2.5. The ice-drift angles are selected to be 0 and 15°. The ice drift speeds are set to be 0.2 and 0.6 m/s, respectively. Therefore, four cases are simulated as listed in Table 4.

The simulated time history of heading and the statistics of turret position for the four cases are shown in Figs. 14–21. When the turret position is located at the centre of gravity of the tanker in all four cases, the tanker becomes unstable as Figs. 14, 16, 18 and 20 show.

Fig. 14 shows that unstable rotation occurs if the turret is located at less than Lpp/20 away from the centre of gravity. The ice-vaning capability tends to be dominant as Lct increases to Lpp/8. The mean turret offset does not vary much and the standard deviation of the offset is almost constant, as seen in Fig. 15. When the ice drift speed increases to 0.6 m/s, Fig. 17 shows that the tanker keeps its heading very well when Lct is larger than Lpp/6. However, the statistics of turret offset shown in Fig. 17 are different from those in Fig. 15 in that both the mean and maximum offsets are very sensitive to the turret location. In particular, the maximum offset at lower speed is obviously smaller than that at higher speed in the case of the same turret position of less than Lpp/8.

For cases 3 and 4, the combined effects of ice-drift angle and turret position on the stability of a moored tanker are considered in Figs. 18–21. Fig. 18 shows three different turret position trends: (1) For Lct less than Lpp/10, the tanker seems unstable; (2) For Lct larger than Lpp/4, the tanker becomes stable heading at 15°; (3) For medium Lct, the heading oscillates around 0°. The simulated turret offset statistics in Fig. 21 are also sensitive to location. It is worth noting

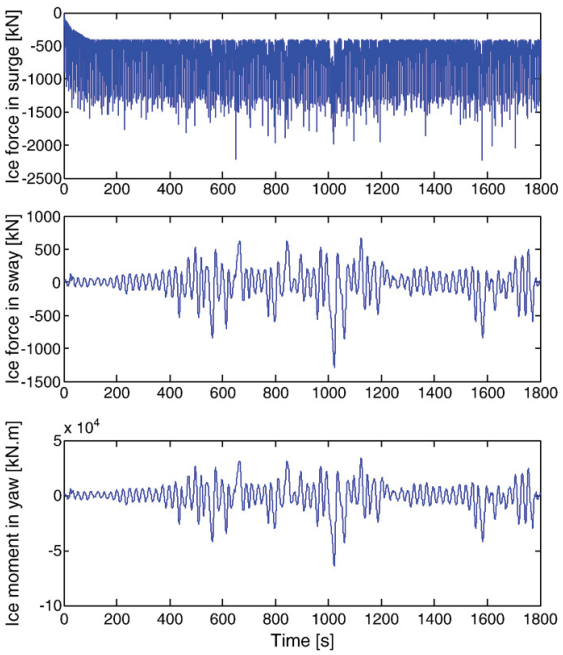

Fig. 11. Time series of ice forces.

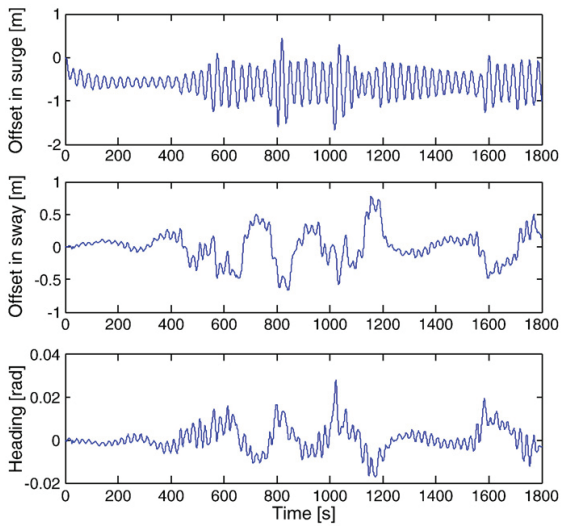

Fig. 13. Time series of turret offset and heading.

Table 4
Matrix of simulated cases.

Case	*Drift speed [m/s]*	*Drift angle [deg]*
1	0.2	0
2	0.6	0
3	0.2	15
4	0.6	15

that the maximum offsets in Fig. 21 are larger than the corresponding values obtained from Fig. 15 due to different ice-drift angles. The difference is mainly attributable to the ice crushing occurring between the ice and the sides of the hull when the ice-drift angle deviates from 0 or 180°, which results in a significant increase in ice forces. As for the mean deviation of the turret, it is interesting that it is larger than that in Fig. 15 when Lct is less than Lpp/5, whereas it is almost the same in the two cases if Lct is larger than Lpp/4. Fig. 20 shows a trend similar to that in Fig. 18 except that the tanker turns to an almost constant angle, −165°, where the tanker is parallel to the ice with stern forward. The response of a moored tanker appears to be more sensitive to turret position in higher ice drift speeds than in lower ice drift speeds, as revealed by comparing Fig. 20 with Fig. 18. Furthermore, Fig. 21 shows that the maximum, mean and standard deviation of turret excursion are not significantly affected by the location of the turret if it is beyond Lpp/4.

The weather-vaning capabilities of a moored tanker in ice have not been well characterised. Hansen and Løset (1999) performed numerical simulations of the horizontal response of a turret moored ship to investigate the effect of the longitudinal position of the moored ship on the stability of the vessel interacting with broken ice. It was found that there seems to be an optimal range of turret position in broken ice.

The present method, based on selected case studies and related analysis of simulation results, also shows that the turret position has a great influence on the horizontal response (and hence stability) of a moored vessel, especially in highly dynamic ice conditions. An optimal range for turret position exists for moored vessels operating in level unbroken ice. Regarding general arrangements, the turret position is as close to mid-ship as possible and for stability purposes as far forward as possible. The optimal turret location for the present case is approximately Lpp/4.

5.4. Parameter sensitivity analysis with heading control

It was demonstrated in Section 5.3 that when the turret position gets close to the centre of gravity of the tanker in level ice, even if the ice moves against the hull in straight manner, it is likely that the hull will rotate due to the non-symmetric action of the ice in the yaw direction and the lack of stabilising capacity.

With the goal of considering the worst stability situations, the heading controller takes effect in the following simulations. Sensitivity studies are carried out with respect to the effects of ice thickness, ice drift speed and mooring stiffness on the dynamics of a moored tanker.

5.4.1. Effect of ice thickness

According to a report of full scale measurements for the Kulluk with a cylindrical hull drilling in the Beaufort Sea and to model test data (Wright, 1999), there is a clear trend of increasing load with increasing ice thickness, although some scatter appears in the data. Comfort (2001) also found that ice loads increase with increasing ice thickness in model tests of the Kulluk and turret-moored tankers. It is desirable to compare the calculated results with full scale data from moored tankers. Unfortunately, such data are still not available due to source limitations. Thus, the effect of ice thickness is studied by numerical simulations.

The ice drift speed is assumed to be constant at 0.6 m/s. The selected ice thickness in the simulation ranges from 0.5 m to 0.7 m with an

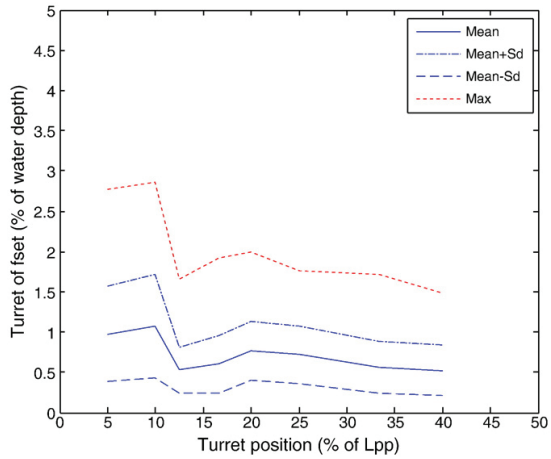

Fig. 15. Statistics of turret offset for case 1.

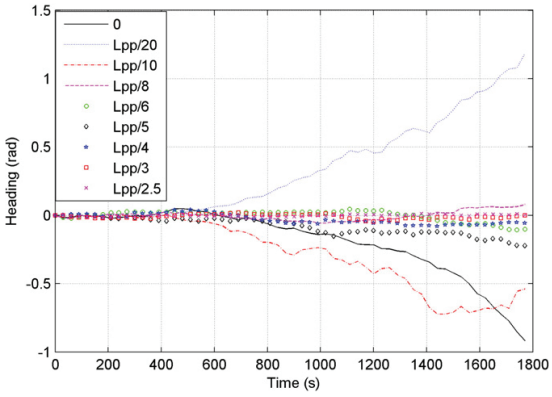

Fig. 14. Heading time series for case 1versus distance (Lct).

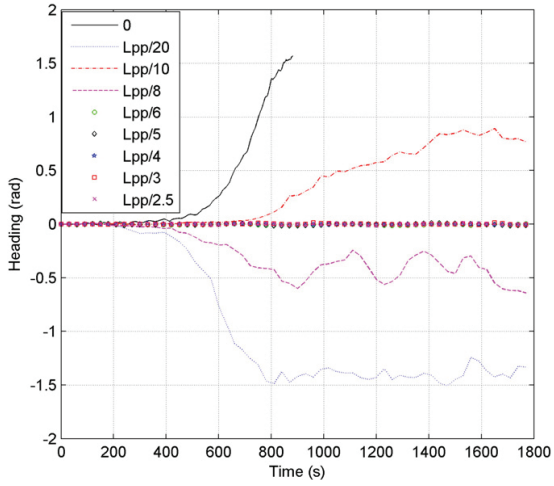

Fig. 16. Heading time series for case 2 versus distance (Lct).

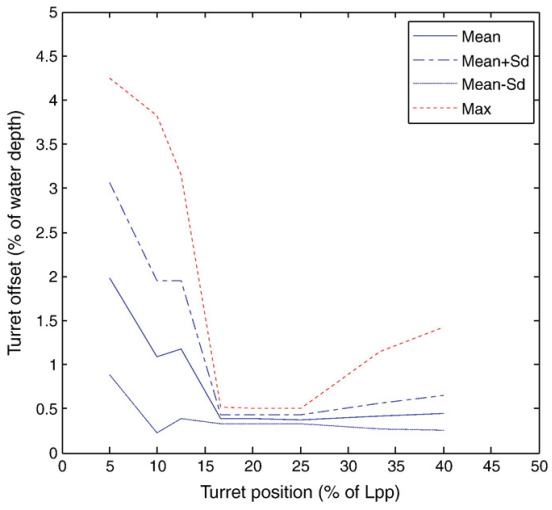

Fig. 17. Statistics of turret offset for case 2.

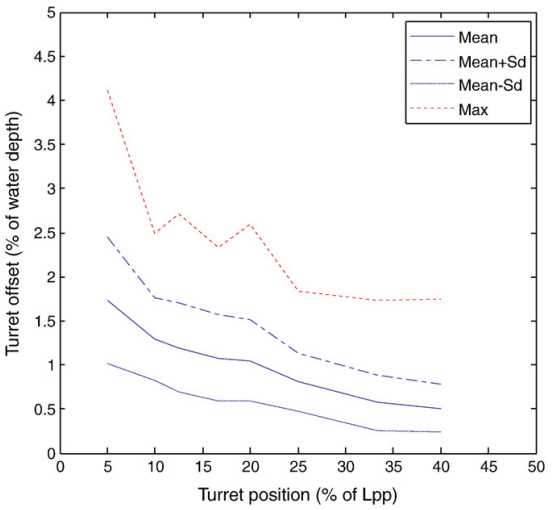

Fig. 19. Statistics of turret offset for case 3.

interval of 0.05 m. The simulation results and ice resistance calculated according to formulations by Lindqvist (1989) are shown in Fig. 22. The simulated ice resistance is close to the ice resistance based on Lindqvist's method when the ice thickness is below 0.4 m. This finding was expected because the ice submersion model is derived from Lindqvist's formulation. However, when the ice thickness increases, the simulated ice resistance tends to exceed that calculated by Lindqvist. Lindqvist's method predicts the ice resistance to be approximately linearly proportional to the ice thickness, whereas the fitted curve derived from the simulated ice resistance shows a power of 1.354. Fig. 22 shows that the simulated ice resistance does not increase with ice thickness monotonically. For instance, the simulated loads did not vary much when the ice thickness was changed from 0.5 m to 0.6 m. This may be attributable to the different icebreaking patterns formed in the interaction between the hull and the two types of ice sheet. Su et al. (2010a) provided more details on this phenomenon.

5.4.2. Effect of ice drift speed

Vessels operating in ice-infested water encounter different ice features with various ice drift speeds. For a moored ship in level ice, the effects of ice drift speed on the ice load acting on the hull must be taken into consideration. Hence, the response of the moored tanker and the corresponding ice force is simulated by varying the ice conditions to further study the influence of ice drift speed on the interaction between a moored tanker and ice.

Ice drift speed plays a very important role in the dynamics of ice loading for moored vessels in broken ice, level ice and ice ridges, as noted earlier. However, little information about the effects of level ice drift speed is available. So far, most information has been obtained from full scale measurements of the Kulluk. Toyama and Yashima (1985) applied a numerical model and a model test to conclude that the surge response was greater at low ice drift speeds. Wright (1999) claimed that there is no obvious effect of ice drift speed on the load levels that the Kulluk experiences. Comfort et al. (1999) also failed to identify any trends when investigating the effects of ice speed on turret moored ships. Recently, Aksnes and Bonnemaire (2009a, 2009b) predicted that a moored ship would experience a large surge motion at low speeds. Aksnes (2010b) reported that local ice forces on the bow waterline increase with drift speed according to model tests. As a new method of simulating the ice-ship

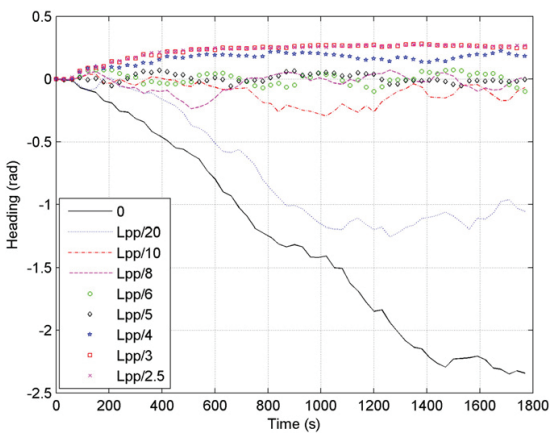

Fig. 18. Heading time series for case 3 versus distance (Lct).

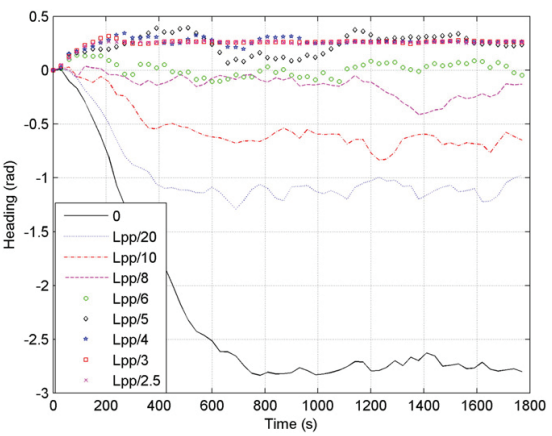

Fig. 20. Heading time series for case 4 versus distance (Lct).

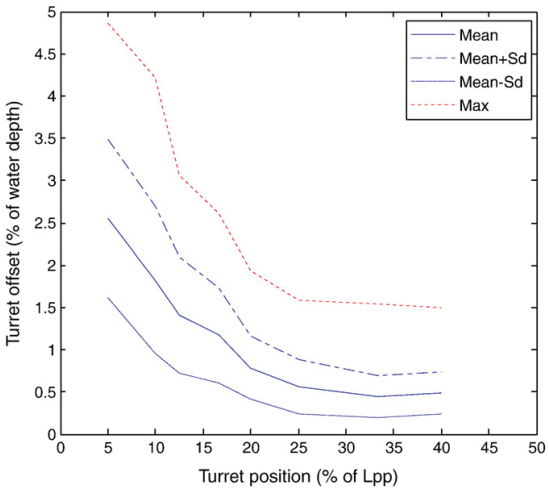

Fig. 21. Statistics of turret offset for case 4.

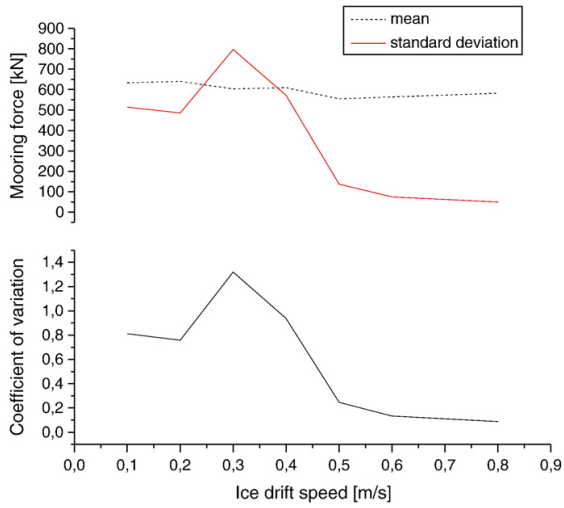

Fig. 23. The mean, standard deviation and coefficient of variation of the mooring force for various ice drift speeds.

interaction, it is of course a good idea to look into the effects of ice drift on the ice loading process.

In this study, the ice thickness is constant at 0.6 m. The ice drift speeds selected for the simulation are 0.1, 0.2, 0.3, 0.4, 0.5, 0.6, 0.8 m/s. The response of a moored vessel in surge is mainly taken into consideration because it dominates the response. The results are presented in terms of representative statistics in Fig. 23, which shows that the mean mooring force is almost constant as the ice drift speed increases, whereas the maximum and standard deviation of the mooring forces are affected significantly by the ice drift speed. The effect velocity varies depending on its range. There is no obvious velocity effect on mooring force deviation when the ice drift speed is relatively low. When the ice drift speed increases from 0.2 m/s to 0.3 m/s, there is an increase in the maximum offset and velocity of the vessel in surge. Then, the amount drops down quickly and tends to approach zero asymptotically as the ice drift speed continues to increase. On the whole, the tanker experiences higher mooring force variance in the plane with lower drift speeds (below 0.4 m/s) compared to that with higher drift speeds. As shown in Figs. 24 and 25, the mean offset does not change much with ice drift speed, whereas the mean velocity of the vessel remains constant at zero. It should be emphasised that the tanker seems to experience significant motion under the influence of ice at lower speeds, which corresponds to high mooring force variance due to the approximately linear relationship between the mooring force and the offset of the tanker. When the ice drift speed increases, the magnitude of the motion and velocity of the tanker tend to decrease rapidly, which indicates that the tanker will be more stationary.

The reason for the observed behaviour may be explained as follows. Once the vessel is approached by incoming ice, crushing occurs in the breaking phase. Because the vessel is moored, it moves away in the same direction with the drifting ice. Then, the ice-breaking force decreases slightly at the beginning of contact and then increases as the ice penetrates the hull further. Thus, the ice-breaking phase in the process of the ice-hull interaction may last for a longer time period than it would have if the tanker was fixed. In this way, the ice-breaking force

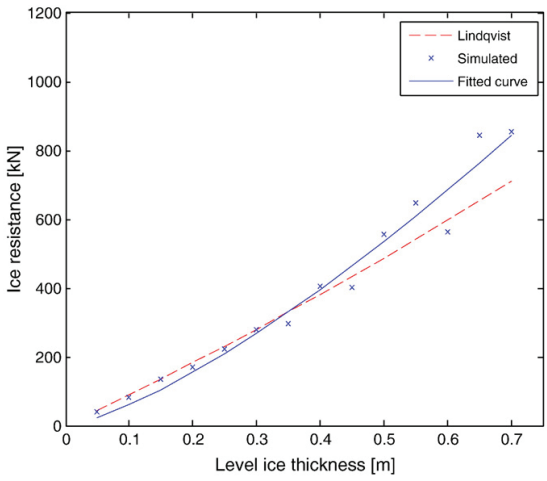

Fig. 22. Ice resistance versus ice thickness.

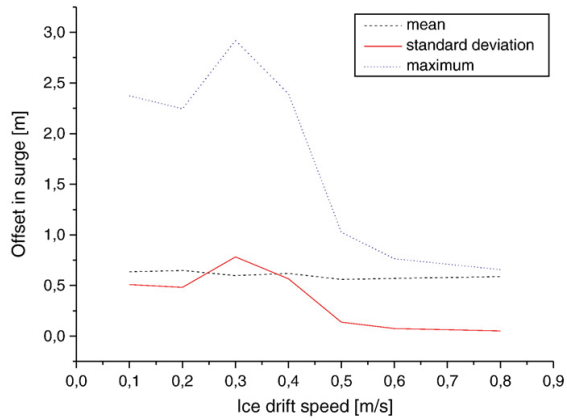

Fig. 24. The mean, standard deviation and maximum of the tanker offset at various ice drift speeds.

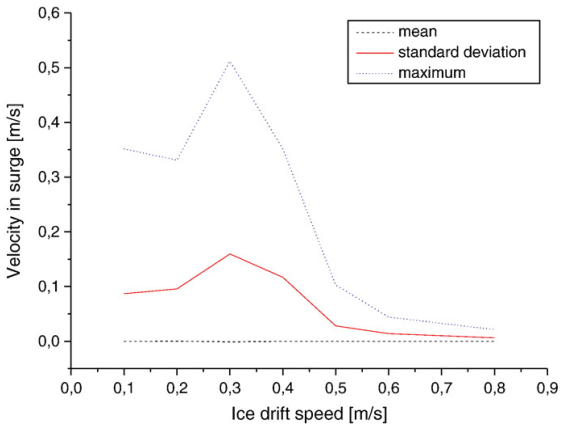

Fig. 25. The mean, standard deviation and maximum of the tanker's velocity at various ice drift speeds.

is significantly influenced by the relative motion between the ice and the tanker. If the ice drift speed is low, the crushing phase lasts longer. Consequently, the force of the ice (including the submersion and sliding forces) is mainly concentrated in a long time period and a low frequency. In contrast, if the drift speed of the ice sheet is high, the ice-breaking process is completed rapidly. This implies that ice-breaking forces with high frequencies dominate the total simulated ice force regardless of the submersion and sliding components, which have comparatively low frequencies. Moreover, a moored vessel always acts as a low-pass filter on ice forces. This means that at high drift speeds, ice forces occurring at a certain instant work as an impulse that is unable to be sensed by the mooring system and thus cannot be transmitted to the mooring system unless the impulse has a period above the vessel's natural period.

Spectral analysis of the simulated ice force at ice drift speeds of 0.1, 0.3 and 0.6 m/s were performed to verify this point (Fig. 26). It is also clear from the ice force spectrum that the main energy shifts towards higher frequencies as the ice sheet velocity increases. When the velocity of the ice sheet is approximately 0.3 m/s, more energy is located around the natural frequency of a moored tanker, which leads to pronounced motion with large amplitude. If the velocity of the ice sheet continues to increase (more than 0.5 m/s), the duration of each ice failure event decreases dramatically, which means that the high frequency range where the main energy of the ice concentrates goes far beyond the tanker's natural frequency so that the tanker may be required to keep still to some extent.

Therefore, the oscillation of the tanker is trivial under high ice drift speed conditions and obvious under low ice drift speed conditions. This analysis leads to the conclusion that the ice drift speed has a greater influence on the standard deviation and maximum than the mean of the mooring force, velocity and offset of the ship, especially at low ice drifting speed.

5.4.3. Effect of linear mooring stiffness

Nixon and Ettema (1987) studied ice-sheet interactions with a cable-moored platform in model tests. Three tests were carried for three levels of mooring system stiffness. The results show that a minimum surge force as a function of inverse mooring stiffness appears to exist, but it is not clear precisely what factors contribute to the minimum. Aksnes and Bonnemaire (2009a, 2009b) also studied the effects of mooring stiffness and found that the amplitude of the oscillations increases with increasing natural period.

In this study, the ice thickness is constant at 0.6 m and the ice drift speed is set to 0.6 m/s. The mooring stiffness is assumed to be linear, and five different levels of mooring stiffness are used: 300, 500, 1000, 2000, and 3000 kN/m. Fig. 27 shows the simulated mean, standard deviation and maximum of the mooring forces in surge at different mooring stiffness levels. The mean mooring force is approximately constant regardless of mooring stiffness, whereas the standard deviation and maximum vary with mooring stiffness. There is no clear trend as to how the standard deviation and maximum change as mooring stiffness increases from 300 to 3000 kN/m. The maximum appears to be more sensitive to mooring stiffness than the deviation.

Spectral analysis of the mooring forces was performed as shown in Fig. 28. It is clear that the main energy for all configurations is concentrated at the natural periods of the model. The first peaks for different mooring systems occur around their corresponding natural frequency. The other peaks occur at almost the same frequency because these peaks are invoked by the ice excitation forces, which are not significantly affected by varying mooring stiffness.

Fig. 29 gives the mean, standard deviation and maximum turret offset in surge as mooring stiffness varies and shows that these values decrease monotonically with increasing mooring stiffness.

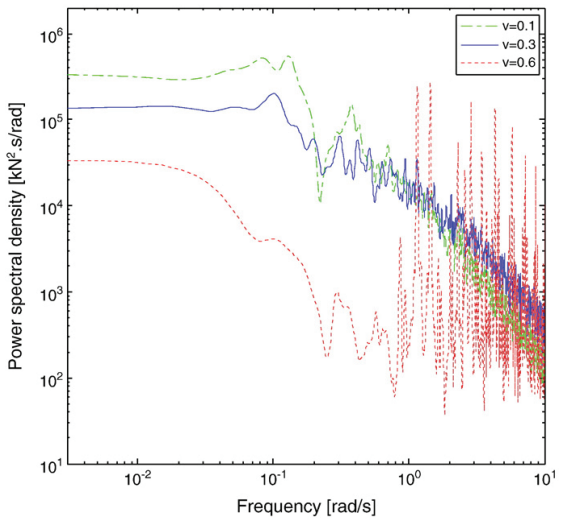

Fig. 26. Power spectral density of ice forces in a surge.

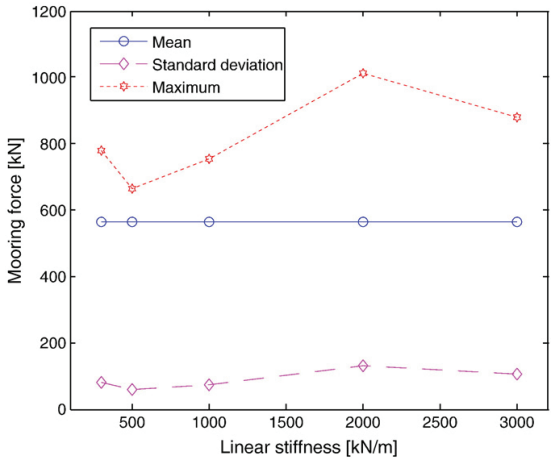

Fig. 27. Mooring force in surge versus linear stiffness.

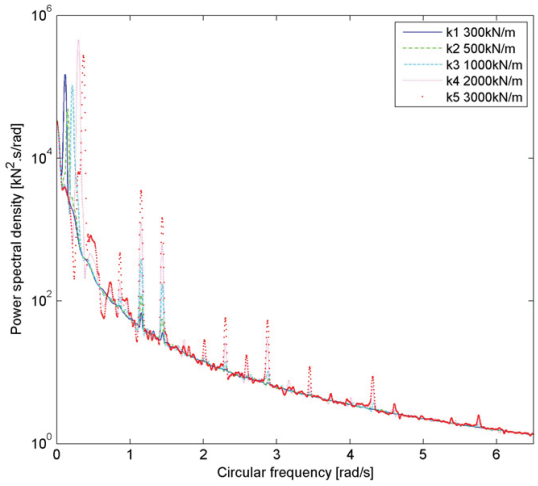

Fig. 28. Power spectral density of mooring force as a function of mooring stiffness in surge.

6. Conclusions

A two-dimensional model of a moored ship in level ice was developed, and it was validated by comparing numerical simulations of the Kulluk with both model and full scale measurements. The influence of turret position on the stability of a moored tanker under various ice drift speeds and angles was investigated. The effects of ice thickness, drift speed and mooring stiffness on the mooring forces and dynamics of a moored structure with heading control were assessed. The findings of the study can be summarised as follows:

- Both model validation and full scale validation with the Kulluk revealed that the presented numerical method accurately simulates moored structures in level ice.
- The longitudinal location of the turret influences the horizontal response and stability of a moored tanker. The influence is more obvious when the ice-drift angle deviates from 0 to 180° and the ice drift speed is comparatively high. For the cases considered in this paper, an optimal turret position exists, namely Lpp/4.

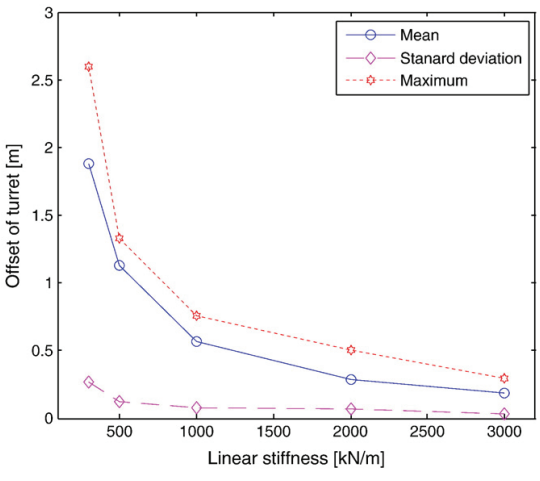

Fig. 29. Turret offset versus linear stiffness.

- The dependency of ice force on ice thickness is clear. The ice resistance calculated by the proposed model deviates from that by Lindqvist at higher ice thickness conditions.
- There is a strong speed effect on the standard deviation and maximum of the mooring force and on the response of structures, especially at low ice drift speeds. The mean mooring force is insensitive to the ice drift speed.
- The mooring stiffness has an effect on the standard deviation and maximum of the mooring forces and the turret offset. The standard deviation and maximum of the mooring force increase non-monotonically with increasing mooring stiffness. The amplitude of the oscillations decreases with increasing mooring stiffness.

All the above conclusions are based specifically on simulations of moored structures. More data are needed to validate this model. Therefore, care should be taken when the method is used for other applications. The moored structure is assumed to have good ice clearing capacity. This assumption is valid for conical structures with ice management (such as the Kulluk) and structures equipped with azimuth thrusters that push broken ice floes away from the bow area with a propeller system. In industrial operations, the structure may encounter ice ridges, which are a significant threat to station keeping. Ice management is thus expected to mitigate the action of ice under severe ice conditions.

To improve the present numerical model for moored vessels, damping terms induced by the hull, mooring lines and any other factors that play an important role in simulating a moored structure in level ice should be studied. It is also suggested performing model tests with a setup similar to that of the simulation would further validate and modify this ice force model. In particular, the ice submersion model should be refined based on field observations and model tests. In addition, the effects of ice ridges and pile up need to be studied, which are of great importance in the actual design of station keeping systems.

Acknowledgements

The authors would like to acknowledge the support of the Research Council of Norway through the Centre for Ships and Ocean Structures at the Norwegian University of Science and Technology in Trondheim, Norway.

References

Aksnes, V., 2010b. A panel method for modeling Level Ice Actions on Moored Ships. Part1: Loacal Ice Force Formulation. Cold Regions Science and Technology 63, 29–39.
Aksnes, V., Bonnemaire, B., 2009a. A simplified approach for modelling stochastic response of moored vessels in level ice. Proceedings of the 20th International Conference on Port and Ocean Engineering under Arctic Conditions. Luleå, Sweden (POAC09-134).
Aksnes, V., Bonnemaire, B., 2009b. Analysis of the behavior of a moored ship in variable ice. Proceedings of the 20th International Conference on Port and Ocean Engineering under Arctic Conditions. Luleå, Sweden (POAC09-25).
Aksnes, V., Bonnemaire, B., Løset, S., Lonoy, C., 2008. Model Testing of the Arctic Tandem Offloading Terminal – Tandem mooring forces and Relative Motions between Vessels. Proceedings of the 19th IAHR International Symposium on Ice. Vancouver, British Columbia, Canada, 2, pp. 687–698.
Aksnes, V., Bonnemaire, B., Koch, R., Lonoy, C., Løset, S., 2010a. Investigation Of Response Of Moored Ships In Level Ice. Proceedings of the HYDRALAB III Joint User Meeting, Hannover.
Bonnemaire, B., Lundamo, T., Evers, K.U., Løset, S., Jensen, A., 2008. Model Testing of the Arctic Tandem Offloading Terminal –Mooring Ice Ridge Loads. Proceedings of the 19th IAHR International Symposium on Ice. Vancouver, British Columbia, Canada, 2, pp. 639–650.
Bonnemaire, B., Aksnes, V., Lundamo, T., Evers, K.U., Løset, S., Ravndal, O., 2010. Ice Basin Testing of A Moored Offloading Icebreaker In Variable Ice Drift: Innovations And New Findings. Proceedings of the HYDRALAB III Joint User Meeting, Hannover.
Comfort, G., et al, 1982, Experimental Studies of Ice Performance of Conical Drilling Unit, ARCTEC Canada Ltd. report 897 submitted to Gulf Canada Resources Ltd.
Comfort, G., 2001. Moored vessel station-keeping in ice-infested waters. An assessment of model test data for various structures and ship shapes. The international Conference on Port and Ocean Engineering under Arctic Conditions (POAC'01), Ottawa, Ontario, Canada.

Comfort, G., Singh, S., Spencer, D., 1999. Evaluation of Ice Model Test Data for Moored Structures. PERD/CHC report, pp. 26–195.
Enkvist, E., Varsta, P., Riska, K., 1979. The Ship-Ice Interaction, vol. 2. The International Conference on Port and Ocean Engineering under Arctic Conditions (POAC), Trondheim, pp. 977–1002.
Evers, K., et al, 1983, Conical Drilling Unit – Model Tests in Ice Ridges, HSVA report E 126/83 submitted to Gulf Canada Resources Ltd.
Fossen, T.I., 2002. Marine Control Systems: Guidance, Navigation and Control of Ships, Rigs and Underwater Vehicles. Marine Cybernetics AS, Trondheim82-92356-00-2.
Hansen, E.H., Løset, S., 1999. Modelling floating offshore units moored in broken ice: comparing simulations with ice tank tests. Cold Regions Science and Technology 29, 107–119.
Keinonen, A.J., Browne, Revill, R.P., Reynolds, A., 1996. Ice breaker Characteristics Synthesis. Report of AKAC Inc. to Transportation Development Centre, July 1996, TP12812 E.
Kotras, T.V., Baird, A.V., Naegle, J.N., 1983. Predicting ship performance in level ice. SNAME Transactions 91, 329–349.
Lindqvist, G., 1989. A Straightforward Method for Calculation of Ice Resistance of Ships. Proceedings of POAC 1989, pp. 722–735.
Lubbad, R., Løset, S., 2011. A numerical model for real-time simulation of ship–ice interaction. Cold Regions Science and Technology 65, 111–127.
Nixon, W.A., Ettema, R., 1987. Ice-sheet Interaction with a Cable-moored Platform. IIHR Report, Iowa,USA.
Nixon, W.A., Ettema, R., 1988. Ice Sheet Interaction With a Cable-Moored Platform, University of Iowa IIHR report 148.
Riska, K., Patey, M., Kishi, S., Kamesaki, K., 2001. Influence of ice conditions on ship transit times in ice. The International Conference on Port and Ocean Engineering under Arctic Conditions (POAC'01), Ottawa, Ontario, Canada, 2, pp. 729–745.
Sayed, M., Barker, A., 2011. Numerical Simulations of Ice Interaction with a Moored Structure. The Offshore Technology Conference, Houston, Texas, USA, OTC22101.
Su, B., Riska, K., Moan, T., 2010. A Numerical Method for the Prediction of Ship Performance in Level Ice. Cold Regions Science and Technology 60, 177–188.
Toyama, Y., Yashima, N., 1985. Dynamic response of moored conical structures to a moving ice sheet. Proceedings of the 8th International Conference on Port and Ocean Engineering under Arctic Conditions, 2. Narssarssuaq, Greenland, pp. 677–688.
User's Manual Riflex, version 3.2.3, 2003. MARINTEK Report No.519619.
Valanto, P., 2001. The resistance of ships in level ice. SNAME Transactions 109, 53–83.
Valkonen, J., Cammaert, G., Larsen, M.M., 2008. Field Program for Simulation of Stationkeeping Conditions for Arctic Drilling and Production Vessels. International Conference and Exhibition on Performance of Ships and Structures in Ice. Banff, Alberta, Canada. ICETECH08-169-RF.
Wang, S., 2001. A Dynamic model for Breaking Pattern of Level Ice by Conical Structures. Ph.D. Thesis, Department of Mechanical Engineering, Helsinki University of Technology, Finland.
Wright, B., 1999. Evaluation of Full Scale Data for Moored Vessel Stationkeeping in Pack Ice. PERD/CHC Report 26–200, Ottawa, Canada.
Zhou, L., Su, B., Riska, K., Moan, T., 2011. Numerical Simulation Of Moored Ship in Level Ice. Proceeding of the 30th international Conference on Offshore Mechanics and Arctic Engineering, Rotterdam, The Netherlands.

Paper 2

Heading control for turret-moored vessel in level ice based on Kalman filter with thrust allocation

Li Zhou, Torgeir Moan, Kaj Riska and Biao Su

Accepted by Journal of Marine Science and Technology (2011)

Heading control for turret-moored vessel in level ice based on Kalman filter with thrust allocation

Li Zhou[a,*], Torgeir Moan[a], Kaj Riska[a,b], Biao Su[a]

[a] Centre for Ships and Ocean Structures, Norwegian University of Science and Technology, Trondheim, Norway

[b] TOTAL S.A. - DGEP/DEV/TEC/GEO - 06D55, Tour Coupole, 2, Place Jean Millier, La Défense 6 - Cedex 45, 92078 PARIS LA DÉFENSE, FRANCE

[*] Corresponding author. Phone: +47 41340189; Fax: +47 73595528; E-mail address: li.zhou@ntnu.no

Abstract

This paper mainly focuses on the heading control of a position-moored vessel operating under level ice regime. A dynamic ice simulator interconnecting the vessel motions with the ice dynamics is used for the design of heading control system. The strategy is to ensure that the vessel is kept at an appropriate position within the safe limits. Using a heading controller based on Kalman filter, the desired control force is computed to counteract the environmental disturbances. A thrust allocation method is developed to go with the heading controller. To keep the ice forces to a reasonable level the moored vessel should be aligned with the ice drift direction and small angles up to 15° in change on heading against the ice flow could be possible. Therefore, heading control of a moored vessel exposed to level ice with drift angle 0° and 15° is simulated since the dynamic positioning system need to resist ice yaw moments and lateral ice forces on the hull. The simulation indicates that the proposed control strategy performs satisfactorily for moored vessel in level ice.

Keywords: Heading control; Kalman filter; Thrust Allocation; Position mooring; Level ice;

1. Station keeping method

The presence of sea ice in the Arctic region poses a challenge for keeping the vessel at location with different purposes in industrial activity of oil exploration and exploitation. Station keeping for vessels in both waves and ice-covered areas can be achieved by three methods: a mooring system; a dynamic positioning system; or a combination of the first and second methods.

The pure mooring method is relatively popular in industry. Relevant experience with moored structures in ice is obtained from drilling operations in the Beaufort Sea. As a conical drilling unit, the Kulluk platform was designed with a variety of special features to improve the performance under ice conditions in the shallow water [1]. The system has a downward sloping circular hull near the waterline that breaks the oncoming ice mainly in flexure and an outward flare near the bottom that clears the broken ice cusps away from the moon pool and mooring lines. The strong mooring system could resist ice forces up to 450 tones. It worked successfully with the downtime in operations less than 10%, but at a cost of extensive ice management by three icebreakers.

Another method is to use dynamic positioning systems for maintaining the vessels in position and on a correct heading. Station keeping with dynamic positioning systems was employed for drilling and diving operations in heavy ice conditions, where the water depth is 30 meters [2]. The operation was supported by two icebreakers. The total ice down time was 22% during six weeks of operation in varying ice conditions. The related drilling operations using dynamic positioning in ice in the Arctic Ocean was also reported by Moran et al. [3]. The site water depth ranges from 1100 meters to 1300 meters. The manual positioning instead of automatic DP operation was applied to achieve a very successful station keeping with nearly no

down time when good ice management with icebreakers is used. Comparing two DP operations, it was found that DP is preferred to be used in deep water. This was also concluded by Allan et al. [4].

Thruster assisted mooring provides a third way of station keeping. Considering the water limitation for DP operation and extensive ice management for mooring system, an appropriate allowance may be made for the effectiveness of thruster systems in reducing mooring loads. In addition, there is also a potential of lowering fuel consumption in shallow and intermediate open water through mooring systems [5]. Kjerstad [6] pointed out that it will be important that the vessel's heading is towards the direction of ice drift. Kuehnlein [7] identified the main challenges for dynamic station keeping in ice, of which he also mentioned that the vessels need to be oriented always against the drifting ice with the bow or the aft end, as the side motions are very limited or even not possible due to vertical side walls. Therefore, a heading controller needs to keep the vessel align with the drifting ice while a mooring system needs to provide a reactive force to compensate for the mean drift loads of the environment due to ice. Wilkman [8] summarized some problems that will be challenging for DP operations in ice, such as forces acting on the vessel, forces caused by ice dynamics, turning yaw moment, changes in ice movement direction, new type of thruster control allocation and so on. In this paper, dynamic ice forces acting on the vessel and turning yaw moment under 0° and 15° ice drift angle are simulated based on the mathematical model of level ice during level ice-hull interaction in Biao et al. [9], Zhou et al. [10,11]. The aim of this paper is to propose a method for simulating the behavior of a moored vessel with heading control based on Kalman filter in level-ice covered seas under different ice drift angles. The overall schematic of control strategy is shown in Fig.1.

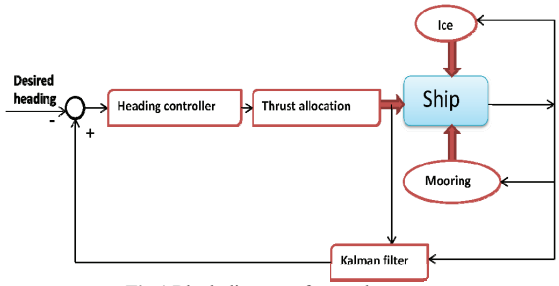

Fig.1 Block diagram of control strategy

2. Mathematical modelling

According to Sørensen [12], the mathematical models of a vessel may be formulated in two complexity levels: a control plant model and a process plant model. The process plant model is a comprehensive description of the real physics of plant dynamics which should be as close as possible. The control plant model is a simplified mathematical description to capture only main characteristics from the process plant model. The process plant model including the kinematics and kinetics is shown in the following.

2.1 Kinematics

Let the Earth-fixed position (x, y) and heading ψ of the vessel relative to an Earth-fixed frame $X_E Y_E Z_E$ be expressed in vector form by $\boldsymbol{\eta} = [x, y, \psi]$and let the vessel-fixed vessel velocities be represented by the state vector $\mathbf{V} = [u, v, r]$. The three modes are referred to as the surge, sway and yaw of a vessel. The origin of the vessel-fixed frame XYZ is located at the vessel centre line in a distance x_g from the center of gravity.

In general, the transformation between the vessel- and Earth-fixed coordinate frames can be described by the three Euler angles; Φ (roll), θ (pitch) and ψ (yaw). The horizontal motion of the vessel is described by one Euler angle only, which is the yaw angle. If only surge, sway and yaw (3-DOF), the relationship between the Earth-fixed position vector and the body-fixed velocity vector is given through a transformation matrix,

$$\dot{\boldsymbol{\eta}} = \mathbf{R}(\psi)\mathbf{V} \tag{1}$$

$$\mathbf{R}(\psi)=\begin{bmatrix} c\psi & -s\psi & 0 \\ s\psi & c\psi & 0 \\ 0 & 0 & 1 \end{bmatrix} \tag{2}$$

where c, s are compact notations for cosine and sine, respectively.

2.2 Vessel kinetics

A process plant model for vessel dynamics in horizontal plan can be expressed as

$$(\mathbf{M}_{RB}+\mathbf{M}_{A})\dot{\mathbf{V}}+\mathbf{C}_{RB}(\mathbf{V})\mathbf{V}+\mathbf{D}(\mathbf{V}_r)=\boldsymbol{\tau}_{ice}+\boldsymbol{\tau}_{mo}+\boldsymbol{\tau}_{th} \tag{3}$$

where $\boldsymbol{M}_{RB}$ is the system inertia matrix and $\boldsymbol{M}_{A}$ is the added mass; $\boldsymbol{\tau}_{ice}$ is the level ice load vector in the body-fixed frame; $\boldsymbol{\tau}_{mo}$ is the mooring force translated from the earth-fixed coordinate system to body-fixed coordinate system by the rotational matrix described in Eq. (2); $\boldsymbol{\tau}_{th}$ is the thruster vector consisting of forces and moments produced by the propulsion system; The skew-symmetric Coriolis-centripetal matrix $\mathbf{C}_{RB}(\mathbf{V})$ is given by

$$\mathbf{C}_{RB}(\mathbf{V})=\begin{bmatrix} 0 & 0 & -m(x_g r+v) \\ 0 & 0 & mu \\ m(x_g r+v) & -mu & 0 \end{bmatrix} \tag{4}$$

where x_g is the longitudinal position of the center of gravity in body-fixed coordinate. When a vessel operates under dynamic positioning where the velocities are small, the Coriolis-centripetal terms $\mathbf{C}_{RB}(\mathbf{V})\mathbf{V}$ can be ignored for control design. The term $\mathbf{D}(\mathbf{V}_r)$ in Eq. (3) represents the damping force due to the motion of the vessel relative to the ambient water. Empirical formulas are often used to calculate the damping forces and moments on a vessel [13], that is

$$\mathbf{D}(\mathbf{V}_r)=\begin{bmatrix} \dfrac{0.075}{(\log_{10}Rn-2)^2}\dfrac{1}{2}\rho S u_r|u_r| \\ \dfrac{1}{2}\rho\left[\int_L dx C_D(x)D(x)\right]v_r|v_r| \\ \dfrac{1}{2}\rho\left[\int_L dx C_D(x)D(x)x\right]v_r|v_r| \end{bmatrix} \tag{5}$$

Where $\mathbf{V}_r=[u_r, v_r, r_r]$ is the motion of the vessel relative to the ambient water; the integration is over the length L of the vessel; R_n is Reynolds number; ρ is the water density; S is the wetted surface of the vessel; $C_D(x)$ is the drag coefficient for cross-flow past an infinitely long cylinder with the cross-sectional area of the vessel at the longitudinal coordinate x. $D(x)$ is the sectional draught.

2.3 Level ice loads

The modelling of ice load acting on a moored vessel in level ice depends highly on the interaction process by which the hull breaks and displaces the ice. Once the ice gets contact with the hull, ice is being crushed. Then the crushing force continues to increase with increasing contact area until its vertical force component gets large enough to cause bending failure of the ice, after which the broken ice floes start to turn along the vessel's hull until they are parallel to the hull. Finally, the floes submerge and slide along the hull as they are pushed by the next broken ice floes. The level ice loads modelling has been presented in details by Zhou et al. [10, 11]. The method was also validated by comparing the simulated results with full scale field measurement of the Kulluk. Therefore, the details are neglected in this paper.

2.4 Mooring system

Comparing with spread mooring system, internal turret mooring system has good weather-vaning capacity to mitigate ice action on the hull since ice drift direction is changing due to current, wind, and so on in most ice-infested waters. In addition, it facilitates the operation of disconnecting and leaving the site quickly and reliably.

The motions of a moored vessel in ice conditions are believed to be significantly influenced by the mooring lines. Mooring systems provide not only time-varying restoring forces but also damping forces, both of which should be taken into consideration in vessel response analysis in the horizontal plane. A horizontal-plane turret mooring system model can be formulated as

$$\boldsymbol{\tau}_{mo} = -\mathbf{R}^{-1}(\psi)\mathbf{g}_{mo}(\boldsymbol{\eta}) - \mathbf{D}_{mo}(\mathbf{V}) \tag{6}$$

where $\mathbf{g}_{mo}(\boldsymbol{\eta})$ and $\mathbf{D}_{mo}(\mathbf{v})$ are the Earth- fixed restoring term and the additional damping, respectively. The nonlinear mooring line characteristics $\mathbf{g}_{mo}(\boldsymbol{\eta})$ can be found by dedicated software programs for slender marine structures, e.g. RIFLEX [14] and others. The mooring damping term $\mathbf{D}_{mo}(\mathbf{V})$ could be obtained based on DNV [15].

3. Heading controller design

3.1 Control plant model

The observer and controller are designed through a control plant model of the DP vessel [16]. It should be noted that only yaw moment is considered. It is assumed that the nonlinear damping $\mathbf{C}_{\mathrm{RB}}(\mathbf{V})$ in yaw is small in Eq. (3) since the vessel's velocity is small in station keeping. The control plant model only considers 3-DOF. The resulting low-frequency model of yaw in (1) and (3) can be simplified such that

$$\dot{\psi} = r \tag{7}$$

$$\dot{b}_{ice} = -T_{ice}^{-1} b_{ice} + E_i w_2 \tag{8}$$

$$m_{66}\dot{r} = \tau_{th} + b_{ice} + w_1 \tag{9}$$

$$y_m = r + v_y \tag{10}$$

where b_{ice} is the bias vector considering both slowly varying disturbances and unmodelled dynamics from ice disturbance; T_{ice} is a diagonal matrix of time constants for estimating slowly varying yaw moment by ice; E_i is the ice gain; m_{66} is the moment of inertia in yaw; w_1 and w_2 are the zero-mean white noises; y_m is the measured output; v_y is the measurement noise.

3.2 Kalman filter design

Based on the control plant model, the state-model of Kalman filter for heading control design could be expressed as from Eq. (7)-(10)

$$\dot{x} = \mathbf{A}x + \mathbf{B}u + \mathbf{E}w \tag{11}$$

$$y_m = \mathbf{H}x + v_y \tag{12}$$

where $x = [\Psi, r, b_{\mathrm{ice}}]^{\mathrm{T}}$ is the state vector; $u = N_{\psi}$ is the control command, where N_{ψ} is defined in Eq. (21); $w = [w1, w2]^{\mathrm{T}}$ represents the process noise vector and

$$\mathbf{A} = \begin{bmatrix} 0 & 1 & 0 \\ 0 & 0 & m_{66}^{-1} \\ 0 & 0 & -T_{ice}^{-1} \end{bmatrix}, \quad \mathbf{B} = \begin{bmatrix} 0 \\ m_{66}^{-1} \\ 0 \end{bmatrix} \tag{13}$$

$$\mathbf{E} = \begin{bmatrix} 0 & 0 \\ m_{66}^{-1} & 0 \\ 0 & E_i \end{bmatrix}, \qquad \mathbf{H} = \begin{bmatrix} 1 & 0 & 0 \end{bmatrix} \tag{14}$$

The model given in Eq. (11) forms the basis of a Kalman filter design. In order to implement the filter on a computer, the model needs to be discretized as [19]

$$x(k+1) = \mathbf{\Phi} x(k) + \mathbf{\Delta} u(k) + \mathbf{\Gamma} w(k) \tag{15}$$

$$y_m(k) = \mathbf{H} x(k) + v_y(k) \tag{16}$$

$$\mathbf{\Phi} = \exp(\mathbf{A}h) \tag{17}$$

$$\mathbf{\Delta} = \mathbf{A}^{-1}(\mathbf{\Phi} - \mathbf{I})\mathbf{B} \tag{18}$$

$$\mathbf{\Gamma} = \mathbf{A}^{-1}(\mathbf{\Phi} - \mathbf{I})\mathbf{E} \tag{19}$$

where h is the sampling time, and the equivalent discrete-time noises $w(k)$ and v_y(k) are Gaussian and white noises with zero mean. For large offshore vessels and rigs, the sampling time is normally in the range of 100–500 ms [17]. Then sampling time used in the following simulation is 100ms.

3.3 Reference Generation

A simplest form of a reference model with a low-pass filter structure is used [16]:

$$\frac{\psi_d(s)}{\psi_s(s)} = \frac{1}{T_m s + 1} \tag{20}$$

where ψ_d denotes the heading command and ψ_s is the generated desired heading; T_m is the time-constant. It should be noted that in order to obtain good tracking performance and stability, bandwidth of the reference model must be lower than that of the vessel control system.

3.4 Heading control design

Pinkster and Nienhuis [18] controlled the x- and y-positions using a PID feedback controller while only derivative action was used for the yaw angle, which is only applicable for large tankers. Aalbers et al. [20] used both derivative and proportional action to control yaw motion. However, Stephens and Meahan [21] proposed that the control of heading requires a full three-term controller including proportional, integral and derivative terms in the design and commissioning of a new thruster assisted mooring system (TAMS) for global producer III.

The heading control law for moored vessel is proposed to be an output PID which is given as

$$N_\psi = -k_p \hat{\psi}_e - k_d \hat{r}_e - k_i \int_0^t \hat{\psi}_e dt \tag{21}$$

where $\hat{\psi}_e = \hat{\psi} - \psi_d$; $\hat{r}_e = \hat{r} - r_d$; $\hat{\psi}$ and $\hat{r}$ are the estimated heading and yaw rate by Kalman filter; ψ_d and r_d are the desired heading and yaw rate, which are the output from the reference model; k_p, k_i, k_d are the PID controller gains; Integrator anti-windup should be implemented in order to avoid that the integrator integrates up beyond the saturation limits of the actuators. The controller gains can be designed by the LQG algorithm [16].

4. Thrust Allocation

4.1 Unsaturated thrust allocation

A general relation between the control demand and the individual actuator demand thrusts is as follows

$$\tau_c = T_a T_{th} \tag{22}$$

where τ_c is the vector of thrust and moment demand from the controller; T_{th} is a vector of thruster demands in Cartesian coordinates, and T_a is the thruster allocation matrix, defined as follows:

$$T_{th} = \begin{bmatrix} T_{1x} & T_{1y} & \cdots & T_{nx} & T_{ny} \end{bmatrix} \tag{23}$$

$$T_a = \begin{bmatrix} t_1 & \cdots & t_n \end{bmatrix} \tag{24}$$

where n is the number of thrusters. In 3 DOF (surge, sway and yaw), the column vectors take the following form:

$$t_i = \begin{cases} \begin{bmatrix} 0 & 0 \\ 0 & 1 \\ 0 & l_{ix} \end{bmatrix} & tunnel\,thruster \\ \begin{bmatrix} 1 & 0 \\ 0 & 0 \\ l_{iy} & 0 \end{bmatrix} & main\ propeller \\ \begin{bmatrix} 1 & 0 \\ 0 & 1 \\ l_{iy} & l_{ix} \end{bmatrix} & azimuth\,thruster \end{cases} \tag{25}$$

Where l_{ix} and l_{iy} denote the longitudinal and transverse position of the i_{th} thruster respectively.

In general, Eq. (22) represents an underdetermined set of equations since the fact the number of columns of thruster arrangement matrix T_a is more than 3. There will be more variables describing the thruster settings than equations to solve (required forces and moment is solved in such a way to minimize the allocated power. One particular solution to the over-determined set of equations is the least-norm or minimum norm solution. The minimum norm solution of T_{th} could be achieved by finding the Moore-Penrose generalized inverse of T_a [19]. Then the solution can be expressed as:

$$T_{th} = T_a^{\dagger} \tau_c \tag{26}$$

$$T_a^{\dagger} = W^{-1} T_a^T (T_a W^{-1} T_a^T)^{-1} \tag{27}$$

$$W = \begin{bmatrix} w_{1x} & & & & 0 \\ & w_{1y} & & & \\ & & \ddots & & \\ & & & w_{rx} & \\ 0 & & & & w_{ry} \end{bmatrix} \tag{28}$$

where $T_a^{\dagger}$ is the generalized inverse of T_a ; W is weighting matrix, in which the element w_{ix} is the cost to use the i_{th} thruster in the surge axis, and w_{iy} is the cost to use them in the sway axis. The higher the cost, the less thrust that will be assigned to the thruster.

Then the solved thrust vector T_{th} can be converted to an azimuth angle command and thrust demand pair for each thruster unit:

$$T_{th} = \begin{bmatrix} \alpha_1 & T_1 & \cdots & \alpha_r & T_r \end{bmatrix}^T \tag{29}$$

$$\alpha_i = \arctan \frac{T_{iy}}{T_{ix}} \tag{30}$$

$$T_i = \sqrt{T_{ix}^2 + T_{iy}^2} \tag{31}$$

4.2 Saturated thrust allocation

If the solution thrust exceeds the thrust limit for any actuator, the solution of Eq.(26) using the pseudo-inverse technique in a least-squares sense will no longer hold and hence the desired thrust and moment demand will not be achieved.

In this paper, the most important mode of control is to maintain the vessel's heading in sense that the bow should be pointing into the prevailing weather in order to mitigate the ice forces acting on the vessel. If the vessel fails to maintain station with the bow oriented to minimize the load, then it would certainly be unable to maintain the station for other more unfavorable heading angles. Therefore, thrust allocation with the heading priority scheme is of concern. The main procedure for the allocation is given in the following.

A. The first step should be to allocate thrusts as in section 4.1, and examine the magnitudes of each demand thrust. If any thruster is saturated, the demand vector for a heading priority control strategy should be modified, in which both the surge and sway demands are taken as zero and only the moment is allocated.

B. The magnitudes of each demand thrust should be rechecked for thruster saturation.

B1. If there is no saturated thruster after allocating the moment, which means that there is some reserve thrust capacity left in each thruster, but not enough to allocate the entire demand. It should be noticed that the azimuth angles and thrust levels are now optimum at this point since meeting the yaw demand is prioritized. With the azimuth angles fixed, the next step is to allocate the thrust required to satisfy the surge or sway. In addition, a ratio could be chosen between surge and sway, which reflects the relative importance of each with respect to the other.

B2. If all are thrusters saturated, there is no recourse except to clamp all thrusts.

B3. If there are still some thrusters saturated, a new method is necessary to meet the moment command to the best of actuators' ability. If there are more than two thrusters unsaturated, then the thrust should be set to the maximum and the azimuth angle should be fixed for each saturated thruster. Then neglecting the saturated thrusters, the next step will allocate the remaining command for unsaturated thrusters. The magnitudes of each demand thrust will be examined again. If no thruster is saturated, the allocation will terminate. Otherwise, the process would be iterated until there is only one thruster unsaturated left. Moment in the command vector is also taken as the most important element for allocation to the last unsaturated thruster. Surge or sway comes to the second, depending on the relative importance in the specific control task.

5. Case study

Only ice loads is taken into consideration due to its prominent influence on the behavior of moored vessels compared to other environmental loads in ice-infested areas. The input parameters including vessel,

mooring system characteristics and ice for the simulation are specified in this section. Then, corresponding results of simulation and the discussions are given.

5.1. Overview

An icebreaking tanker named MT Uikku as a double-hull icebreaking motor tanker that was constructed to meet the standards of the highest Finnish-Swedish Ice Class, IA Super, is modeled. The primary dimensions of MT Uikku are given in Table 1.

The mooring system used in the simulations is the same as that used in Zhou et al. [11] consisting of twelve identical mooring lines with three lines in each group. Each2 mooring line has an identical chain-wire-chain configuration. The angle between adjacent mooring lines at each corner is 10 degrees.

The MT Uikku was equipped with an 11.4 MW azipod unit [22]. The present propulsion system is not able to perform the dynamic positioning due to inefficient thruster allocation and insufficient capacity. A new thruster configuration needs to be designed for station-keeping operations. The tunnel thruster or the transverse thruster which produces only transverse force is desired to be used, considering that the moment generation will be more conducive to sway force generation rather than surge. In addition, the azimuth thrusters are attractive in dynamic positioning systems since they can produce forces in different directions. Thus a new actuator setup of moored MT Uikku is shown in Fig.2. There are four thrusters in all with two azimuth thrusters (thruster #1 and #2) and two transverse thrusters (thruster #3 & 4), where Ti and αi are thrust and azimuth angle for the ith thuster. It should be noted that Ti will always be positive for all thrusters. It means that thrust reversal is obtained by 180° rotation of the thruster or reversal propeller rotating for azimuth thrusters and only reversal propeller rotating for transverse thrusters. Therefore, the azimuth angles for thrusters #3 (α3) and # 4 (α4) will be either 90° or -90°. The individual maximum thrust delivered by thruster is assumed to be 600 kN.

For the weighting matrix described in Eq. (28), the higher the weighting factors, the less thrust that will be assigned to the thruster in the selected axis when calculating the solution. In the preliminary selection, the weighting factors are all equal. Considering the interaction the thruster interaction between thruster #1 and #2 due to direct their propeller wash at each other, the weighting factor for the sway axis is modified to increase the weighting factor to some extent. The main particulars related to the thruster locations and weighting factors are listed in Table 2.

Table 1. Primary dimensions of MT Uikku

Primary dimensions	value	unit
Length over all	164.4	m
Length between perpendiculars	150.0	m
Breadth moulded	22.2	m
Draught	12	m
Displacement	22600	ton
Deadweight	15750	ton
Block coefficient	0.72	

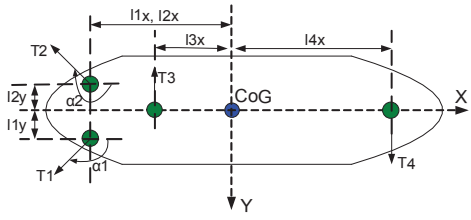

Fig.2 The schematic of thruster arrangement

Table 2. Main particulars for thrusters

Thruster No.	Location (m)		Weighting factor	
	l_{ix}	l_{iy}	w_{ix}	w_{iy}
#1	-85	5	1	10
#2	-85	-5	1	10
#3	-70	0	1	1
#4	55	0	1	1

Level ice is considered with uniform ice properties shown in Table 3. The thickness of level ice is assumed to be constant at 0.6 m in the case study, considering the possible capacity of the overall thruster-assisted moored icebreaking tanker. The ice drift velocity is also important in studying the dynamic of moored vessels in ice, where the dynamics of moored is the most severe at speed 0.3 m/s [11]. Therefore ice drift speed at 0.3 m/s is selected in the following simulations.

The ice is assumed to move towards the hull, illustrated in Fig.3, where the ice drifting angle and turret location are defined. The optimal turret position with Lct =Lpp/4 are assumed. Typically, the angle of attack is from 0° to 15° [15]. Considering the capacity of actuators, two scenarios with ice drifting angle at 0° and15° are considered in the simulation. The initial ice edge is defined as a given pre-broken boundary, which is not symmetric (shown in Fig.4). When the ice sheet keeps intruding the vessel with heading controller, ice force and vessel motion will get more and more stable and not substantially affected by the initial condition.

Table 3. Ice characteristics

Parameter	Symbol	Value	Unit
Density	ρi	880	kg/m3
Young's modulus	E	5400	MPa
Poisson ratio	γ	0.33	
Crushing strength	σc	2.3	MPa
Flexural strength	σf	0.5	MPa
Frictional coefficient	μi	0.15	

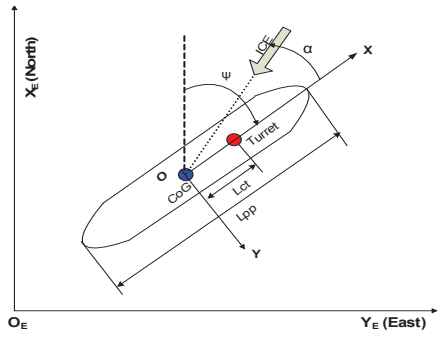

Fig.3 Definition of turret location and drifting angle

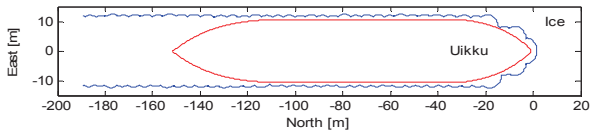

Fig. 4 Initial ice boundary in Earth-fixed coordinate

5.2 Results and discussions

As mentioned before, a variable ice drifting direction is believed to pose a challenge for moored structures since they have to vane against the ice drifting direction to minimize the impact on the hull. Provided that the ice suddenly turns the drifting direction towards the tanker side, then the best way for the tanker is to adjust the heading to make sure that the ice is moving towards the symmetric axis in surge.

The origin of earth-fixed coordinate is fixed at the turret position. The initial heading angle ψ shown in Fig.3 is set at 0°. The cases considered in the simulation are given in Table 4. In case HC1, the heading controller tries to keep the initial heading angle under the action of drifting level ice while for case HC2, it simulates the situation that the hull suffers from a sudden change in ice drift direction at 15° and then the heading controller as well as propulsion system acts to rotate the hull to bow into the oncoming ice. The other cases simulated here is to demonstrate the effect of heading control on the whole system.

Table 4. Cases for simulation

Case Name	Control Description	Ice thickness (m)	Ice drift speed (m/s)	Drifting angle (deg)	Desired heading(deg)	Simulation duration (s)	Sampling time (s)
HC1	Heading control	0.6	0.3	0	0	1000	0.1
NHC1	No control	0.6	0.3	0	--	1000	0.1
HC2	Heading control	0.6	0.3	15	15	1000	0.1
NHC2	No control	0.6	0.3	15	--	1000	0.1

5.2.1 Effect of heading control

A D-controller as well as additional P-controller if necessary, rather than integral action was suggested to be used in the thruster assisted positioning mooring system by Fossen [19]. Therefore, only derivative and proportional actions are taken into account in the control system. The proportional gain k_p is chosen so that the natural period of the slowly oscillating ship is from 100-200 s in yaw [13]. The derivative gain k_d can be set to be around 60% of the critical damping in yaw based on the proportional gain k_p. In the present simulation, $k_p = 8.4 \bullet 10^{10}$ Nm/rad and $k_d = 8.0 \bullet 10^{11}$ Nms/rad are used.

The corresponding simulated time series of turret position and heading in earth-fixed coordinate in level ice for case HC1 and NHC1 are presented in Fig.5. Fig.5 (lower) shows that the heading controller on the tanker works well in terms of keeping the heading of the hull so that the heading is constant at 0° excerpt for very small variations less than 0.5 degree. However, the hull without heading controller could also resist the disturbance of the nonsymmetrical yaw moment induced by intruding level ice sheet with some flexibility (within 2 degrees) due to its own capacity when the turret is located at Lpp/4. It is also found from Fig5 that the mean of turret offset in case HC1 is almost the same as that in case NHC1, but the maximum of turret offset in case HC1 is a little larger than that in case NHC1 and thus the corresponding global resultant mooring force in case HC1 is a little larger than that in case NHC1, as shown in Fig.6. A reason might explain. The ice breaking force acting on the bow is not always symmetric about central longitudinal section during simulation. In the free mode, the minor rotation may be conducive to break ice with less energy. If the vessel is fixed on the heading, extra effort may be needed to continuously break ice. Thus, the instantaneous icebreaking force on the vessel without heading control may be lower than that on the constrained vessel with heading control.

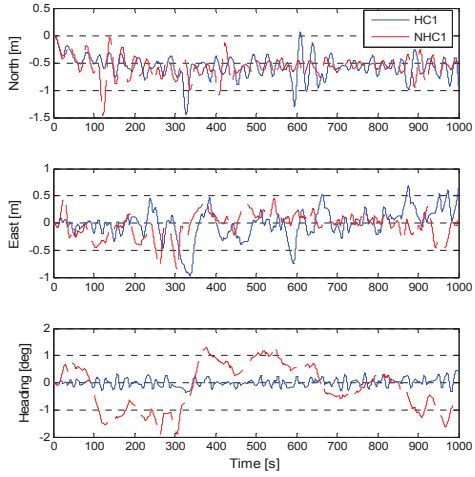

Fig.5 Earth-fixed position and heading of turret

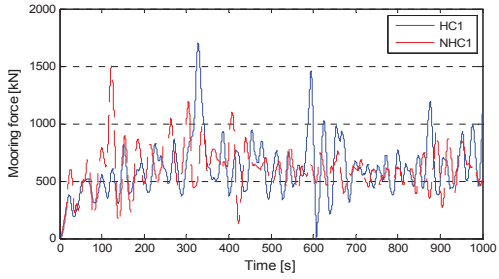

Fig.6 Earth-fixed horizontal resultant mooring force

The corresponding simulated time series of turret position and heading in earth-fixed coordinate in level ice for case HC2 and NHC2 are presented in Fig.7. Fig.7(lower) shows that the hull without heading controller rotates slowly from 0° to 21° and tends to oscillate around 15° under the disturbance from intruding level ice sheet. The heading doesn't converge to the desired value within 1000 s in the simulation. The heading controller makes the hull rotate to the desired heading (15°) within 200 s and then keeps it constant at 15° excerpt for very small variations. The corresponding time series of global resultant mooring force in horizontal plane for both cases are presented in Fig.8, where the maximum global mooring force (2690 kN) for the hull without heading control are significantly larger than that (1420 kN)for the hull with heading control.

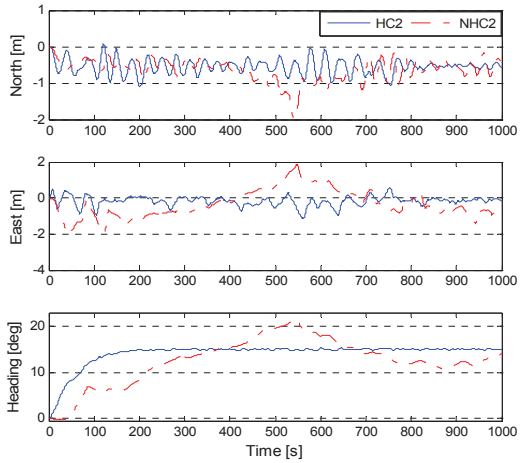

Fig.7 Earth-fixed position of turret and heading relative to field zero point

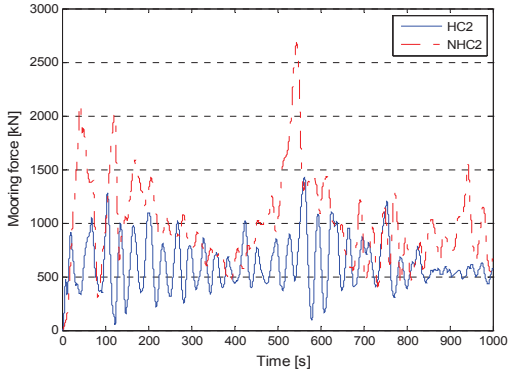

Fig.8 Earth-fixed horizontal resultant mooring force

5.2.2 Performance of Kalman filter

To implement a Kalman filter, the covariance of the measurement noise and process noise in the model are necessary. The heading measurement noise is associated with compass. Balchen et al. [23] used white heading measurement nouse with standard deviation 0.2 degrees in simulation experiments. In the present simulation, the Kalman filter is designed using the assumption of a Gaussian, white heading measurement noise with standard deviation 0.1 degree, and a measurement sample rate of 100 ms. The time constant in Eq.(20) is 100 s. The process noise values can be chosen by applying Bryson's inverse square method [24]. Since the anticipated maximum values of the yaw moment due to ice could be very large, the covariance of the noise w_2 is taken as 0. The covariance of the noise w_1 is chosen as $5 \bullet 10^{-2}$.

Fig.9 (Upper) shows the simulated desired, measured and estimated heading for case HC1 while Fig.9 (Lower) shows the absolute error between the actual heading and estimated heading. The plots show reasonable performance with heading excursion of 0.4 degrees. The maximum estimated heading error is around 0.2°. This may seem a little large so that the Kalman filter's tracking capability needs to be

improved. However, the improved tracking will result in more aggressive actuator utilization to some extent. This is also mentioned by Jenssen et al. [25].

Fig.10 (Upper) shows the simulated desired, measured and estimated heading for case HC2 while Fig.10 (Lower) shows the absolute error between the actual heading and estimated heading. The estimated heading follows the actual heading satisfactorily. In the rotation stage, there exists a small absolute estimation error in heading for case HC2.

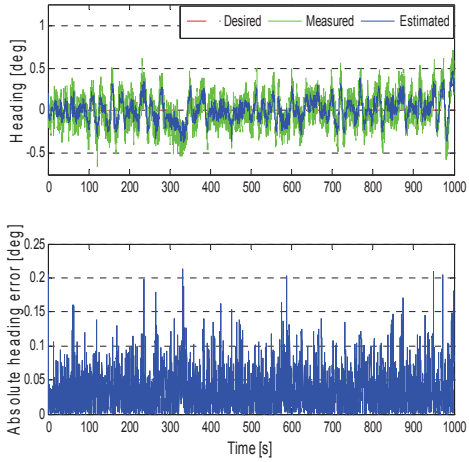

Fig.9 Simulated data of Kalman-based filter for case HC1

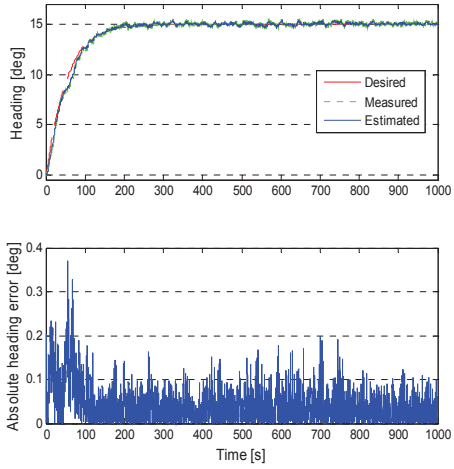

Fig.10 Simulated data of Kalman-based filter for case HC2

5.2.3 Performance of thrusters

The modeling of thruster dynamics is not included in the simulation. In order to study the dynamics of heading introduced by ice, the maximum rate that each thruster can change thrust as a result of inertia of the motor, the propeller together with then other components in the drive system and the maximum slew

rate for changing thrust direction are not taken into consideration in the present simulation of thrust allocation. The ratio of the delivered thrust to the maximum thrust for each thruster in time domain for case HC1 is shown in Fig.11. From Fig.11 it is seen that the allocated forces display large variations and the transverse thrusters (thruster #3 and #4) are much more used than the main azimuthing thrusters (thruster #1 and #2). The corresponding azimuth angle is shown in Fig.12. From Fig.12 it is found that the signs of allocated angles change frequently due to ice dynamics.

The time history of the ratio of the delivered thrust to the maximum thrust and the corresponding azimuth angle for each thruster in case HC2 are shown in Figs.13 and14, respectively. From Fig.13, it is seen that compared to the case HC1, all thrusters are much more dependent and even get saturated during transient rotation process in order to follow the desired heading and finally make the hull head up towards the drifting ice. Similarly to case HC1, the allocated azimuth angles in case HC2 displays large oscillations from Fig.14.

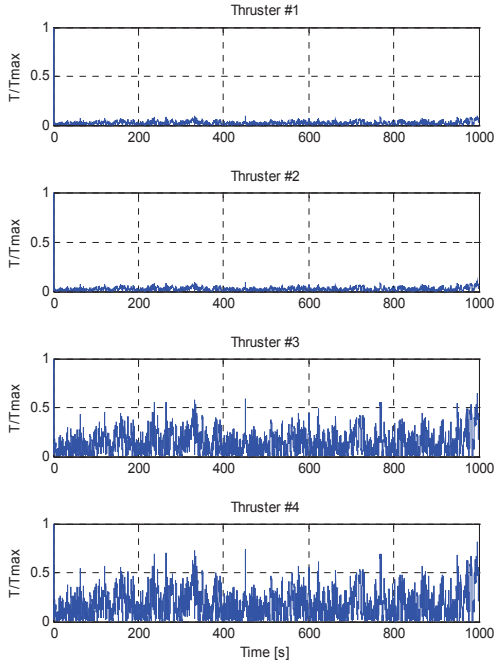

Fig.11 Allocated force in case HC1

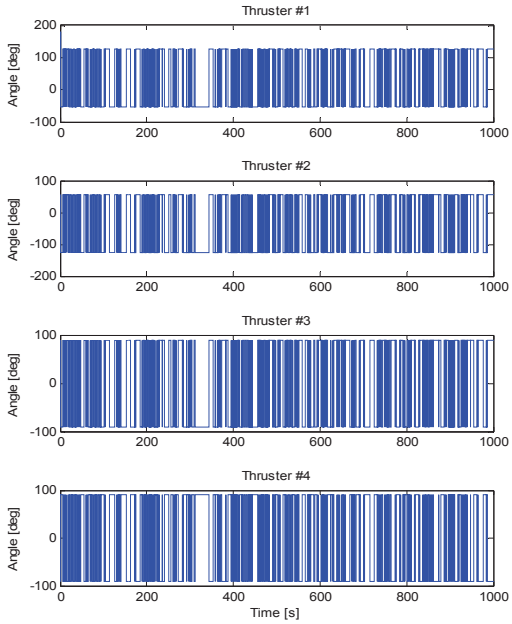

Fig.12 Allocated angle in case HC1

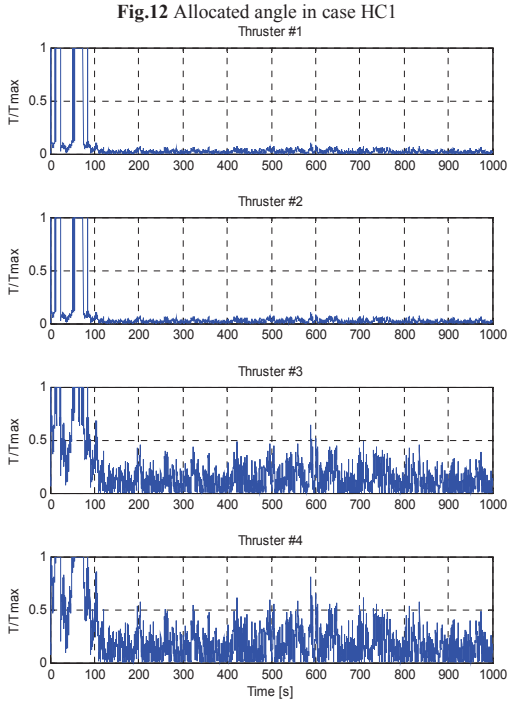

Fig.13 Allocated force in case HC2

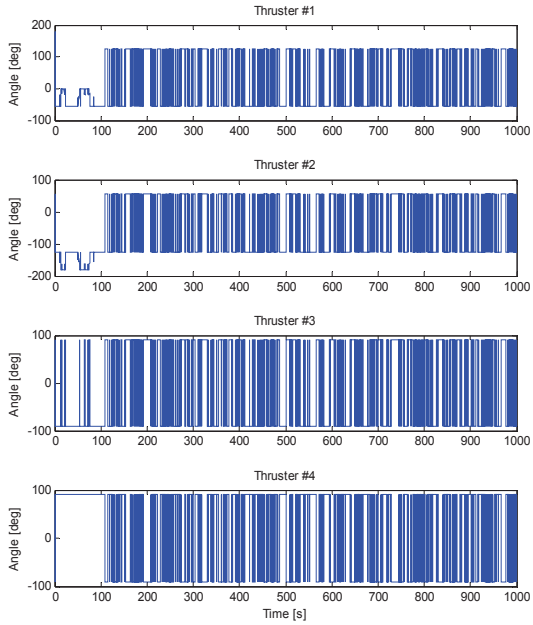

Fig.14 Allocated angle in case HC2

6. Conclusions

This paper simulates the dynamic behavior of heading controlled moored icebreaking tanker in level-ice and designed heading controller based on Kalman filter. In addition, a thrust allocation method suitable for the heading controller is proposed. From the simulation, there are some significant findings which are worth pointing as follows:

- Heading controller based on Kalman filter is feasible to keep the moored vessels aligned with the encountering level ice with changing drift direction. However, when the actual heading does not deviate from the expected one, the utilization of heading controller might deteriorate the performance of system and thus increase the mooring forces. Therefore, it is preferable to switch on and off to reduce the fuel consumption of position moored vessels. It is noted that to have good ice-vaning capacity, the location of turret is important. When the turret gets close to the center of the gravity of the floating tanker in level ice, it is likely that the hull will rotate due to the non-symmetric ice action in yaw direction and lack of stability capacity. The ideal location seems to be around one quarter of the length between two perpendiculars forward the center of the gravity.
- Based on numerical simulation in the present paper, the turn moment due to ice disturbance is changing rapidly. The designed Kalman filter could track the changing of heading. Improving the tracking capacity is possible, but at a cost of heading filtering and aggressive thruster usage. How to balance the problem is still a challenge.
- All thrusters are used extensively in the turning process. The requirement for propulsion system is high in terms of increased thruster usage and additional wear and maintenance when heading control system compensates the quickly changing ice disturbance. Therefore, the dynamic characteristics of actuators need to be considered in the design of DP control system to ice conditions.

All the above conclusions are based specifically on the simulations. More data are desired to validate this model. The effects of ice ridges and pile up should be studied, which are believed to have influence on the actual design of station keeping systems. At present, most industrial station keeping operations are conducted under the ice management with extensive utilization of icebreakers. The combined heading control and mooring system is still at an early stage, but it is promising. If it comes true, then the cost of ice management will reduce significantly.

7. References

1. Wright B (1999) Evaluation of Full Scale Data for Moored Vessel Stationkeeping in Pack Ice. PERD/CHC Report 26-200, Ottawa, Canada

2. Keinonen A, Wells H, Dunderdale P, Pilkington R, Miller G, Brovin A (2000) Dynamic positioning operation in ice, offshore sakhalin, may – june 1999. The 10th ISOPE. Seattle, USA. pp. 683–690

3. Moran K, Backman J, Farrell JW (2006) Deepwater drilling in the arctic ocean's permanent sea ice. Vol. 302 of the Proc. of the Integrated Ocean Drilling Program (IODP)

4. Allan R, Barr A, Seamen D, Duggal A (2009) Station Keeping Solutions for a Mobile Drilling Unit in Arctic Environments. Proceedings of the 20th International Conference on Port and Ocean Engineering under Arctic Conditions, Luleå, Sweden, POAC09-82

5. Strand JP, Sørensen AJ, Fossen TI (1998) Design of automatic thruster assisted position mooring systems for ships. Modelling, Identification and Control, Vol. 19, No. 2, pp. 65–71

6. Kjerstad N (2011) Ice Navigation. Tapir Academic Press, Trondheim

7. Kuehnlein WL (2009) Philosophies for dynamic positioning in ice-covered waters. Offshore Technology Conference, OTC 20019, Houston, Texas, USA

8. Wilkman G, Suojanen RA, Saarinen S, Mattsson T, Leiviskä T (2009) DP In Ice Conditions - Challenges and Opportunities. DYNAMIC POSITIONING CONFERENCE,Houston, USA

9. Su B, Riska K, Moan T (2010) A numerical method for the prediction of ship performance in level ice. Cold Regions Science and Technology 60, 177–188

10. Zhou L, Su B, Riska K, Moan T (2011) Numerical Simulation of Moored Ship in Level Ice. Proceeding of the 30th international Conference on Offshore Mechanics and Arctic Engineering, Rotterdam, The Netherlands

11. Zhou L, Su B, Riska K, Moan T (2012) Numerical simulation of moored structure station keeping in level ice, Cold Regions Science and Technology 71, 54-66.

12. Sørensen AJ (2005) Structural issues in the design and operation of marine control systems. IFAC Journal of Annual Reviews in Control 29(1), 125–149

13. Faltinsen OM (1990) Sea loads on ships and offshore structures. Cambridge University Press, Cambridge

14. User's Manual Riflex, version 3.2.3 (2003), MARINTEK Report No.519619

15. DNV – Det Norske Veritas (2004). Positioning mooring. Offshore Standard DNV-OS-E301

16. Sørensen AJ (2006) Lecture Notes: Modelling and Control. Marine Cybernetics. Trondheim, Norway

17. Fossen TI, Perez T (2009). Kalman Filtering for Positioning and Heading Control of Ships and Offshore Rigs. Control Systems, IEEE, Volume: 29 Issue:6, 32-46

18. Pinkster JA, Nienhuis U (1996) Dynamic positioning of large tankers at sea. Proceedings of the offshore technology conference (OTC'96), Houston, TX

19. Fossen TI (2010) Guidance and Control of Marine Craft. Marine Cybernetics. Trondheim, Norway

20. Aalbers AB, Janse SAW, Boom WC (1995) DP assisted and Passive Mooring for FPSO's. Proceedings of the offshore technology conference, Houston, OTC 7722

21. Stephens RI, Meahan A (2007) Design and Commissioning of a New Thruster Assisted Mooring System (TAMS) For Global Producer III. DYNAMIC POSITIONING CONFERENCE, Design & Control, Houston, USA

22. Hänninen S, Ojanen M, Uuskallio A, Vuorio J (2007) Recent Development of Podded Propulsion in Arctic Shipping. Recent Development of Offshore Engineering in Cold Regions, POAC-07, Dalian, China

23. Balchen JG, Jenssen NA, Mathisen E, Sælid S (1980) A Dynamic Positioning System Based on Kalman Filtering and Optimal Control. Modeling, Identification and Control 1(3), 135-163

24. Bryson AE, Ho YC (1969) Applied Optimal Control. Ginn and Co., Boston, USA

25. Jenssen NA, Muddesitti S, Phillips D, Backstrom K (2009) DP in Ice Conditions. DYNAMIC POSITIONING CONFERENCE, Arctic, Houston, USA

Paper 3

Station Keeping Capacity of a Moored Structure with Heading Control in Level Ice

Li Zhou, Kaj Riska and Torgeir Moan

Published in the 21st IAHR International Symposium on Ice, Dalian, China, 2012

21st IAHR International Symposium on Ice
"Ice Research for a Sustainable Environment", Li and Lu (ed.)
Dalian, China, June 11 to 15, 2012

Station Keeping Capacity of a Moored Structure with Heading Control in Level Ice

Li Zhou[1*], Kaj Riska[1,2], and Torgeir Moan[1]

1. Centre for Ships and Ocean Structures, Norwegian University of Science and Technology, Trondheim, Norway
2. ILS Oy, Helsinki, Finland
[*] *li.zhou@ntnu.no*

This paper deals with a simulation of heading control of a moored icebreaking tanker under level ice regime. A dynamic ice simulator interconnecting the vessel motions with the ice dynamics is used for the design of control system. In open water, the vessel with Dynamic Positioning (DP) is controlled to move in horizontal plane with surge, sway and yaw as required. This is not the case for DP in level ice. It is almost impossible to move a vessel to the side since the transverse ice load would be very large far being beyond the DP capacity. Therefore, the DP system needs to orientate the vessel to be always against the drifting ice with ship's ice breaking bow breaking the ice. In order to implement the station keeping operation at an appropriate position in level ice, yaw must be controlled by the DP system while surge and sway drift must be compensated by the mooring system. The moored tanker with heading control is simulated in the time domain. The corresponding results are analyzed in order to establish the effect of heading control on station keeping. It is found that the vessel with the heading control can be operated in more severe ice conditions than without DP control. Hence the operating season for moored ships can be extended.

1. Introduction

The Dynamic Positioning (DP) system has become a rapidly growing technology for station keeping in the marine offshore industry of ships and semi-submersibles since 1960s. It offers better station-keeping accuracy and mobile flexibility, and also it is more cost effective for deepwater operations than traditional mooring systems. At present, most of the modern deepwater semi-submersible rigs are equipped with a DP system.

In basic design, the DP capability assessment of a vessel is based on static environmental and propulsion forces. The capability plot, often presented as a polar diagram with a number of envelops, is used to establish the vessel's capability to keep position in a certain environment with a certain combination of thrusters. The environmental forces and moments are increased until they are exactly balanced by the maximum available thrust offered by the thruster configuration (Gonsholt and Nygård, 2002). Thus, a limiting weather condition is obtained as a combination of a mean wind speed, significant wave height and a sea current speed. Normally all three environmental forces are acting from the same direction. Therefore, various calculations need to be carried out like environmental force in open water, which consists of mainly wind force, wave drift forces and current drag forces acting from various directions on the vessel to induce motion on horizontal plane, and propulsion forces from thrusters considering propeller, rudder and thruster efficiency in various directions based on hull interaction, propeller interaction, thruster interaction etc.

The DP capability analysis is well developed. Kongsberg Maritime AS has used the commercial computer program StatCap to assess the DP capability for a ship called Adams Arrow, where the correctness of the DP capability analysis is inextricably related to the correctness of input data (Kongsberg Maritime As, 2008). Mahfouz and El-Tahan (2006) also developed a software program, the Capability Polar Plot Program (CPPP) for DP vessels. Later, they presented a new method of predicting the Capability-Polar-Plots for offshore platforms using the combination of the artificial neural networks (NNs) and the capability polar plots program (Mahfouz, 2007). As an alternative to the static analysis, time domain simulations would be more desirable to establish the limiting environmental conditions since it could investigate the performance of the vessel and assess station keeping ability to a higher accuracy, especially for vessels operating in ice-covered water. The ice force on the vessel will change rapidly, which leads to a severe dynamic response. Thus, the dynamic effect introduced by ice is non-trivial in assessing the DP capabiity.

In this paper, the performances of a moored icebreaking tanker and the tanker with heading control in level ice are simulated in time domain. The limiting ice thickness where moored ships with and without heading control can operate in station keeping mode is of the main concern.

2. Mathematical Modelling

In the paper, planar motions are considered in the ship's performance. Two reference frames are used, namely Earth-fixed frame ($X_EY_EZ_E$) and body-fixed frame (XYZ), see Fig.1.

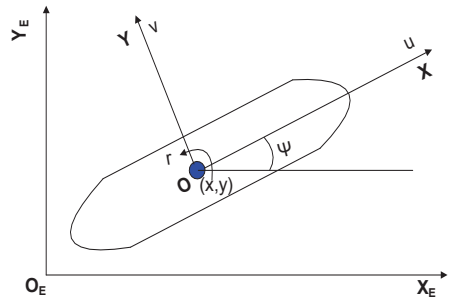

Figure 1. Earth-fixed ($X_EY_EZ_E$) and body-fixed (XYZ) reference frames in horizontal plane.

The horizontal position and orientation of the vessel in the Earth-fixed coordinate system are defined by $\boldsymbol{\eta} \triangleq [x, y, \psi]$, where the first two variables describe the position, while the last one describes the heading angle. Correspondingly, the translational and rotational body-fixed velocities are defined by $\mathbf{v} \triangleq [u, v, r]$. The body-fixed general velocities are transformed to the Earth-fixed frame by

$$\dot{\boldsymbol{\eta}} = \mathbf{J}(\boldsymbol{\eta})\mathbf{v}, \qquad \textbf{[1]}$$

where

$$\mathbf{J}(\boldsymbol{\eta}) = \begin{bmatrix} c\psi & -s\psi & 0 \\ s\psi & c\psi & 0 \\ 0 & 0 & 1 \end{bmatrix}, \qquad \textbf{[2]}$$

where $c\psi$, $s\psi$ is compact notation of $cos\psi$ and $sin\psi$ respectively.

2.1 Level Ice Forces

Only ice loads is taken into consideration due to their prominent influence on the behavior of moored vessels, as compared to other environmental loads. The modelling of ice loads acting on a moored ship in level ice depends highly on the interaction process by which the hull breaks and displaces the ice. Once the ice gets in contact with the hull, ice is being crushed. Then the crushing force continues to increase with increasing contact area until its vertical force component gets large enough to cause bending failure of the ice, after which the broken ice floes start to turn along the ship's hull until they are parallel to the hull. Finally, the floes submerge and slide along the hull as they are pushed by the next broken ice floes. Considering the

interaction between vessel and level ice, the level ice loads modeling has been presented in Zhou et al. (2011; and 2012) , Biao et al.(2010). Therefore, the details are omitted in this paper.

2.2 Mooring Forces

The internal turret mooring system has good weather-vaning capacity to mitigate ice action on the hull since ice drift direction is changing due to current, wind, and so on in most ice-infested waters. In addition, it facilitates the operation of disconnecting and leaving the site quickly and reliably. The motions of a moored ship in ice conditions are believed to be significantly influenced by the mooring lines. Mooring systems do not only provide time-varying restoring forces but also damping forces, both of which should be taken into consideration in vessel response analysis in the horizontal plane. A horizontal-plane turret mooring system model can be formulated as

$$\boldsymbol{\tau}_{mo} = -\mathbf{J}^{-1}(\eta)\mathbf{g}_{mo}(\eta) - \mathbf{d}_{mo}(v) \qquad \textbf{[3]}$$

where $\boldsymbol{\tau}_{mo}$ is the global mooring force; $\mathbf{g}_{mo}(\eta)$ and $\mathbf{d}_{mo}(v)$ are the Earth- fixed restoring term and the additional damping, respectively. The nonlinear mooring line characteristics $\mathbf{g}_{mo}(\eta)$ can be found by dedicated software programs for marine slender structures, e.g. RIFLEX (2003) and others.

2.3 Thruster Forces

The main function of the thrusters in DP systems is to develop the required forces to counteract the environmental disturbance forces acting on the vessel. DP controller calculates the command forces based on the filtered state signals, such as the position and heading error. Then the total command forces will be allocated to the individual thruster in an optimal way. The main structure of heading control system will be introduced briefly. A simplest form of a reference model with a low-pass filter structure is used to generate a smooth trajectory, which the vessel is expected to follow in laplace form:

$$\frac{\psi_d(s)}{\psi_s(s)} = \frac{1}{T_m s + 1}, \qquad \textbf{[4]}$$

where ψ_d denotes the heading command and ψ_s is the generated desired heading; T_{ms} is the time-constant parameter, as a time delay in the process of generating a smooth reference trajectory from the present heading to desired heading.

The heading control law for moored vessel is proposed to be an output PID which is given as

$$N_\psi = -k_p \hat{\psi}_e - k_d \hat{r}_e - k_i \int_0^t \hat{\psi}_e dt \qquad \textbf{[5]}$$

where N_ψ is the moment command; $\hat{\psi}_e = \hat{\psi} - \psi_d$; $\hat{r}_e = \hat{r} - r_d$; $\hat{\psi}$ and $\hat{r}$ are the estimated heading and yaw rate by Kalman filter; ψ_d and r_d are the desired heading and yaw rate, which are the output from the reference model; k_p, k_i, k_d are the PID controller gains.

An optimal thrust allocation could be achieved by finding the Moore-Penrose generalized inverse of the thrust allocation matrix (Fossen, 2010).Thruster efficiency in various directions based on hull interaction, propeller interaction; thruster interaction etc is one of the most difficult variables to get under control. There are many factors influencing the efficiency. The best method to get hold of these efficiencies is to do full scale tests and the second best is model tests. However, it is difficult for authors to take it into account in the simulations.

3. Numerical Simulations and Results

3.1 Overview

An icebreaking tanker named MT Uikku is modeled. The primary dimensions of MT Uikku are given in Table 1.

Table 1. Primary dimensions of MT Uikku.

Primary dimensions	value	unit
Length over all	164.4	m
Length between perpendiculars	150.0	m
Breadth moulded	22.2	m
Draught	12	m
Displacement	22600	ton
Deadweight	15750	ton
Block coefficient	0.72	

Since the present propulsion system is not able to perform the dynamic positioning, a new thruster configuration needs to be designed for station-keeping operations. The tunnel thruster or the transverse thruster which produces only transverse force is desired to be used, considering that the moment generation will be more conducive to sway force generation rather than surge. In addition, the azimuth thrusters are attractive in dynamic positioning systems since they can produce forces in different directions. Thus a new actuator setup of moored MT Uikku is shown in Fig.2. There are four thrusters in all with two azimuth thrusters (thruster #1 and #2) and two transverse thrusters (thruster #3 and # 4). The individual maximum thrust delivered by each thruster is assumed to be 600 kN. The thruster locations are listed in Table 2.

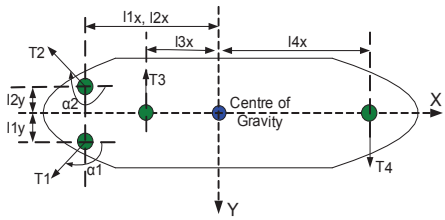

Figure 2. Schematic illustration of a new thruster arrangement of the MT Uikku.

Table 2. Thruster location.

Thruster No.	Location (m)	
	lx	*ly*
#1	-85	5
#2	-85	-5
#3	-70	0
#4	55	0

Level ice is considered with uniform ice properties shown in Table 3. The normal ice drift speed ranges from a few cm/sec to 0.6 m/sec encountered in the Beaufort Sea (Wright, 1999). According to Zhou et al. (2012), the ice drift velocity is also important in studying the dynamic of moored vessels in ice. The dynamics of moored is the most severe at speed 0.3 m/s. Therefore ice drift speed at 0.3 m/s is selected in the following simulations. The initial ice edge is defined as a given pre-broken boundary, which is not symmetric (shown in Fig.3). When the ice sheet keeps intruding the vessel with heading controller, ice force and ship motion will get more and more stable and will not be affected substantially by the initial condition.

Table 3. Ice characteristics.

Parameter	Symbol	Value	Unit
Density	ρi	880	kg/m3
Young's modulus	E	5400	MPa
Poisson ratio	γ	0.33	
Crushing strength	σc	2.3	MPa
Flexural strength	σf	0.5	MPa
Frictional	μi	0.15	

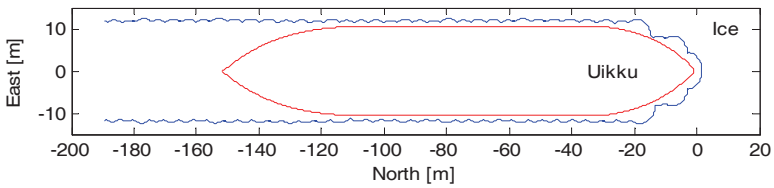

Figure 3. Initial ice boundary in Earth-fixed coordinate.

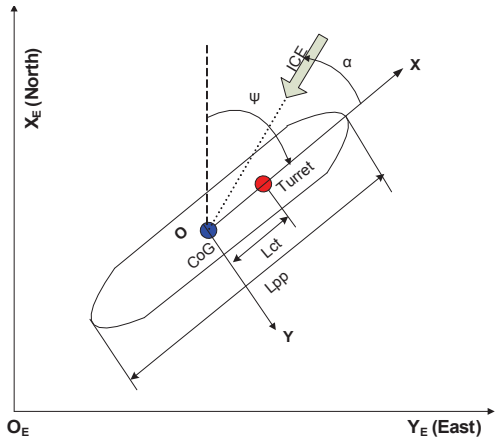

Figure 4. Definition of turret location and drifting angle.

The water depth is 100 meters. The global mooring stiffness is linear at 1000 kN/m. The mooring damping ratio based on DNV (2004) is chosen to be 10%. The initial heading of the tanker is set at 0 degree. The ice is assumed to move towards the hull, illustrated in Fig.4, where the ice drifting angle and turret location are defined. The optimal turret position with Lct =Lpp/4 are fixed. In addition, the setting for heading control system is the same for all simulations in order to make the results comparable.

3.2 Examples of Time Series

In the simulation, all the settings shown in the section 3.1 are fixed except ice drift angle and ice thickness. When ice drifts at a certain angle towards the hull, the vessel will respond to the ice disturbance. The resulting horizontal turret offsets in time domain are recorded until the tanker gets stable. If the maximum turret offset is below the limitation of station keeping operation, assuming 5% of water depth in this paper, i.e. 5 meters, then the ice thickness is increased until the maximum ice thickness is derived. Thus, the maximum ice thickness and range of ice drift angles under which the vessel operates in a stable fashion are needed to be estimated.

Two cases without heading control (HC) at ice thickness 0.4, 0.5 and 0.6 meter are given as an example. The ice drift angle is 80 degrees. The simulated time series of heading change and turret offset are shown in Fig. 5. From Fig.5, it is clear that the tanker rotates slowly until the heading approaches the ice drift angle. During the whole turning process, the turret deviates from the original position. The corresponding offset records are presented in Fig.6. At hi=0.4, the maximum offset is 3.2 meters, below the limitation (5 meters). For an ice thickness of hi=0.5, the maximum offset is 5.0 meters. When ice thickness increases to 0.6 meter, the maximum offset is 5.7 meters, larger than the limitation. Therefore 0.5 meter is found as the limiting ice thickness which the moored tanker without HC could hold in station keeping operation.

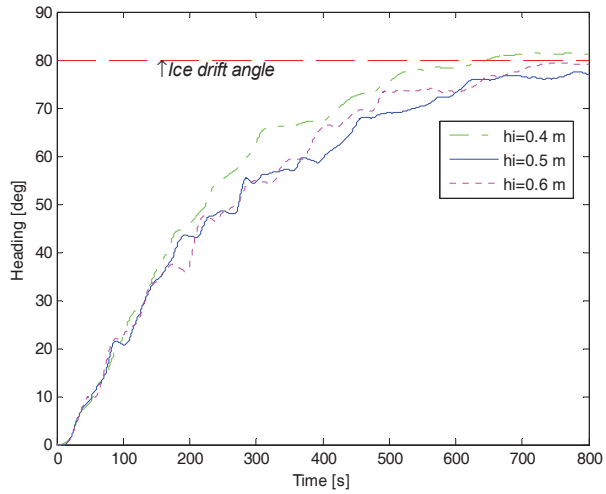

Figure 5. Heading change of moored tanker without HC.

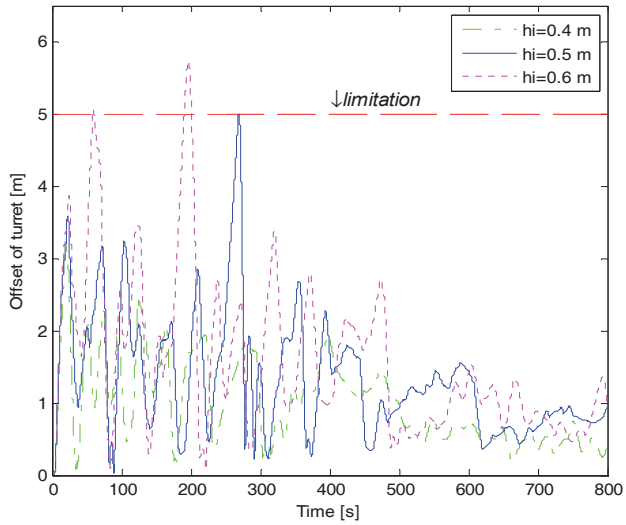

Figure 6. Turret offset of moored tanker without HC.

3.3 Results and Discussions

More cases for moored tanker without HC and with HC are simulated in order to finding the limiting ice thickness. The ice drift angle of interest in this work ranges from -90 degrees to 90 degrees. The limiting ice thicknesses at different ice drift angled that the tanker could resist are tabulated in Table 4. The polar plot is shown in Fig.7.

Table 4. The limiting ice thickness for moored tanker without HC and with HC.

Ice drift angle (deg)	Without HC (m)	With HC (m)
0	1.3	1.3
10	1.1	1.1
20	0.75	1.1
30	0.8	1.1
40	0.65	1.0
50	0.6	1.0
60	0.7	0.85
70	0.45	0.8
80	0.5	0.65
90	0.5	0.8

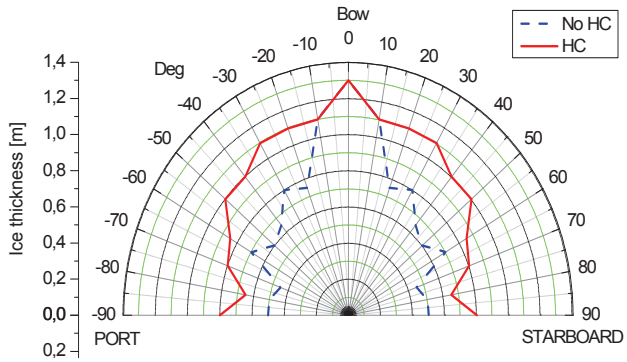

Figure 7. Capacity plot for moored tanker without HC and with HC.

It is interesting to see some special findings related to the simulated results shown in Fig.7 as follows:

a) The maximum limiting ice thickness is 1.3 meters at 0 degree. The least limiting ice thickness is 0.45 meter at 70 degrees for moored tanker without HC and 0.65 meter at 80 degrees for moored tanker with HC. In general, the limiting ice thickness decreases as the ice drift angle increases for both No HC case and HC case, but not monotonously. This may be attributed to the dynamics of vessel introduced by drifting ice with different angles.

b) Using heading control to assist moored tanker enhances the station keeping capacity significantly except for cases with ice drift angle at 0 and 10 degrees. Although heading control setting is the same for all HC cases, the commanded force by controller is different case by case, depending on the heading error between the ice drift angle and the present heading. This means that when heading control is used, the calculated forces from control system in cases with ice drift angle at 0 and 10 degrees are less than those in other cases. The effort made by heading control system is less and thus it doesn't make significant influence on the station keeping ability of the tanker.

The result shows that HC is useful to increase the station keeping capacity of moored tanker, especially when the ice drifting angle is large. It should be noted that the present model may overestimate the station keeping capacity of moored tanker since the modeling of ice pile up or accumulation is neglected. For moored tanker without good ice clearing capacity, it is important to take it into consideration. The station keeping capability in the paper is based on input data subject to uncertainties, which may influence on the correctness and accuracy of the results herein. Any change or alteration made to the input data such as vessel dimensions, ice properties, thruster data or configuration, water depth, mooring system characteristics or any other input data on which the analysis is based may alter the results hereof.

4. Conclusions

Based on a dynamic ice simulator interconnecting the vessel motions with the ice dynamics, this paper presents a simulation of heading control of a moored icebreaking tanker in level ice. Both moored tanker without HC and with HC were simulated in order to find the maximum ice thickness that the moored tanker can resist in station keeping operation under the drifting ice from different directions. The corresponding results were compared in different ice conditions. The main outcome of the paper shows that the limiting ice thickness for a moored ship can be increased by using a DP control and hence offers an extension of the operating season for moored ships.

Acknowledgments

The authors would like to acknowledge the support of the Research Council of Norway through the Centre for Ships and Ocean Structures at the Norwegian University of Science and Technology in Trondheim, Norway.

References

DNV – Det Norske Veritas, 2004. Positioning mooring. Offshore Standard DNV-OS-E301.

Fossen, T. I., 2010. Guidance and control of marine craft. Marine Cybernetics. Trondheim, Norway.

Gonsholt, A., and Nygård, B., 2002. DP design studies. Dynamic Positioning Conference, Design, Houston, USA, 1–14.

Kongsberg Maritime As, 2008. DP capability analysis adams arrow. Project: DP 43092, Report 1056504.

Mahfouz, A. B., and El-Tahan, H. W., 2006. On the use of capability polar plots program on the dynamic positioning systems for marine vessels. Ocean Engineering, 33, 1070–1089.

Mahfouz, A. B., 2007. Predicting the capability-polar-plots for dynamic positioning systems for offshore platforms using artificial neural networks. Ocean Engineering, 34, 1151–1163.

Su, B., Riska, K., and Moan, T., 2010. A numerical method for the prediction of ship performance in level ice. Cold Regions Science and Technology, 60, 177–188.

User's Manual Riflex, version 3.2.3, 2003. MARINTEK Report No.519619.

Wright, B., 1999. Evaluation of full scale data for moored vessel station keeping in pack ice. PERD/CHC Report 26–200, Ottawa, Canada, 103 pp.

Zhou, L., Su, B., Riska, K., and Moan, T., 2011. Numerical simulation of moored ship in level ice. Proceedings of the 30th International Conference on Offshore Mechanics and Arctic Engineering, Rotterdam, Netherlands, 855–863.

Zhou, L., Su, B., Riska, K., and Moan, T., 2012. Numerical simulation of moored structure station keeping in level ice. Cold Regions Science and Technology, 71, 54–66.

Paper 4

Experiments on level ice loading on an icebreaking tanker with different ice drift angles

Li Zhou, Kaj Riska, Rüdiger von Bock und Polach, Torgeir Moan and Biao Su

Published in Cold Regions Science and Technology 85 (2013), 79-93

Is not included due to copyright

Paper 5

Numerical modeling of ice load on an icebreaking tanker: comparing simulations with model tests

Li Zhou, Kaj Riska, Torgeir Moan and Biao Su

Accepted by Cold Regions Science and Technology (2012)

Is not included due to copyright

R A P P O R T E R
UTGITT VED
INSTITUTT FOR MARIN TEKNIKK
(tidligere: FAKULTET FOR MARIN TEKNIKK)
NORGES TEKNISK-NATURVITENSKAPELIGE UNIVERSITET

Report No.	Author	Title
	Kavlie, Dag	Optimization of Plane Elastic Grillages, 1967
	Hansen, Hans R.	Man-Machine Communication and Data-Storage Methods in Ship Structural Design, 1971
	Gisvold, Kaare M.	A Method for non-linear mixed -integer programming and its Application to Design Problems, 1971
	Lund, Sverre	Tanker Frame Optimalization by means of SUMT-Transformation and Behaviour Models, 1971
	Vinje, Tor	On Vibration of Spherical Shells Interacting with Fluid, 1972
	Lorentz, Jan D.	Tank Arrangement for Crude Oil Carriers in Accordance with the new Anti-Pollution Regulations, 1975
	Carlsen, Carl A.	Computer-Aided Design of Tanker Structures, 1975
	Larsen, Carl M.	Static and Dynamic Analysis of Offshore Pipelines during Installation, 1976
UR-79-01	Brigt Hatlestad, MK	The finite element method used in a fatigue evaluation of fixed offshore platforms. (Dr.Ing. Thesis)
UR-79-02	Erik Pettersen, MK	Analysis and design of cellular structures. (Dr.Ing. Thesis)
UR-79-03	Sverre Valsgård, MK	Finite difference and finite element methods applied to nonlinear analysis of plated structures. (Dr.Ing. Thesis)
UR-79-04	Nils T. Nordsve, MK	Finite element collapse analysis of structural members considering imperfections and stresses due to fabrication. (Dr.Ing. Thesis)
UR-79-05	Ivar J. Fylling, MK	Analysis of towline forces in ocean towing systems. (Dr.Ing. Thesis)
UR-80-06	Nils Sandsmark, MM	Analysis of Stationary and Transient Heat Conduction by the Use of the Finite Element Method. (Dr.Ing. Thesis)
UR-80-09	Sverre Haver, MK	Analysis of uncertainties related to the stochastic modeling of ocean waves. (Dr.Ing. Thesis)
UR-81-15	Odland, Jonas	On the Strength of welded Ring stiffened cylindrical Shells primarily subjected to axial Compression

UR-82-17	Engesvik, Knut	Analysis of Uncertainties in the fatigue Capacity of Welded Joints
UR-82-18	Rye, Henrik	Ocean wave groups
UR-83-30	Eide, Oddvar Inge	On Cumulative Fatigue Damage in Steel Welded Joints
UR-83-33	Mo, Olav	Stochastic Time Domain Analysis of Slender Offshore Structures
UR-83-34	Amdahl, Jørgen	Energy absorption in Ship-platform impacts
UR-84-37	Mørch, Morten	Motions and mooring forces of semi submersibles as determined by full-scale measurements and theoretical analysis
UR-84-38	Soares, C. Guedes	Probabilistic models for load effects in ship structures
UR-84-39	Aarsnes, Jan V.	Current forces on ships
UR-84-40	Czujko, Jerzy	Collapse Analysis of Plates subjected to Biaxial Compression and Lateral Load
UR-85-46	Alf G. Engseth, MK	Finite element collapse analysis of tubular steel offshore structures. (Dr.Ing. Thesis)
UR-86-47	Dengody Sheshappa, MP	A Computer Design Model for Optimizing Fishing Vessel Designs Based on Techno-Economic Analysis. (Dr.Ing. Thesis)
UR-86-48	Vidar Aanesland, MH	A Theoretical and Numerical Study of Ship Wave Resistance. (Dr.Ing. Thesis)
UR-86-49	Heinz-Joachim Wessel, MK	Fracture Mechanics Analysis of Crack Growth in Plate Girders. (Dr.Ing. Thesis)
UR-86-50	Jon Taby, MK	Ultimate and Post-ultimate Strength of Dented Tubular Members. (Dr.Ing. Thesis)
UR-86-51	Walter Lian, MH	A Numerical Study of Two-Dimensional Separated Flow Past Bluff Bodies at Moderate KC-Numbers. (Dr.Ing. Thesis)
UR-86-52	Bjørn Sortland, MH	Force Measurements in Oscillating Flow on Ship Sections and Circular Cylinders in a U-Tube Water Tank. (Dr.Ing. Thesis)
UR-86-53	Kurt Strand, MM	A System Dynamic Approach to One-dimensional Fluid Flow. (Dr.Ing. Thesis)
UR-86-54	Arne Edvin Løken, MH	Three Dimensional Second Order Hydrodynamic Effects on Ocean Structures in Waves. (Dr.Ing. Thesis)
UR-86-55	Sigurd Falch, MH	A Numerical Study of Slamming of Two-Dimensional Bodies. (Dr.Ing. Thesis)
UR-87-56	Arne Braathen, MH	Application of a Vortex Tracking Method to the Prediction of Roll Damping of a Two-Dimension

		Floating Body. (Dr.Ing. Thesis)
UR-87-57	Bernt Leira, MK	Gaussian Vector Processes for Reliability Analysis involving Wave-Induced Load Effects. (Dr.Ing. Thesis)
UR-87-58	Magnus Småvik, MM	Thermal Load and Process Characteristics in a Two-Stroke Diesel Engine with Thermal Barriers (in Norwegian). (Dr.Ing. Thesis)
MTA-88-59	Bernt Arild Bremdal, MP	An Investigation of Marine Installation Processes – A Knowledge - Based Planning Approach. (Dr.Ing. Thesis)
MTA-88-60	Xu Jun, MK	Non-linear Dynamic Analysis of Space-framed Offshore Structures. (Dr.Ing. Thesis)
MTA-89-61	Gang Miao, MH	Hydrodynamic Forces and Dynamic Responses of Circular Cylinders in Wave Zones. (Dr.Ing. Thesis)
MTA-89-62	Martin Greenhow, MH	Linear and Non-Linear Studies of Waves and Floating Bodies. Part I and Part II. (Dr.Techn. Thesis)
MTA-89-63	Chang Li, MH	Force Coefficients of Spheres and Cubes in Oscillatory Flow with and without Current. (Dr.Ing. Thesis
MTA-89-64	Hu Ying, MP	A Study of Marketing and Design in Development of Marine Transport Systems. (Dr.Ing. Thesis)
MTA-89-65	Arild Jæger, MH	Seakeeping, Dynamic Stability and Performance of a Wedge Shaped Planing Hull. (Dr.Ing. Thesis)
MTA-89-66	Chan Siu Hung, MM	The dynamic characteristics of tilting-pad bearings
MTA-89-67	Kim Wikstrøm, MP	Analysis av projekteringen for ett offshore projekt. (Licenciat-avhandling)
MTA-89-68	Jiao Guoyang, MK	Reliability Analysis of Crack Growth under Random Loading, considering Model Updating. (Dr.Ing. Thesis)
MTA-89-69	Arnt Olufsen, MK	Uncertainty and Reliability Analysis of Fixed Offshore Structures. (Dr.Ing. Thesis)
MTA-89-70	Wu Yu-Lin, MR	System Reliability Analyses of Offshore Structures using improved Truss and Beam Models. (Dr.Ing. Thesis)
MTA-90-71	Jan Roger Hoff, MH	Three-dimensional Green function of a vessel with forward speed in waves. (Dr.Ing. Thesis)
MTA-90-72	Rong Zhao, MH	Slow-Drift Motions of a Moored Two-Dimensional Body in Irregular Waves. (Dr.Ing. Thesis)
MTA-90-73	Atle Minsaas, MP	Economical Risk Analysis. (Dr.Ing. Thesis)
MTA-90-74	Knut-Aril Farnes, MK	Long-term Statistics of Response in Non-linear Marine Structures. (Dr.Ing. Thesis)
MTA-90-	Torbjørn Sotberg, MK	Application of Reliability Methods for Safety

75		Assessment of Submarine Pipelines. (Dr.Ing. Thesis)
MTA-90-76	Zeuthen, Steffen, MP	SEAMAID. A computational model of the design process in a constraint-based logic programming environment. An example from the offshore domain. (Dr.Ing. Thesis)
MTA-91-77	Haagensen, Sven, MM	Fuel Dependant Cyclic Variability in a Spark Ignition Engine - An Optical Approach. (Dr.Ing. Thesis)
MTA-91-78	Løland, Geir, MH	Current forces on and flow through fish farms. (Dr.Ing. Thesis)
MTA-91-79	Hoen, Christopher, MK	System Identification of Structures Excited by Stochastic Load Processes. (Dr.Ing. Thesis)
MTA-91-80	Haugen, Stein, MK	Probabilistic Evaluation of Frequency of Collision between Ships and Offshore Platforms. (Dr.Ing. Thesis)
MTA-91-81	Sødahl, Nils, MK	Methods for Design and Analysis of Flexible Risers. (Dr.Ing. Thesis)
MTA-91-82	Ormberg, Harald, MK	Non-linear Response Analysis of Floating Fish Farm Systems. (Dr.Ing. Thesis)
MTA-91-83	Marley, Mark J., MK	Time Variant Reliability under Fatigue Degradation. (Dr.Ing. Thesis)
MTA-91-84	Krokstad, Jørgen R., MH	Second-order Loads in Multidirectional Seas. (Dr.Ing. Thesis)
MTA-91-85	Molteberg, Gunnar A., MM	The Application of System Identification Techniques to Performance Monitoring of Four Stroke Turbocharged Diesel Engines. (Dr.Ing. Thesis)
MTA-92-86	Mørch, Hans Jørgen Bjelke, MH	Aspects of Hydrofoil Design: with Emphasis on Hydrofoil Interaction in Calm Water. (Dr.Ing. Thesis)
MTA-92-87	Chan Siu Hung, MM	Nonlinear Analysis of Rotordynamic Instabilities in Highspeed Turbomachinery. (Dr.Ing. Thesis)
MTA-92-88	Bessason, Bjarni, MK	Assessment of Earthquake Loading and Response of Seismically Isolated Bridges. (Dr.Ing. Thesis)
MTA-92-89	Langli, Geir, MP	Improving Operational Safety through exploitation of Design Knowledge - an investigation of offshore platform safety. (Dr.Ing. Thesis)
MTA-92-90	Sævik, Svein, MK	On Stresses and Fatigue in Flexible Pipes. (Dr.Ing. Thesis)
MTA-92-91	Ask, Tor Ø., MM	Ignition and Flame Growth in Lean Gas-Air Mixtures. An Experimental Study with a Schlieren System. (Dr.Ing. Thesis)
MTA-86-92	Hessen, Gunnar, MK	Fracture Mechanics Analysis of Stiffened Tubular

		Members. (Dr.Ing. Thesis)
MTA-93-93	Steinebach, Christian, MM	Knowledge Based Systems for Diagnosis of Rotating Machinery. (Dr.Ing. Thesis)
MTA-93-94	Dalane, Jan Inge, MK	System Reliability in Design and Maintenance of Fixed Offshore Structures. (Dr.Ing. Thesis)
MTA-93-95	Steen, Sverre, MH	Cobblestone Effect on SES. (Dr.Ing. Thesis)
MTA-93-96	Karunakaran, Daniel, MK	Nonlinear Dynamic Response and Reliability Analysis of Drag-dominated Offshore Platforms. (Dr.Ing. Thesis)
MTA-93-97	Hagen, Arnulf, MP	The Framework of a Design Process Language. (Dr.Ing. Thesis)
MTA-93-98	Nordrik, Rune, MM	Investigation of Spark Ignition and Autoignition in Methane and Air Using Computational Fluid Dynamics and Chemical Reaction Kinetics. A Numerical Study of Ignition Processes in Internal Combustion Engines. (Dr.Ing. Thesis)
MTA-94-99	Passano, Elizabeth, MK	Efficient Analysis of Nonlinear Slender Marine Structures. (Dr.Ing. Thesis)
MTA-94-100	Kvålsvold, Jan, MH	Hydroelastic Modelling of Wetdeck Slamming on Multihull Vessels. (Dr.Ing. Thesis)
MTA-94-102	Bech, Sidsel M., MK	Experimental and Numerical Determination of Stiffness and Strength of GRP/PVC Sandwich Structures. (Dr.Ing. Thesis)
MTA-95-103	Paulsen, Hallvard, MM	A Study of Transient Jet and Spray using a Schlieren Method and Digital Image Processing. (Dr.Ing. Thesis)
MTA-95-104	Hovde, Geir Olav, MK	Fatigue and Overload Reliability of Offshore Structural Systems, Considering the Effect of Inspection and Repair. (Dr.Ing. Thesis)
MTA-95-105	Wang, Xiaozhi, MK	Reliability Analysis of Production Ships with Emphasis on Load Combination and Ultimate Strength. (Dr.Ing. Thesis)
MTA-95-106	Ulstein, Tore, MH	Nonlinear Effects of a Flexible Stern Seal Bag on Cobblestone Oscillations of an SES. (Dr.Ing. Thesis)
MTA-95-107	Solaas, Frøydis, MH	Analytical and Numerical Studies of Sloshing in Tanks. (Dr.Ing. Thesis)
MTA-95-108	Hellan, Øyvind, MK	Nonlinear Pushover and Cyclic Analyses in Ultimate Limit State Design and Reassessment of Tubular Steel Offshore Structures. (Dr.Ing. Thesis)
MTA-95-109	Hermundstad, Ole A., MK	Theoretical and Experimental Hydroelastic Analysis of High Speed Vessels. (Dr.Ing. Thesis)
MTA-96-110	Bratland, Anne K., MH	Wave-Current Interaction Effects on Large-Volume Bodies in Water of Finite Depth. (Dr.Ing. Thesis)

MTA-96-111	Herfjord, Kjell, MH	A Study of Two-dimensional Separated Flow by a Combination of the Finite Element Method and Navier-Stokes Equations. (Dr.Ing. Thesis)
MTA-96-112	Æsøy, Vilmar, MM	Hot Surface Assisted Compression Ignition in a Direct Injection Natural Gas Engine. (Dr.Ing. Thesis)
MTA-96-113	Eknes, Monika L., MK	Escalation Scenarios Initiated by Gas Explosions on Offshore Installations. (Dr.Ing. Thesis)
MTA-96-114	Erikstad, Stein O., MP	A Decision Support Model for Preliminary Ship Design. (Dr.Ing. Thesis)
MTA-96-115	Pedersen, Egil, MH	A Nautical Study of Towed Marine Seismic Streamer Cable Configurations. (Dr.Ing. Thesis)
MTA-97-116	Moksnes, Paul O., MM	Modelling Two-Phase Thermo-Fluid Systems Using Bond Graphs. (Dr.Ing. Thesis)
MTA-97-117	Halse, Karl H., MK	On Vortex Shedding and Prediction of Vortex-Induced Vibrations of Circular Cylinders. (Dr.Ing. Thesis)
MTA-97-118	Igland, Ragnar T., MK	Reliability Analysis of Pipelines during Laying, considering Ultimate Strength under Combined Loads. (Dr.Ing. Thesis)
MTA-97-119	Pedersen, Hans-P., MP	Levendefiskteknologi for fiskefartøy. (Dr.Ing. Thesis)
MTA-98-120	Vikestad, Kyrre, MK	Multi-Frequency Response of a Cylinder Subjected to Vortex Shedding and Support Motions. (Dr.Ing. Thesis)
MTA-98-121	Azadi, Mohammad R. E., MK	Analysis of Static and Dynamic Pile-Soil-Jacket Behaviour. (Dr.Ing. Thesis)
MTA-98-122	Ulltang, Terje, MP	A Communication Model for Product Information. (Dr.Ing. Thesis)
MTA-98-123	Torbergsen, Erik, MM	Impeller/Diffuser Interaction Forces in Centrifugal Pumps. (Dr.Ing. Thesis)
MTA-98-124	Hansen, Edmond, MH	A Discrete Element Model to Study Marginal Ice Zone Dynamics and the Behaviour of Vessels Moored in Broken Ice. (Dr.Ing. Thesis)
MTA-98-125	Videiro, Paulo M., MK	Reliability Based Design of Marine Structures. (Dr.Ing. Thesis)
MTA-99-126	Mainçon, Philippe, MK	Fatigue Reliability of Long Welds Application to Titanium Risers. (Dr.Ing. Thesis)
MTA-99-127	Haugen, Elin M., MH	Hydroelastic Analysis of Slamming on Stiffened Plates with Application to Catamaran Wetdecks. (Dr.Ing. Thesis)
MTA-99-128	Langhelle, Nina K., MK	Experimental Validation and Calibration of Nonlinear Finite Element Models for Use in Design of Aluminium Structures Exposed to Fire. (Dr.Ing.

		Thesis)
MTA-99-129	Berstad, Are J., MK	Calculation of Fatigue Damage in Ship Structures. (Dr.Ing. Thesis)
MTA-99-130	Andersen, Trond M., MM	Short Term Maintenance Planning. (Dr.Ing. Thesis)
MTA-99-131	Tveiten, Bård Wathne, MK	Fatigue Assessment of Welded Aluminium Ship Details. (Dr.Ing. Thesis)
MTA-99-132	Søreide, Fredrik, MP	Applications of underwater technology in deep water archaeology. Principles and practice. (Dr.Ing. Thesis)
MTA-99-133	Tønnessen, Rune, MH	A Finite Element Method Applied to Unsteady Viscous Flow Around 2D Blunt Bodies With Sharp Corners. (Dr.Ing. Thesis)
MTA-99-134	Elvekrok, Dag R., MP	Engineering Integration in Field Development Projects in the Norwegian Oil and Gas Industry. The Supplier Management of Norne. (Dr.Ing. Thesis)
MTA-99-135	Fagerholt, Kjetil, MP	Optimeringsbaserte Metoder for Ruteplanlegging innen skipsfart. (Dr.Ing. Thesis)
MTA-99-136	Bysveen, Marie, MM	Visualization in Two Directions on a Dynamic Combustion Rig for Studies of Fuel Quality. (Dr.Ing. Thesis)
MTA-2000-137	Storteig, Eskild, MM	Dynamic characteristics and leakage performance of liquid annular seals in centrifugal pumps. (Dr.Ing. Thesis)
MTA-2000-138	Sagli, Gro, MK	Model uncertainty and simplified estimates of long term extremes of hull girder loads in ships. (Dr.Ing. Thesis)
MTA-2000-139	Tronstad, Harald, MK	Nonlinear analysis and design of cable net structures like fishing gear based on the finite element method. (Dr.Ing. Thesis)
MTA-2000-140	Kroneberg, André, MP	Innovation in shipping by using scenarios. (Dr.Ing. Thesis)
MTA-2000-141	Haslum, Herbjørn Alf, MH	Simplified methods applied to nonlinear motion of spar platforms. (Dr.Ing. Thesis)
MTA-2001-142	Samdal, Ole Johan, MM	Modelling of Degradation Mechanisms and Stressor Interaction on Static Mechanical Equipment Residual Lifetime. (Dr.Ing. Thesis)
MTA-2001-143	Baarholm, Rolf Jarle, MH	Theoretical and experimental studies of wave impact underneath decks of offshore platforms. (Dr.Ing. Thesis)
MTA-2001-144	Wang, Lihua, MK	Probabilistic Analysis of Nonlinear Wave-induced Loads on Ships. (Dr.Ing. Thesis)
MTA-2001-145	Kristensen, Odd H. Holt, MK	Ultimate Capacity of Aluminium Plates under Multiple Loads, Considering HAZ Properties. (Dr.Ing. Thesis)

MTA-2001-146	Greco, Marilena, MH	A Two-Dimensional Study of Green-Water Loading. (Dr.Ing. Thesis)
MTA-2001-147	Heggelund, Svein E., MK	Calculation of Global Design Loads and Load Effects in Large High Speed Catamarans. (Dr.Ing. Thesis)
MTA-2001-148	Babalola, Olusegun T., MK	Fatigue Strength of Titanium Risers – Defect Sensitivity. (Dr.Ing. Thesis)
MTA-2001-149	Mohammed, Abuu K., MK	Nonlinear Shell Finite Elements for Ultimate Strength and Collapse Analysis of Ship Structures. (Dr.Ing. Thesis)
MTA-2002-150	Holmedal, Lars E., MH	Wave-current interactions in the vicinity of the sea bed. (Dr.Ing. Thesis)
MTA-2002-151	Rognebakke, Olav F., MH	Sloshing in rectangular tanks and interaction with ship motions. (Dr.Ing. Thesis)
MTA-2002-152	Lader, Pål Furset, MH	Geometry and Kinematics of Breaking Waves. (Dr.Ing. Thesis)
MTA-2002-153	Yang, Qinzheng, MH	Wash and wave resistance of ships in finite water depth. (Dr.Ing. Thesis)
MTA-2002-154	Melhus, Øyvin, MM	Utilization of VOC in Diesel Engines. Ignition and combustion of VOC released by crude oil tankers. (Dr.Ing. Thesis)
MTA-2002-155	Ronæss, Marit, MH	Wave Induced Motions of Two Ships Advancing on Parallel Course. (Dr.Ing. Thesis)
MTA-2002-156	Økland, Ole D., MK	Numerical and experimental investigation of whipping in twin hull vessels exposed to severe wet deck slamming. (Dr.Ing. Thesis)
MTA-2002-157	Ge, Chunhua, MK	Global Hydroelastic Response of Catamarans due to Wet Deck Slamming. (Dr.Ing. Thesis)
MTA-2002-158	Byklum, Eirik, MK	Nonlinear Shell Finite Elements for Ultimate Strength and Collapse Analysis of Ship Structures. (Dr.Ing. Thesis)
IMT-2003-1	Chen, Haibo, MK	Probabilistic Evaluation of FPSO-Tanker Collision in Tandem Offloading Operation. (Dr.Ing. Thesis)
IMT-2003-2	Skaugset, Kjetil Bjørn, MK	On the Suppression of Vortex Induced Vibrations of Circular Cylinders by Radial Water Jets. (Dr.Ing. Thesis)
IMT-2003-3	Chezhian, Muthu	Three-Dimensional Analysis of Slamming. (Dr.Ing. Thesis)
IMT-2003-4	Buhaug, Øyvind	Deposit Formation on Cylinder Liner Surfaces in Medium Speed Engines. (Dr.Ing. Thesis)
IMT-2003-5	Tregde, Vidar	Aspects of Ship Design: Optimization of Aft Hull with Inverse Geometry Design. (Dr.Ing. Thesis)

IMT-2003-6	Wist, Hanne Therese	Statistical Properties of Successive Ocean Wave Parameters. (Dr.Ing. Thesis)
IMT-2004-7	Ransau, Samuel	Numerical Methods for Flows with Evolving Interfaces. (Dr.Ing. Thesis)
IMT-2004-8	Soma, Torkel	Blue-Chip or Sub-Standard. A data interrogation approach of identity safety characteristics of shipping organization. (Dr.Ing. Thesis)
IMT-2004-9	Ersdal, Svein	An experimental study of hydrodynamic forces on cylinders and cables in near axial flow. (Dr.Ing. Thesis)
IMT-2005-10	Brodtkorb, Per Andreas	The Probability of Occurrence of Dangerous Wave Situations at Sea. (Dr.Ing. Thesis)
IMT-2005-11	Yttervik, Rune	Ocean current variability in relation to offshore engineering. (Dr.Ing. Thesis)
IMT-2005-12	Fredheim, Arne	Current Forces on Net-Structures. (Dr.Ing. Thesis)
IMT-2005-13	Heggernes, Kjetil	Flow around marine structures. (Dr.Ing. Thesis
IMT-2005-14	Fouques, Sebastien	Lagrangian Modelling of Ocean Surface Waves and Synthetic Aperture Radar Wave Measurements. (Dr.Ing. Thesis)
IMT-2006-15	Holm, Håvard	Numerical calculation of viscous free surface flow around marine structures. (Dr.Ing. Thesis)
IMT-2006-16	Bjørheim, Lars G.	Failure Assessment of Long Through Thickness Fatigue Cracks in Ship Hulls. (Dr.Ing. Thesis)
IMT-2006-17	Hansson, Lisbeth	Safety Management for Prevention of Occupational Accidents. (Dr.Ing. Thesis)
IMT-2006-18	Zhu, Xinying	Application of the CIP Method to Strongly Nonlinear Wave-Body Interaction Problems. (Dr.Ing. Thesis)
IMT-2006-19	Reite, Karl Johan	Modelling and Control of Trawl Systems. (Dr.Ing. Thesis)
IMT-2006-20	Smogeli, Øyvind Notland	Control of Marine Propellers. From Normal to Extreme Conditions. (Dr.Ing. Thesis)
IMT-2007-21	Storhaug, Gaute	Experimental Investigation of Wave Induced Vibrations and Their Effect on the Fatigue Loading of Ships. (Dr.Ing. Thesis)
IMT-2007-22	Sun, Hui	A Boundary Element Method Applied to Strongly Nonlinear Wave-Body Interaction Problems. (PhD Thesis, CeSOS)
IMT-2007-23	Rustad, Anne Marthine	Modelling and Control of Top Tensioned Risers. (PhD Thesis, CeSOS)
IMT-2007-24	Johansen, Vegar	Modelling flexible slender system for real-time simulations and control applications
IMT-	Wroldsen, Anders Sunde	Modelling and control of tensegrity structures. (PhD

2007-25		Thesis, CeSOS)
IMT-2007-26	Aronsen, Kristoffer Høye	An experimental investigation of in-line and combined inline and cross flow vortex induced vibrations. (Dr. avhandling, IMT)
IMT-2007-27	Gao, Zhen	Stochastic Response Analysis of Mooring Systems with Emphasis on Frequency-domain Analysis of Fatigue due to Wide-band Response Processes (PhD Thesis, CeSOS)
IMT-2007-28	Thorstensen, Tom Anders	Lifetime Profit Modelling of Ageing Systems Utilizing Information about Technical Condition. (Dr.ing. thesis, IMT)
IMT-2008-29	Berntsen, Per Ivar B.	Structural Reliability Based Position Mooring. (PhD-Thesis, IMT)
IMT-2008-30	Ye, Naiquan	Fatigue Assessment of Aluminium Welded Box-stiffener Joints in Ships (Dr.ing. thesis, IMT)
IMT-2008-31	Radan, Damir	Integrated Control of Marine Electrical Power Systems. (PhD-Thesis, IMT)
IMT-2008-32	Thomassen, Paul	Methods for Dynamic Response Analysis and Fatigue Life Estimation of Floating Fish Cages. (Dr.ing. thesis, IMT)
IMT-2008-33	Pákozdi, Csaba	A Smoothed Particle Hydrodynamics Study of Two-dimensional Nonlinear Sloshing in Rectangular Tanks. (Dr.ing.thesis, IMT)
IMT-2007-34	Grytøyr, Guttorm	A Higher-Order Boundary Element Method and Applications to Marine Hydrodynamics. (Dr.ing.thesis, IMT)
IMT-2008-35	Drummen, Ingo	Experimental and Numerical Investigation of Nonlinear Wave-Induced Load Effects in Containerships considering Hydroelasticity. (PhD thesis, CeSOS)
IMT-2008-36	Skejic, Renato	Maneuvering and Seakeeping of a Singel Ship and of Two Ships in Interaction. (PhD-Thesis, CeSOS)
IMT-2008-37	Harlem, Alf	An Age-Based Replacement Model for Repairable Systems with Attention to High-Speed Marine Diesel Engines. (PhD-Thesis, IMT)
IMT-2008-38	Alsos, Hagbart S.	Ship Grounding. Analysis of Ductile Fracture, Bottom Damage and Hull Girder Response. (PhD-thesis, IMT)
IMT-2008-39	Graczyk, Mateusz	Experimental Investigation of Sloshing Loading and Load Effects in Membrane LNG Tanks Subjected to Random Excitation. (PhD-thesis, CeSOS)
IMT-2008-40	Taghipour, Reza	Efficient Prediction of Dynamic Response for Flexible amd Multi-body Marine Structures. (PhD-thesis, CeSOS)
IMT-2008-41	Ruth, Eivind	Propulsion control and thrust allocation on marine vessels. (PhD thesis, CeSOS)

IMT-2008-42	Nystad, Bent Helge	Technical Condition Indexes and Remaining Useful Life of Aggregated Systems. PhD thesis, IMT
IMT-2008-43	Soni, Prashant Kumar	Hydrodynamic Coefficients for Vortex Induced Vibrations of Flexible Beams, PhD thesis, CeSOS
IMT-2009-43	Amlashi, Hadi K.K.	Ultimate Strength and Reliability-based Design of Ship Hulls with Emphasis on Combined Global and Local Loads. PhD Thesis, IMT
IMT-2009-44	Pedersen, Tom Arne	Bond Graph Modelling of Marine Power Systems. PhD Thesis, IMT
IMT-2009-45	Kristiansen, Trygve	Two-Dimensional Numerical and Experimental Studies of Piston-Mode Resonance. PhD-Thesis, CeSOS
IMT-2009-46	Ong, Muk Chen	Applications of a Standard High Reynolds Number Model and a Stochastic Scour Prediction Model for Marine Structures. PhD-thesis, IMT
IMT-2009-47	Hong, Lin	Simplified Analysis and Design of Ships subjected to Collision and Grounding. PhD-thesis, IMT
IMT-2009-48	Koushan, Kamran	Vortex Induced Vibrations of Free Span Pipelines, PhD thesis, IMT
IMT-2009-49	Korsvik, Jarl Eirik	Heuristic Methods for Ship Routing and Scheduling. PhD-thesis, IMT
IMT-2009-50	Lee, Jihoon	Experimental Investigation and Numerical in Analyzing the Ocean Current Displacement of Longlines. Ph.d.-Thesis, IMT.
IMT-2009-51	Vestbøstad, Tone Gran	A Numerical Study of Wave-in-Deck Impact usin a Two-Dimensional Constrained Interpolation Profile Method, Ph.d.thesis, CeSOS.
IMT-2009-52	Bruun, Kristine	Bond Graph Modelling of Fuel Cells for Marine Power Plants. Ph.d.-thesis, IMT
IMT 2009-53	Holstad, Anders	Numerical Investigation of Turbulence in a Sekwed Three-Dimensional Channel Flow, Ph.d.-thesis, IMT.
IMT 2009-54	Ayala-Uraga, Efren	Reliability-Based Assessment of Deteriorating Ship-shaped Offshore Structures, Ph.d.-thesis, IMT
IMT 2009-55	Kong, Xiangjun	A Numerical Study of a Damaged Ship in Beam Sea Waves. Ph.d.-thesis, IMT/CeSOS.
IMT 2010-56	Kristiansen, David	Wave Induced Effects on Floaters of Aquaculture Plants, Ph.d.-thesis, IMT/CeSOS.
IMT 2010-57	Ludvigsen, Martin	An ROV-Toolbox for Optical and Acoustic Scientific Seabed Investigation. Ph.d.-thesis IMT.
IMT 2010-58	Hals, Jørgen	Modelling and Phase Control of Wave-Energy Converters. Ph.d.thesis, CeSOS.

IMT IMT 2010- 59	Shu, Zhi	Uncertainty Assessment of Wave Loads and Ultimate Strength of Tankers and Bulk Carriers in a Reliability Framework. Ph.d. Thesis, IMT.
IMT 2010-60	Shao, Yanlin	Numerical Potential-Flow Studies on Weakly-Nonlinear Wave-Body Interactions with/without Small Forward Speed, Ph.d.thesis, IMT.
IMT 2010-61	Califano, Andrea	Dynamic Loads on Marine Propellers due to Intermittent Ventilation. Ph.d.thesis, IMT.
IMT 2010-62	El Khoury, George	Numerical Simulations of Massively Separated Turbulent Flows, Ph.d.-thesis, IMT
IMT 2010-63	Seim, Knut Sponheim	Mixing Process in Dense Overflows with Emphasis on the Faroe Bank Channel Overflow. Ph.d.thesis, IMT
IMT 2010-64	Jia, Huirong	Structural Analysis of Intect and Damaged Ships in a Collission Risk Analysis Perspective. Ph.d.thesis CeSoS.
IMT 2010-65	Jiao, Linlin	Wave-Induced Effects on a Pontoon-type Very Large Floating Structures (VLFS). Ph.D.-thesis, CeSOS.
IMT 2010-66	Abrahamsen, Bjørn Christian	Sloshing Induced Tank Roof with Entrapped Air Pocket. Ph.d.thesis, CeSOS.
IMT 2011-67	Karimirad, Madjid	Stochastic Dynamic Response Analysis of Spar-Type Wind Turbines with Catenary or Taut Mooring Systems. Ph.d.-thesis, CeSOS.
IMT - 2011-68	Erlend Meland	Condition Monitoring of Safety Critical Valves. Ph.d.-thesis, IMT.
IMT – 2011-69	Yang, Limin	Stochastic Dynamic System Analysis of Wave Energy Converter with Hydraulic Power Take-Off, with Particular Reference to Wear Damage Analysis, Ph.d. Thesis, CeSOS.
IMT – 2011-70	Visscher, Jan	Application of Particla Image Velocimetry on Turbulent Marine Flows, Ph.d.Thesis, IMT.
IMT – 2011-71	Su, Biao	Numerical Predictions of Global and Local Ice Loads on Ships. Ph.d.Thesis, CeSOS.
IMT – 2011-72	Liu, Zhenhui	Analytical and Numerical Analysis of Iceberg Collision with Ship Structures. Ph.d.Thesis, IMT.
IMT – 2011-73	Aarsæther, Karl Gunnar	Modeling and Analysis of Ship Traffic by Observation and Numerical Simulation. Ph.d.Thesis, IMT.
Imt – 2011-74	Wu, Jie	Hydrodynamic Force Identification from Stochastic Vortex Induced Vibration Experiments with Slender Beams. Ph.d.Thesis, IMT.
Imt – 2011-75	Amini, Hamid	Azimuth Propulsors in Off-design Conditions. Ph.d.Thesis, IMT.

IMT – 2011-76	Nguyen, Tan-Hoi	Toward a System of Real-Time Prediction and Monitoring of Bottom Damage Conditions During Ship Grounding. Ph.d.thesis, IMT.
IMT- 2011-77	Tavakoli, Mohammad T.	Assessment of Oil Spill in Ship Collision and Grounding, Ph.d.thesis, IMT.
IMT- 2011-78	Guo, Bingjie	Numerical and Experimental Investigation of Added Resistance in Waves. Ph.d.Thesis, IMT.
IMT- 2011-79	Chen, Qiaofeng	Ultimate Strength of Aluminium Panels, considering HAZ Effects, IMT
IMT- 2012-80	Kota, Ravikiran S.	Wave Loads on Decks of Offshore Structures in Random Seas. Ph.d.thesis, CeSOS.
IMT- 2012-81	Sten, Ronny	Dynamic Simulation of Deep Water Drilling Risers with Heave Compensating Sysetm, IMT.
IMT- 2012-82	Berle, Øyvind	Risk and resilience in global maritime supply chains, IMT.
IMT- 2012-83	Fang, Shaoji	Fault Tolerant Position Mooring Control Based on Structural Reliability, IMT.
IMT- 2012-84	You, Jikun	Numerical studies on wave forces and moored ship motions in intermediate and shallow water, IMT.
IMT- 2012-85	Xiang, Xu	Maneuvering of two interacting ships in waves, CeSOS
IMT- 2012-86	Dong, Wenbin	Time-domain fatigue response and reliability analysis of offshore wind turbines with emphasis on welded tubular joints and gear components, CeSOS
IMT- 2012-87	Al Ryati, Nabil	Technical Condition Indexes for Auxiliary Marine Diesel Engines, IMT
IMT- 2012-88	Zhu, Suji	Investigation of Wave-Induced Nonlinear Load Effects in Open Ships considering Hull Girder Vibrations in Bending and Torsion, CeSOS
IMT- 2012-89	Ushakov, Sergey	Particulate matter emission characteristics from diesel engines operating on conventional and alternative marine fuels, IMT